7-1-2016

LOW TEMPERATURE TENSILE TESTING OF INDEPENDENTLY FABRICATED GOLD THIN FILM SAMPLES

Adnan Raza

Adnan Raza
Candidate

Mechanical Engineering
Department

This thesis is approved, and it is acceptable in quality and form for publication:

Approved by the Dissertation Committee:

Dr. Zayd C. Leseman , Chairperson

Dr. Yu Lin Shen

Dr. Mehran Tehrani

LOW TEMPERATURE TENSILE TESTING OF INDEPENDENTLY FABRICATED GOLD THIN FILM SAMPLES

by

ADNAN RAZA

B.E MECHANICAL ENGINEERING
NATIONAL UNIVERSITY OF SCIENCES & TECHNOLOGY,
PAKISTAN, 2014

THESIS

Submitted in Partial Fulfillment of the
Requirements for the Degree of

Masters of Science
Mechanical Engineering

The University of New Mexico
Albuquerque, New Mexico

July, 2016

DEDICATION

To my Parents. Everything I am is because of them.

ACKNOWLEDGEMENTS

I would like to acknowledge the countless contributions of so many people in my life without whom this thesis would not have been possible. These people made my stay at the University of New Mexico very special and I am grateful for their efforts.

Dr. Zayd C. Leseman, my research advisor has been a great blessing during the last two years. He enabled me to travel half way around the world from Pakistan to USA for this program. He provided me with the much needed technical guidance and financial support. He was extremely patient and mentored me with admirable commitment. He has been a constant source of inspiration for me and this work would definitely not have been possible without his support, encouragement and suggestions.

My friends and colleagues in our research group made my stay very enjoyable and memorable. I would like to thank my dear friend Mohammad Hosein Ghasemi Baboly for his help, support and friendship. From teaching me COMSOL to giving me valuable advice from time to time, he has always been there for me. He is like an elder brother to me and I am grateful for having him in my life. He is also graduating with me this semester and gets annoyed when I call him Dr. Baboly. I wish him nothing but the very best in life.

I am also grateful to my dear friend Mirza Elahi, for his technical guidance and companionship. Being a NanoFab guru, he was my guide in all of the fabrications processes I used to make my MEMS devices at the UNM cleanroom. Another great friend I would like to appreciate is my buddy Patrick King. His constant willingness to help and his impressive resourcefulness has been of immense comfort for me. I am grateful to them all for the evenings we shared at Starbucks and wish them the absolute best in life.

I would like to extend my special thanks to Dr. Azeem Sarwar who has been a constant source of inspiration and support for me. I am thankful to him for believing in my abilities and introducing me to Dr. Zayd Leseman. All of this would never have been possible without his efforts for which I am ever grateful.

I am also grateful to my brother Asad Raza for shouldering my share of familial responsibilities towards our family and to my younger brother Haseeb Raza and of course my mother for being so patient with me. It is because of their prayers and patience that I was able to concentrate fully on my studies and finally succeed.

Inevitably I have missed a lot of people but I would like to let them know they are no less important to me and they have my immense gratitude.

LOW TEMPERATURE TENSILE TESTING OF INDEPENDENTLY FABRICATED GOLD THIN FILM SAMPLES

BY

ADNAN RAZA

B.E. Mechanical, National Univ. of Sciences & Technology, Pakistan, 2014

M.S., University of New Mexico, Albuquerque, NM, USA, 2016

ABSTRACT

Tensile testing of free standing thin films is of great importance for determining their material properties. Samples have always been co fabricated with the MEMS device being used as the test apparatus. Consequently, a new device has to be used each time a new sample is tested, resulting in loss of precision. The proposed idea is to independently fabricate free standing gold thin film samples and transfer them to a separately fabricated cascaded thermal actuator setup. Thermal actuators are desirable due to the large deflections and forces they provide while maintaining a relatively low thermal gradient across the test specimen. 250 nm thick Gold samples are fabricated with varying lengths of 50,100, 500, 625 & 750 μm with corresponding thermal actuators. Also, to study the drastic effects of change in temperature on the tensile behavior of these samples, a lab scale cryostat capable of experimentation in the 4 K -300 K temperature range is also developed and presented in detail in the first half of this thesis.

TABLE OF CONTENTS

LIST OF FIGURES

Chapter 1

INTRODUCTION

1.1 BACKGROUND AND MOTIVATION

Advancement in semiconductor fabrication technology, particularly bulk and surface micromachining techniques for Silicon opened up doors to a new era of miniaturized devices known as Micro Electromechanical Devices (MEMS). These devices offer new capabilities, improved performance and lower costs due to batch production over traditional transducers and sensors. The years to come will surely see the rise of the MEMS industry, revolutionizing everyday life as we know it.[1] [2]. They are already being used today in many physical, chemical and biological applications [3]–[5]. A number of these application make use of thin metal films. In particular micro switching devices where these films are used as an ohmic contact material.

Gold is an important material used for thin film structures in the MEMS industry. It is valued because of its inertness and high thermal stability. Gold has a Young's modulus of 79 GPa and a high melting temperature of 1064^0C. So it can be used as a thin film structure at higher temperatures with good resistance to mechanical failure.

Nano-structured thin films exhibit elastic and plastic behavior which is significantly different than bulk materials. The reason being the volume ratios of material defects such as grain boundaries, dislocations and interstitials become significant and become a chief contributor to the physical and mechanical properties. Metal thin films tend to be stronger than their bulk counterparts in exchange for reduced ductility. Moreover, these properties further change drastically as the temperature drops. The elasticity decreases and the strength increases as the temperature goes down. Hardly any data is available for tensile

testing of thin Gold films in the temperature range of 77K-300K. So, the author attempts to study these properties at reduced temperatures in a custom designed cryostat.

Gold is not new to the semiconductor or MEMS industry and several experiments have been conducted to study their material properties. Tensile testing has been done with the samples being co-fabricated along with the test apparatus. Khawar et al [6] used cascaded thermal actuators for tensile testing of Platinum thin films. These samples were co-fabricated along with the actuator setup. The main problem with co-fabricated samples is that they can only be used once and a new apparatus has to be made for another tensile test. As no two devices fabricated are exactly the same so this leads to a loss in precision and accuracy. In this thesis the author introduces a novel concept of tensile testing of samples, independently fabricated from the test apparatus. Hundreds of samples are fabricated separately from the thermal actuators and are then transfer to the test site. In this way the same test apparatus can be used repeatedly with many interchangeable samples. Using the same devices for the testing insures repeatability of the test and the sheer number of the samples alone contribute much towards a high precision.

Vinci et al described Nano-indentation as an effective means of determining physical and thermal properties of various free standing thin films including Gold thin films. [7] Zhu et al used a parallel plate actuator to study a poly silicon sample and a carbon nano wire. The poly silicon sample was co-fabricated along with the actuator, while the carbon nano wire was welded on the device using 'Focused Ion Beam' (FIB).[8] But none have actually tested independently fabricated Gold thin film samples like the author proposes, thus warranting the novelty of this work.

1.2 SCOPE

The scope of this thesis is the tensile testing of independently fabricated and free standing Gold thin film samples. The samples will have lengths of 50, 100, 500, 625 & 750 µm with a film thickness of 250 nm. The experiments will be carried out at room temperature as well as in the temperature range of 77-300 K. This additional requirement of reduced temperature testing in turn produces a need for a custom built 'Cryostat' with provisions for electrical connectivity and optical access.

1.3 OVERVIEW/ORGANIZATION

The thesis is divided into 9 chapters. The second chapter talks about the design process for the cryostat needed for the low temperature tensile tests. It includes the general design criteria, material selection and finite element analysis of the proposed design. Chapter 3 takes the final recommendations for the cryostat design and shapes the manufacturing flow through a CAD model. It also contains details of the final product and the special features it contains. Chapter 4 is about the experimental setup used to test the cryostat and the results obtained. Chapter 5 explains the need for a custom sample holder for the cryostat and draws out some recommendations through FEA for an optimized design. In Chapter 6 the manufacturing flow and design features for the sample holder are presented. It also contains the experimental results obtained by testing the operation of the holder in the cryostat. Chapter 7 is dedicated to the theory behind the thermal actuators used for the tensile testing and design of test samples. Chapter 8 talks about the fabrication process for these actuators and samples. Chapter 9 is for the experimental setup used to test out the thermal actuators and contains results of the fab process and recommendations for future work.

Chapter 2

CRYOSTAT DESIGN & ANALYSIS

2.1 INTRODUCTION

A cryostat is essential for the low temperature testing of the MEMS thermal actuators. Several commercial models are available for various minimum temperatures, presence or absence of optical access, electrical connectivity, temperature control etc. As is the case with all commercial merchandise, better performance and added features come at a high cost. Thus, the goal is to design, manufacture and test a cost effective, lab scale cryostat. Several resources are available to achieve this goal. A few of the resources that the author benefitted from are presented in [9]–[12]. The main focus is to facilitate the experimentation at the test site. The cryostat can be designed to cool down the sample directly, through contact with low temperature vapors from a cryogenic liquid at a selected rate or it can be indirectly cooled through conduction, where the sample is in contact with the cryogenic liquid through a series of cascaded structures. The second option is selected as it provides the opportunity to have the sample in vacuum without any kind of direct contact which could be harmful to the delicate MEMS structures. An optical access is a must for observing the behavior of the test specimen. Electrical access is also needed to form connections with the device to carry out experiments. In light of this discussion, an overall design criterion is presented in the following section.

2.2 OVERALL DESIGN CRITERIA

The following criteria has been set up for the design of the cryostat:

1. Stable design, no vibrations
2. The test specimen should be in vacuum
3. Optical access to the test specimen required
4. Electrical access to the test specimen required
5. Minimum thermal losses from the test specimen and the cooling reservoirs
6. Easy changeover of sample

2.3 SELECTION OF BUILDING MATERIAL

The design process starts with the selection of commercially available stainless steel pipes to be used to form the cylindrical cavities for the cryogenic reservoirs. SS 304 and SS 316 are the most widely used low carbon steels. Both SS 304 and SS 316 are strong, corrosion resistant, can withstand thermal shocks, have low thermal conductivity and high heat capacity making them ideal building materials for cryostats. SS 316 is used in applications where magnetic fields are involved and is more expensive as compared to SS 304. As the design criteria does not include a provision for magnetic fields so SS 304, which weakly magnetizes is used as a more cost effective alternate. After careful thought, table1 shows the pipe sizes that were chosen to form the various chambers for the cryostat.

Table1: Commercially Available SS304 Pipe Sizes

#	Material, Catalog Entry	(O.D x I.D x Thickness)
1	SS304, Schedule-40, 1-1/2	(1.9 x 1.610 x 0.145)"
2	SS304, Schedule-10, 6	(6.625 x 6.357 x 0.134)"
3	SS304, Schedule-40, 8	(8.625 x 7.981 x 0.322)"
4	SS304, Schedule-40, 10	(10.75 x 10.02 x 0.365) "
5	SS304, Schedule-40, 12	(12.75 x 12.00 x 0.375)"

The placement of these pipes and the various chambers which they form is shown in figure1. Afterwards, these cross sectional dimensions are taken to an FEA software where their lengths are decided to optimize the volumes based on a simulation criterion.

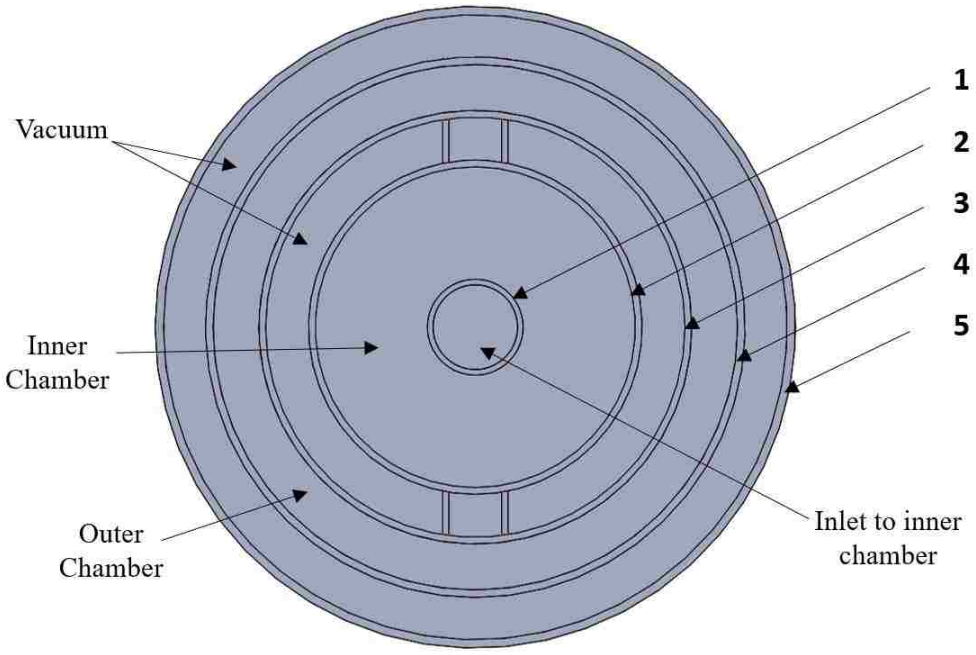

Figure 1: Cross Section of Cryostat

2.4 CRYOSTAT FINITE ELEMENT ANALYSIS

COMSOL Multiphysics version 4.2a is the selected FEA tool for optimizing the cryostat design. An axisymmetric model has been setup for this purpose thereby taking advantage of the cryostat's geometry. The model is shown in figure 2.

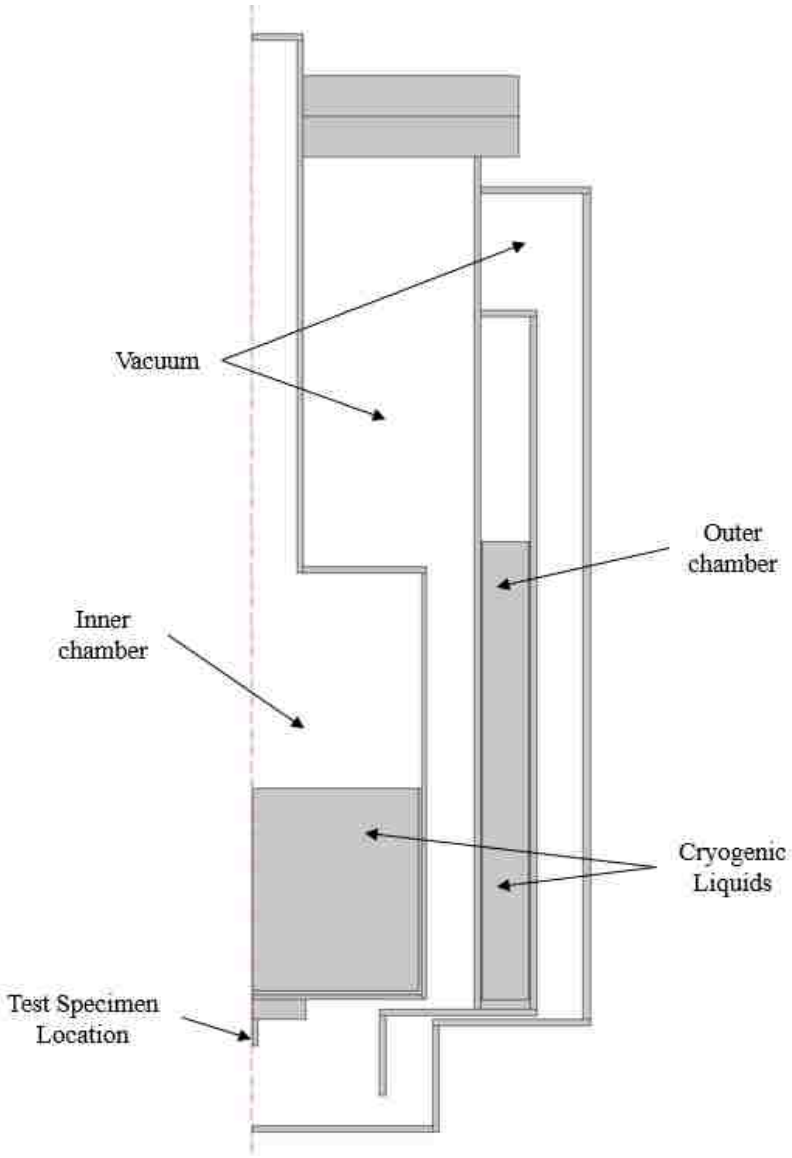

Figure 2: COMSOL Model

2.5 GEOMETRIC PROVISIONS FOR MINIMIZATION OF HEAT GAINS

2.5.1 CONDUCTION

Conduction is the chosen mechanism for drawing out heat from the test specimen to the cryogenic liquids. The cryogenic liquid in the inner chamber takes away heat from its bottom plate and walls. The walls then conduct this cooling effect throughout the entire structure. In the other direction the bottom plate for the inner chamber cools a 'Sample Holder' which in turn cools the test specimen. Further provisions have been taken to minimize conduction losses for the inner chamber as it holds the test specimen. These provisions include:

1. Making the neck for the inner chamber as long as possible because SS 304 has low thermal conductivity and high heat capacity. Thus making the heat transfer from the exposed top area to the inner chamber more difficult.
2. Avoiding direct contact between the outer and the inner chamber as much as possible.

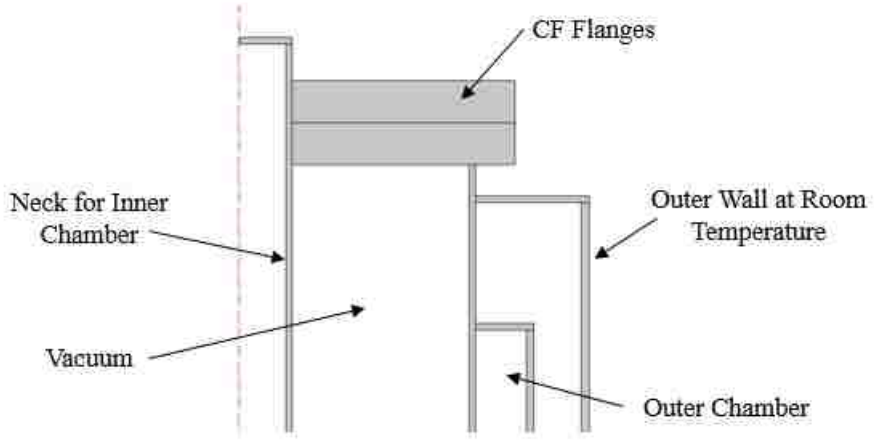

Figure 3: Provisions for Minimizing Heat Gain for Inner Chamber

It can be seen in the figure 3 that the connection point for the outer wall is the extension of the inner chamber. The inner chamber also cools the CF flanges which are in direct contact with the neck of the inner chamber.

2.5.2 CONVECTION

The regions between the inner & outer chamber and between the outer chamber and outer most wall (exposed to the atmosphere) collectively constitute the 'Vacuum Jacket'. Air is removed from this region through a vacuum pump thus eliminating convective heat gains for the cryogenic reservoirs and the test specimen.

2.5.3 RADIATION

As explained earlier, cooling the inner chamber is more important than the outer chamber as it holds the test specimen. The outer chamber is surrounded by the outer wall which is at room temperature. But, the inner chamber is surrounded by the outer chamber which will eventually achieve 77 K. So in this way the outer chamber receives much more heat through radiation than the inner chamber. Further provisions taken for test specimen will be explained in the sample holder design section.

2.6 OPTIMIZATION

The FEA model is optimized based upon the following design criteria:

1. Maximize capacity vs. consumption for the cryogenic liquids in the inner and outer chamber
2. The chamber capacity must at least 4 and 6 liters, for the inner and outer chambers respectively (Close to capacities for similar, commercially available models)

3. Cool down time for the test specimen must be reasonable. (Around 15 minutes which is close to that of commercially available models of the same capacity)
4. Factor of safety for both the pressure vessels should at least be 6 for both liquid nitrogen and liquid helium.

The design variables are the lengths of all cylinders. Considering the scope of the optimization study two cases have to be solved for an optimal design:

1. Operation of cryostat from room temperature to 77 K
2. Operation of cryostat from 77 K to 4.5 K

2.6.1 CASE 1: OPERATION FROM 300 K to 77 K

Initially, both inner and outer chambers are empty and the whole structure starts out at room temperature. A vacuum pump is used to suck out air from the 'Vacuum Jacket'. Then liquid nitrogen is poured into the inner and outer chambers to cool them down. So the cryogenic liquid for case-1 is liquid nitrogen in both chambers, which are kept half full by intuition to balance the initial boil off and pouring in of the liquid nitrogen. This is validated afterwards in the 'Experimental Results' section.

MATERIAL PROPERTIES

Thermophysical properties of materials vary drastically with drastic changes in temperature. The operational temperature range here is between 300 K and 77 K and in the subsequent case it will be between 77 K and 4.5 K. So the radical changes in thermophysical properties, such as the thermal conductivity and heat capacity have to be accounted for the materials involved. These properties are input to COMSOL as a function

of temperature, over the entire operational range. Failure to do so will result in unrealistic and untrustworthy results. NIST offers a convenient library of thermophysical properties for select materials over a range of temperatures from cryogenic temperatures to higher than room temperature.[9] The plots shown in figure 4 and 5 have been generated for the thermal conductivity and the heat capacity for Stainless Steel 304, which is the primary material in this simulation. These plots are generated through MATLAB using the NIST material library database.

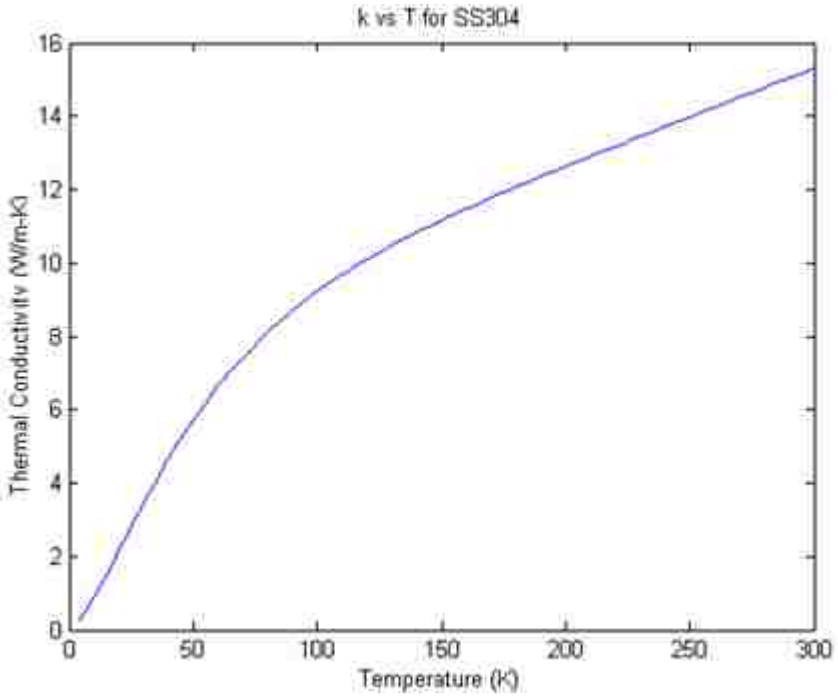

Figure 4: Thermal Conductivity of SS 304

The other property required for this simulation is density which does not change as much for SS 304. Consequently, a fixed value of 8000 Kg/m^3 has been used.

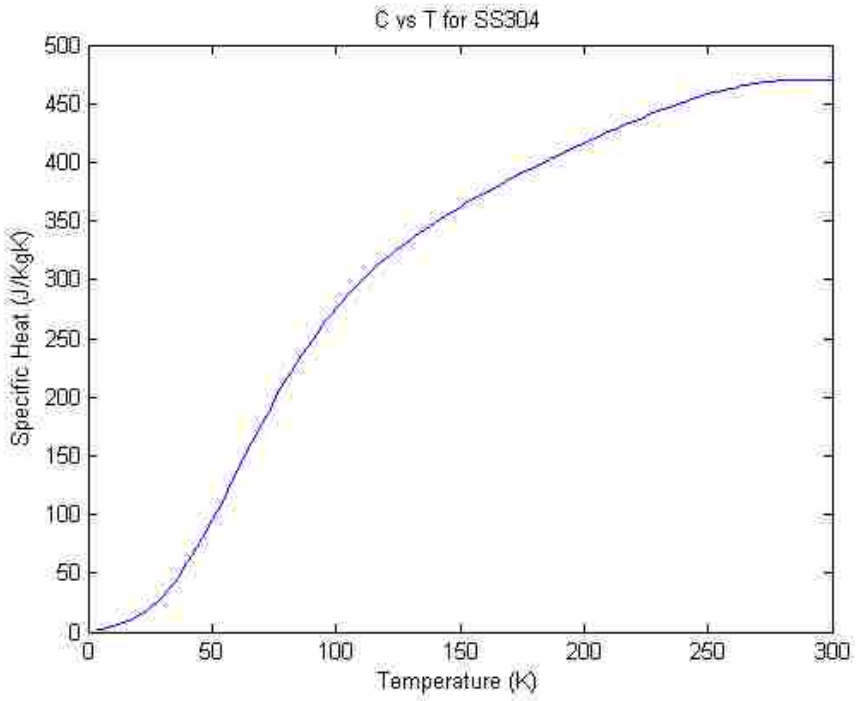

Figure 5: Heat Capacity for SS 304

Another material of importance in this simulation is liquid nitrogen. Liquid nitrogen has a boiling point of 77K, specific heat capacity of 2.04 KJ/Kg-K, thermal conductivity of 139.6mW/m-K and a density of 808 Kg/m^3. At the boiling point the temperature remains the same so the thermophysical properties associated with it will also remain the same. As soon as the liquid nitrogen comes in contact with the metal surface in both the chambers it immediately takes in heat and that layer boils off. It is then replacing by another layer and the cycle continues. The liquid nitrogen in both the chambers is being continuously replenished as to keep its level same. So it is safe to assume that we can get sensible results by giving the cryogenic liquids in both the chambers, fixed properties at their boiling point which will not change during the entire course of operation.

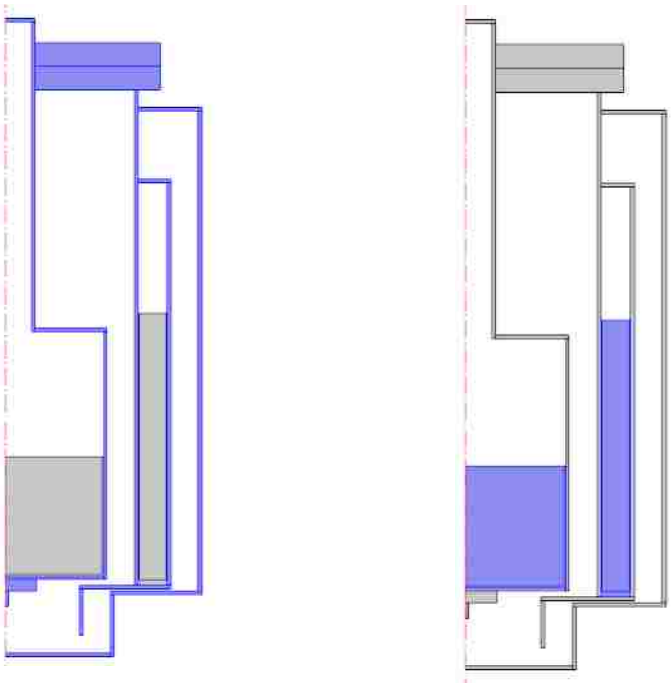

Figure 6: Highlighted Areas show Material Assignment for SS 304 (Left) and Liquid Nitrogen (Right) for Case 1

INITIAL CONDITIONS, BOUNDARY CONDITIONS & LOADS

Initially the whole cryostat is at room temperature except the two cryogenic reservoirs. A special approach is taken to model the cryogenic reservoirs. This will simulate a scenario which is as real as possible. Here an important modeling assumption is taken, that the properties of the bulk of the cryogenic liquid remain the same except for a narrow strip along the point of contact. This region behaves as a buffer zone between the bulk of the liquid and the hot metal surface. It is arbitrarily assumed that this layer contains 1% of the total volume. So at 99% of the volume a boundary at fixed temperature of 77 K is setup.

If this provision is not taken, then two other scenarios are possible. First, 100% volume of the cryogenic liquid is given the initial condition of 77K without a fixed temperature boundary. Transient analysis showed that within the realistic time frames, heat

gains due to convection heating on the outer jacket dominate the cooling effect due to the cryogenic liquids and the temperature graphs level down at a much higher temperature than 77 K (The simulation showed it to be 212 K). This is not realistic and hence is discarded. It will be shown later that the experimental data contradicts this approach and the original approach yields the most realistic results.

The second scenario is that in addition to the initial temperature of the cryogenic reservoirs being 77K, a fixed temperature boundary condition of 77K is added at the liquid – metal interface. This leads the simulation to believe that the sample temperature drops from 300 K to 77 K in less than a second. This if of course, unrealistic as well so the only realistic representation of the actual phenomenon occurring at the liquid – metal interface is the one implemented.

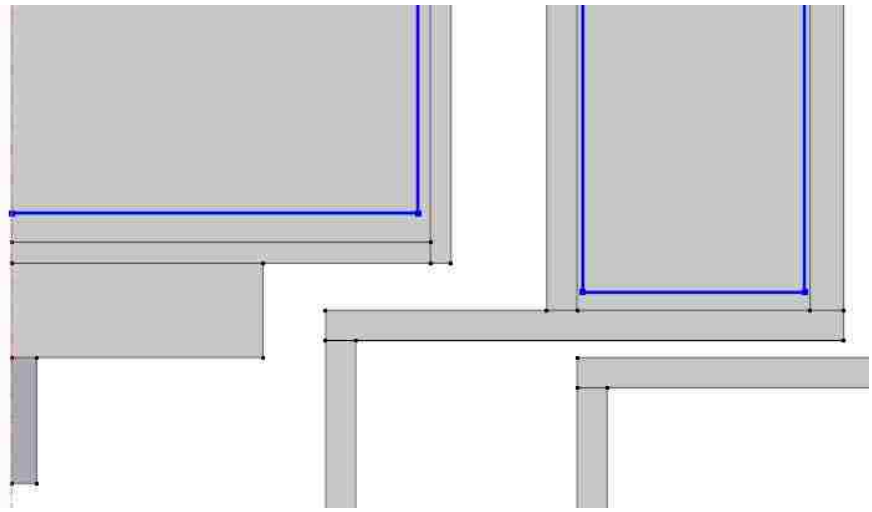

Figure 7: Simulating Boiling of Cryogenic Liquids (Fixed T Boundary in Blue)

In the end, an 'Inward Flux' has been setup on the outer most surface of the cryostat. The surrounding air is at 300 K and has a coefficient of convection as $h = 10 \frac{W}{m^2}$ for natural convection of air. This becomes the heat source in the model and heats up the outer jacket

with convection. Then this heat is carried through conduction to the test specimen. Figure 8 is a visual representation of the various initial and boundary conditions.

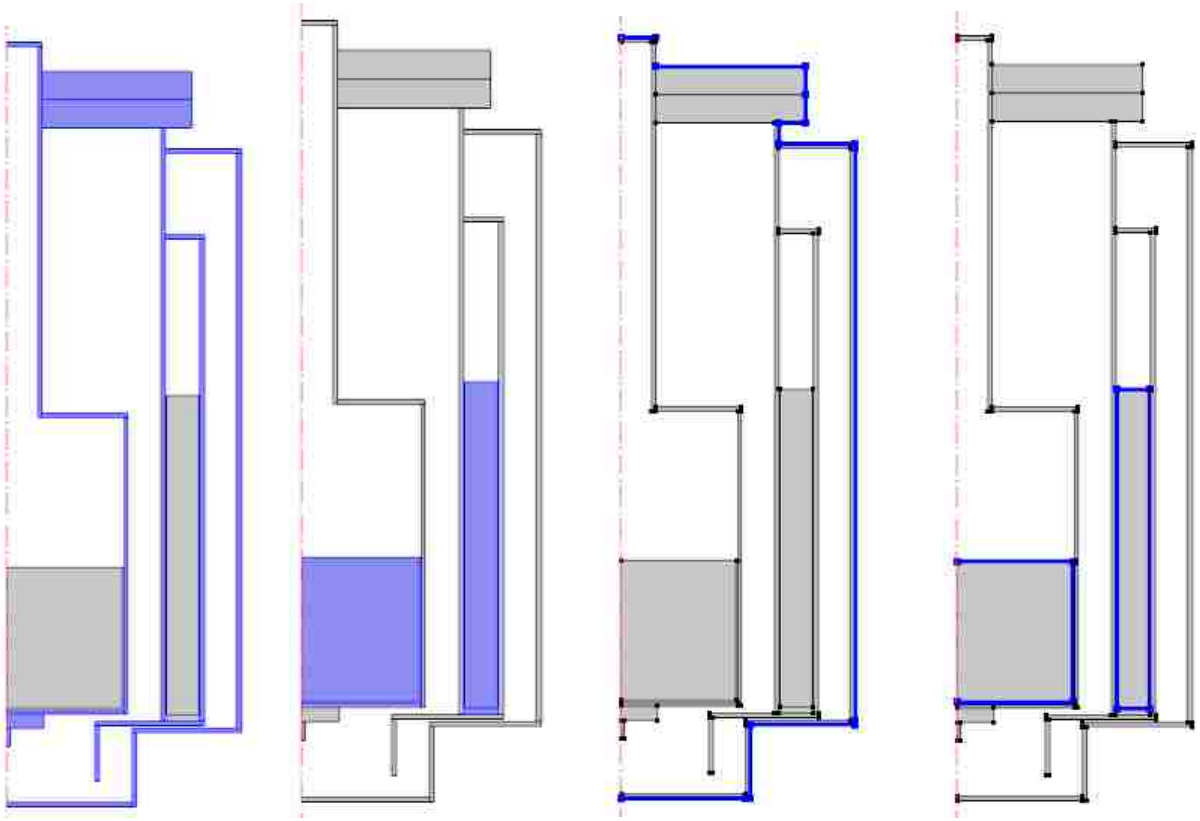

Figure 8: Initial Conditions for case 1 a) 300K, b) 77K, Boundary Conditions for Case1 c) 10W/inch2, 300K inward Flux, d) 77K fixed temperature (Similar to figure 7)

MESH REFINEMENT

The regions close to the liquid-metal interface are subjected to high temperature and flux gradients. Thus a mesh refinement study is necessary to get well converged results. Tetrahedral elements were used throughout the model with varying size. The mesh setting for the entire model except for the walls and bottom of the inner and outer chamber and

the bodies of the cryogenic liquid are set to ‘Extra Fine’. These excluded regions are then given a custom mesh size of ¼ the smallest element size for ‘Extra Fine’ setting in COMSOL. The results were studied for temperature and flux at the liquid-metal interface for the inner chamber with varying mesh size up to the final settings described above. The results lie within a 0.1% range. A setting of ‘Extremely Fine’ mesh size was also used but that increased the computational memory and time requirements four times with 0.01% change in results with respect to the ‘Extra Fine’ setting. Thus the optimal meshing conditions are the ones used for this analysis. Figure 9 shows the overall mesh and the regions of mesh refinement.

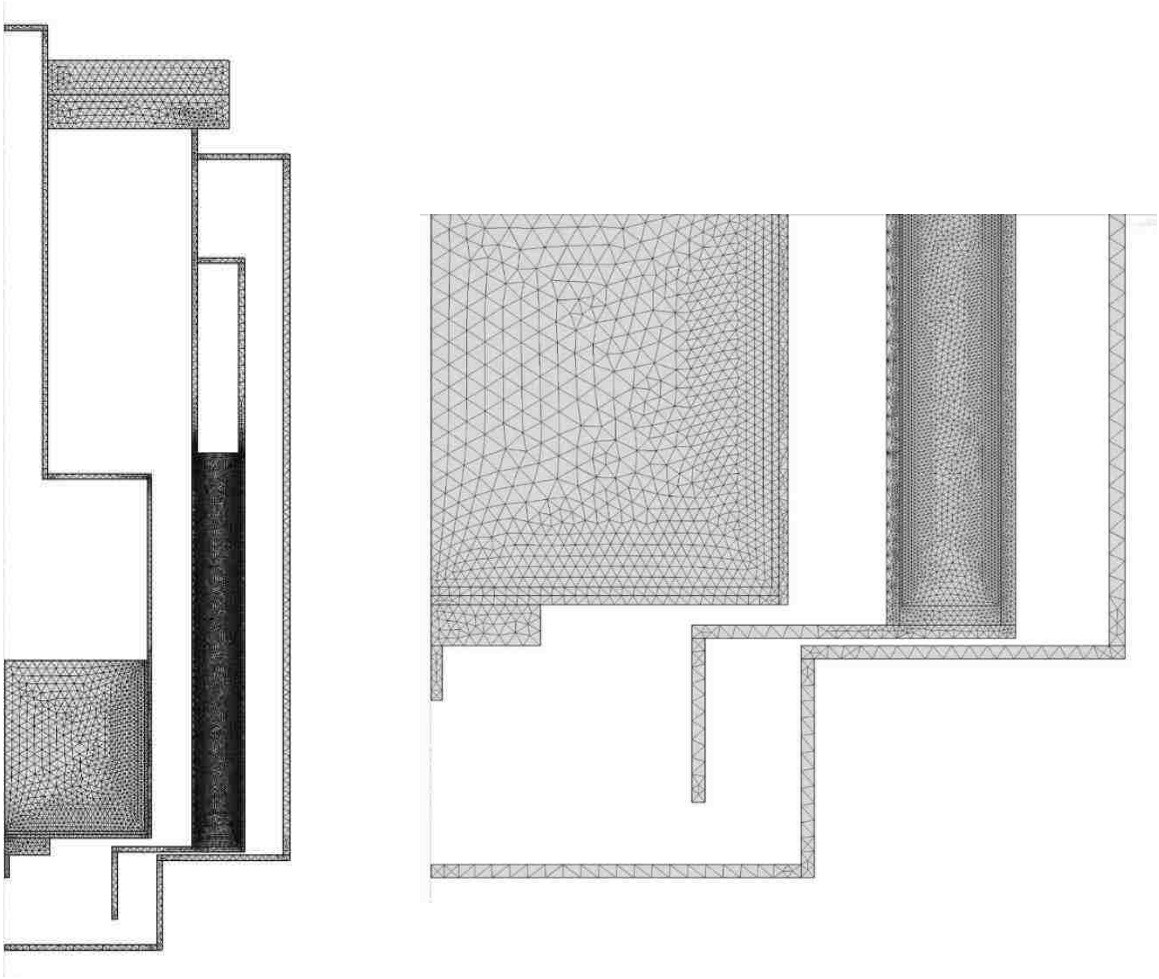

Figure 9: Overall Mesh (Left) & Regions of Mesh Refinement (Right)

CONSUMPTION RATES

Optimization of the cryostat model requires the calculation of consumption rates for the cryogenic liquids in the inner and outer chambers. The three step involved are shown in figure 10.

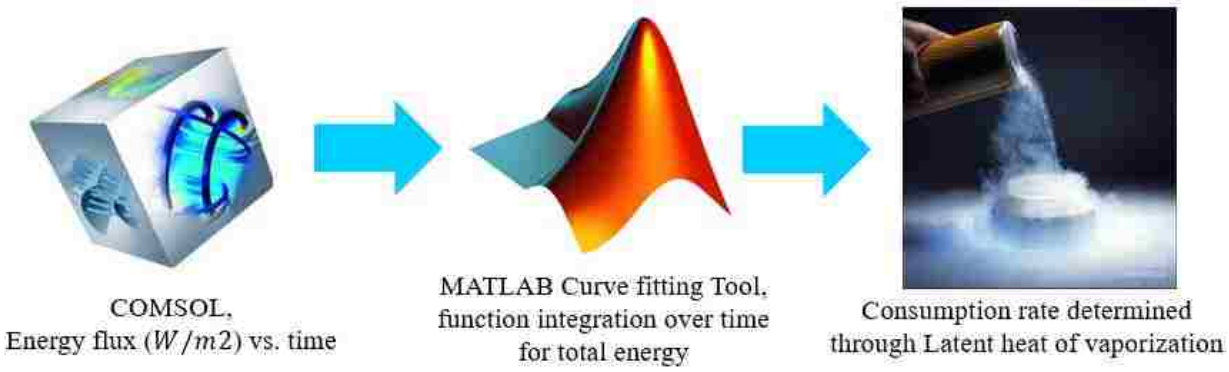

Figure 10: Steps Involved in Calculation of Consumption Rates for Cryogenic Liquids

1. The first step is to draw out the rate at which the cryogenic liquids are taking in heat. For this purpose, the 'Line Average' is taken at the liquid – metal interface over the concerned period of time during a transient analysis. This comes out to be in W/inch^2. This is then converted into 'Power' by multiplying it by the surface area of the liquid – metal interface. The unit comes out to be Watts or Joules per second.

2. The second step is to convert the power obtained in step 1 into total energy by integrating it over the time period involved. This is done by exporting the data into MATLAB and then using a curve fitting tool to generate a function that gives the power at each time. This function is then integrated over the concerned period of time to get

the exact value of energy that the cryogenic liquids absorbed. The unit now becomes Joules.

3. The third step is simply to convert the total energy obtained in the previous step to the amount of cryogenic liquid evaporated through its latent heat of evaporation. This gives the total amount of liquid consumed over that period of time hence the consumption rate. This liquid when it boils off, still has a lot of cooling power as its initial temperature is just above the liquid's boiling point so as this gas makes its escape it takes away the heat from the walls of the chambers and the inlet/exit pathways, thus lowering their temperature as well. This is not taken into consideration to counter the losses that might incur during the actual operation of the cryostat.

The consumption rate decays exponentially from the start of operation till the quasi steady state (As it cannot actually achieve steady state without taking infinite time). Thus we need a fixed reference time frame to compare the performance of different design iterations. 15 minutes (900 sec) is selected as reference time frame as it is in accordance with the problem

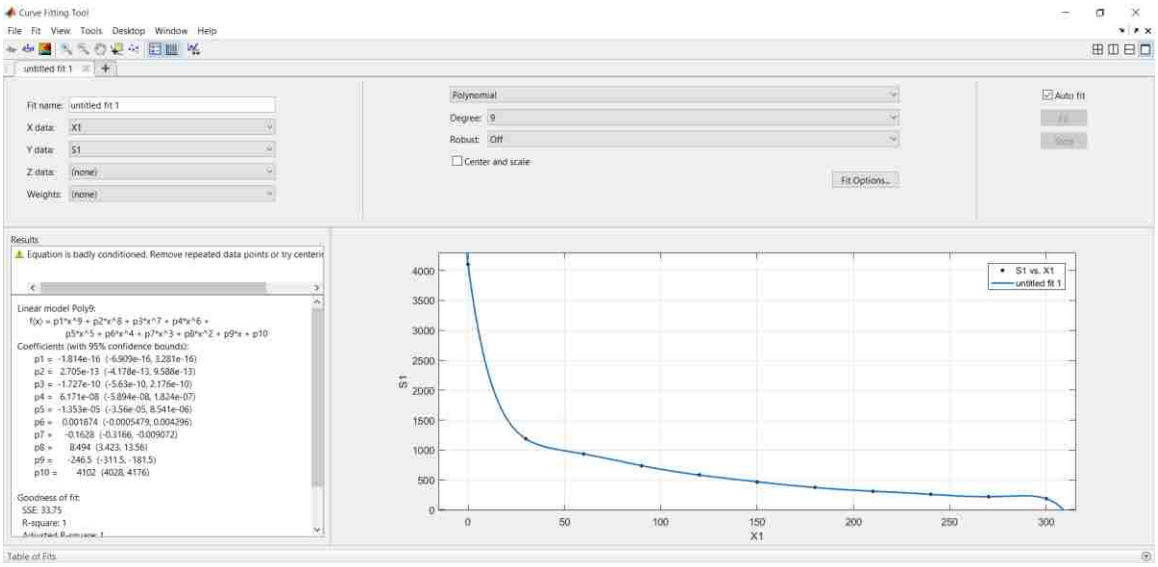

Figure 11: Curve Fitting Flux across Walls of Inner Chamber (0-300 sec)

statement for this simulation. The flux gradient is found to be so high that MATLAB is unable to fit a polynomial curve through the points for the 900 sec duration even with a polynomial order of 9 with co-efficient accuracy up to 16 digits for the 10 polynomial constants involved. Thus the process had to be divided into two curves, from 0-300 sec and 300-900 sec. The figures 11 & 12 show the curve fitting process for these two time intervals

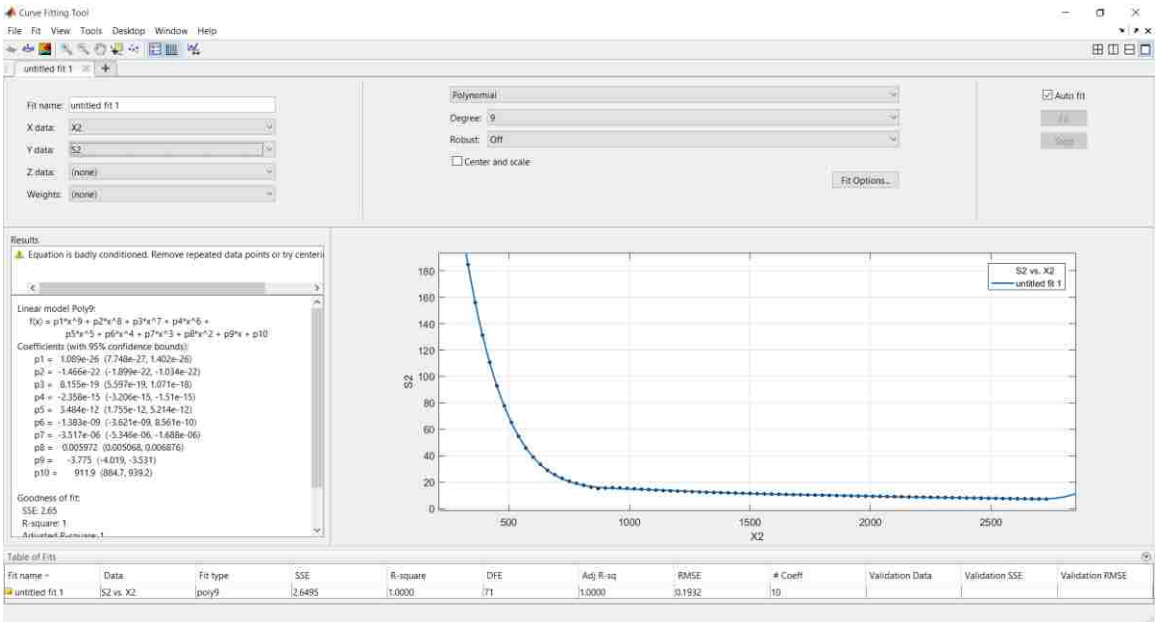

Figure 12: Curve Fitting Flux across Walls of Inner Chamber (300-2700 sec)

The optimization process starts with the length of the inner chamber. This in turn decides its capacity and consumption rate for the liquid it contains. All the other lengths are dealt with accordingly. The first iteration is for L=r for the inner chamber which puts the capacity around 4 Liters. Then the process is repeated for L=2r, 3r, and L=4r. Afterwards the refinement process is carried out for L=2.5r. A visual to these capacities in proportion to the cryostat size is shown in figure 13.

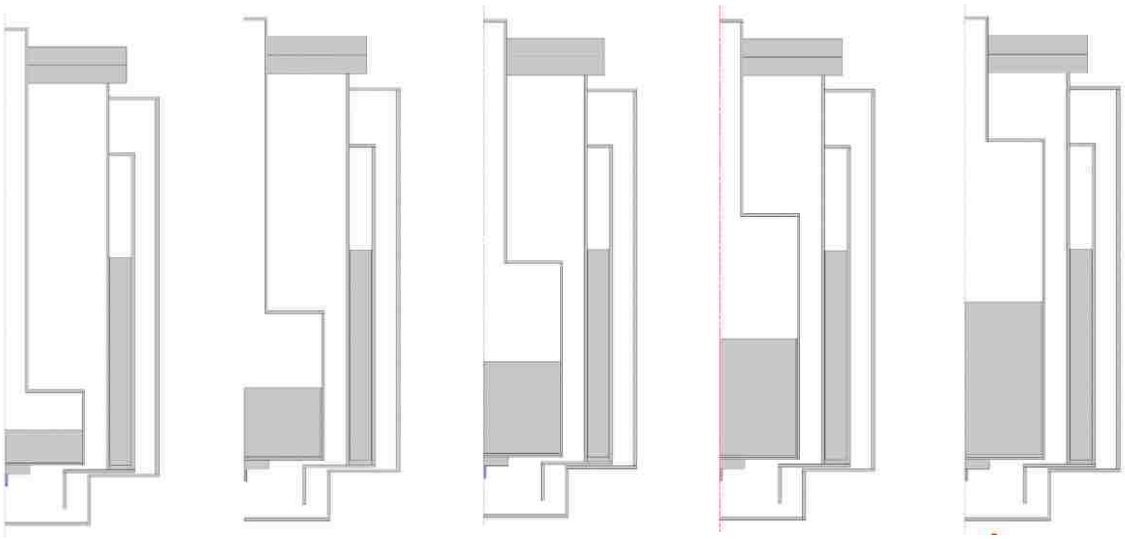

Figure 13:: Design Iterations for Inner Chamber Length (Left to Right: L=r, 2r, 2.5r, 3r, 4r)

The relative performance of each design iteration is observed by comparing the consumption rate at 15 minutes (Start of quasi steady state, converted to per hour) vs. the capacity of the inner chamber.

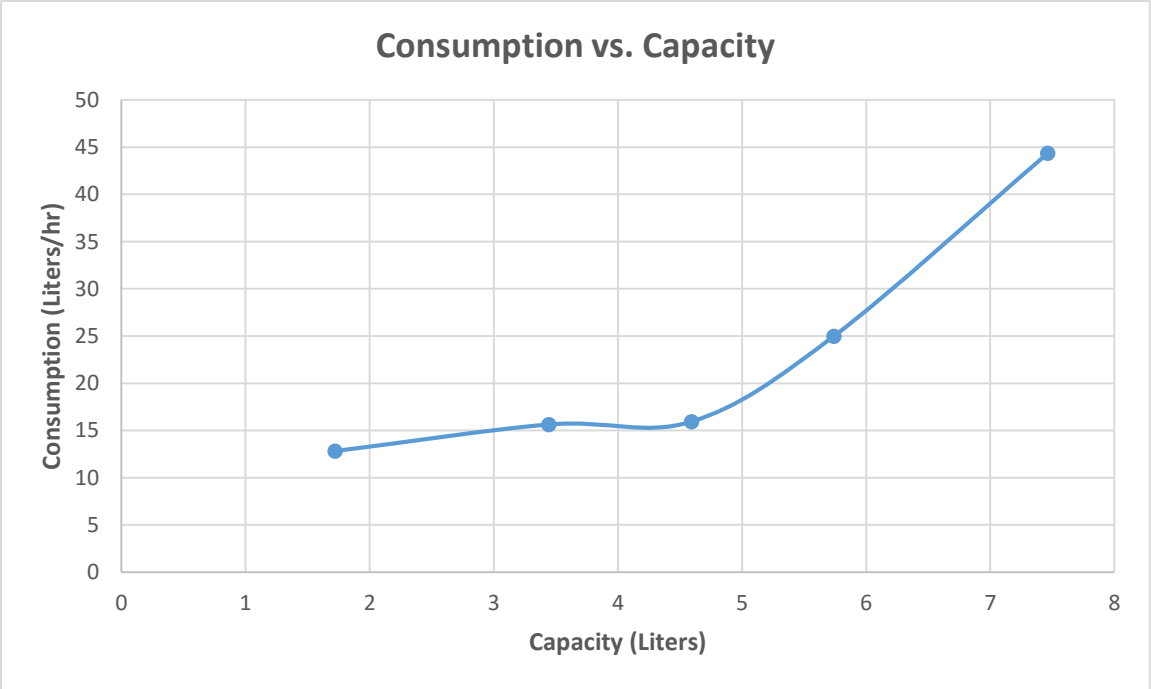

Figure 14: Consumption vs Capacity for Cryostat Design Iterations

Another more useful graph is plotted from figure 14 by dividing the capacity by its corresponding consumption and the result is presented as figure 15, which clearly shows iteration 3 with L=2.5r and capacity around 4.6 liters to be the optimal design.

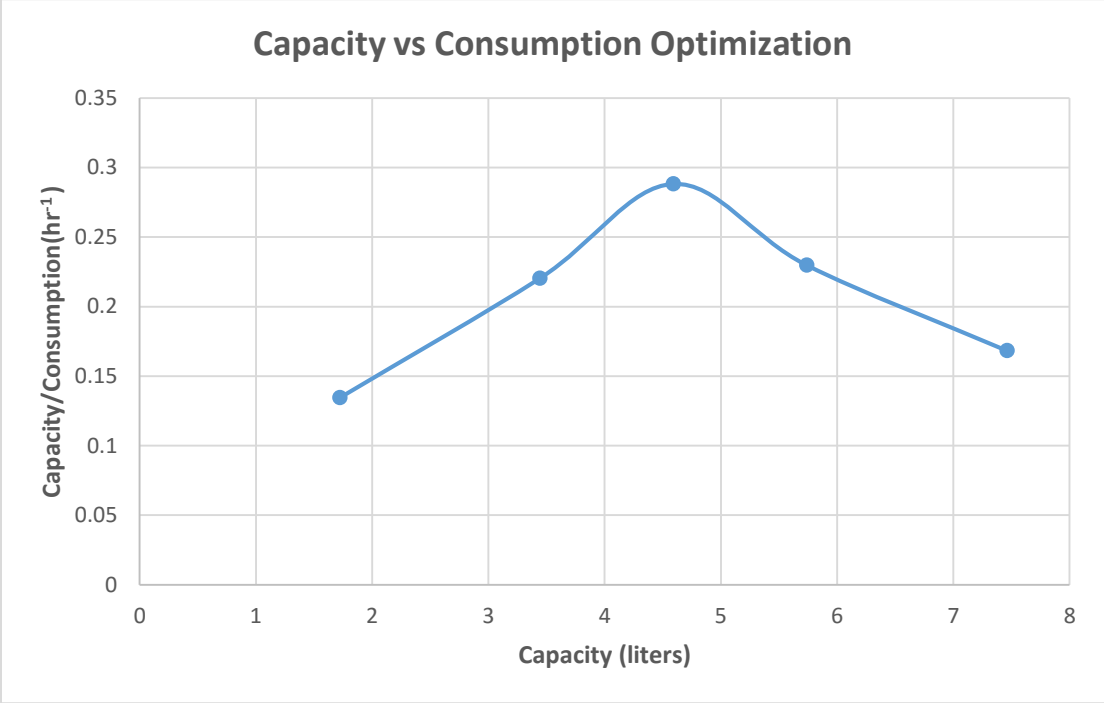

Figure 15: Comparison of Design Iterations for Optimal Inner Chamber Length

The steady state simulation shows very little difference in consumption rates after an infinite amount of time for different iterations. The instantaneous consumption rate at 15 minutes was taken as a relative measure for performance for ease of calculation. The instantaneous consumption rate varies in a similar fashion to the flux or the power drawn out from the walls and bottom of the inner chamber. So instead of going through lengthy calculations for determining the total liquid consumed by 15 minutes, their behavior at 15 minutes is taken as a representation of the volume consumed before it. Figure 16 shows the decay of the spontaneous power drawn from the inner chamber over time.

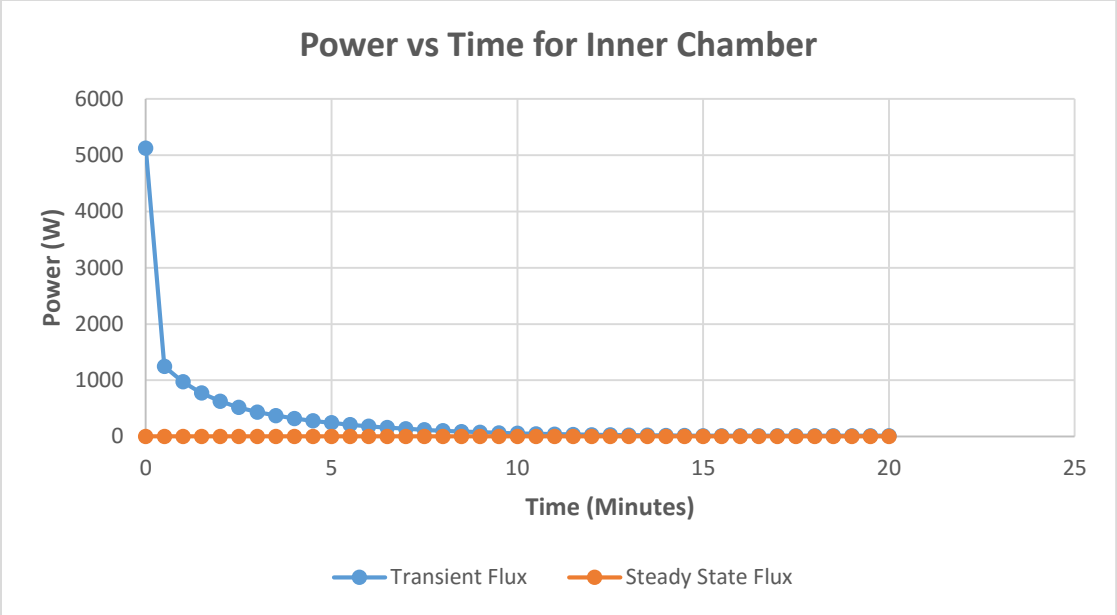

Figure 16: Instantaneous Power from the Walls and Bottom of the Inner Chamber for the Optimized model- Case 1

At this point in the optimization process any changes to the outer chamber will affect the performance of the inner chamber as well. The results from the default length for the outer chamber are analyzed are found to be within acceptable bounds. So they are accepted without any changes and the consumption rate is calculated for the same 15-minute interval. Figure 17 shows the exponential decay of the power from the outer chamber. As the cryogenic liquid in both of these chambers is liquid nitrogen at this point so their heat absorbing capacity per time looks almost exactly the same. Although the actual area and the capacity for both these chambers varies and so does the actual heat that they take away. This response would be drastically different when the cryogenic liquid in the inner chamber changes to liquid helium which has a much higher potential to take away heat mostly due to the huge difference between their boiling points.

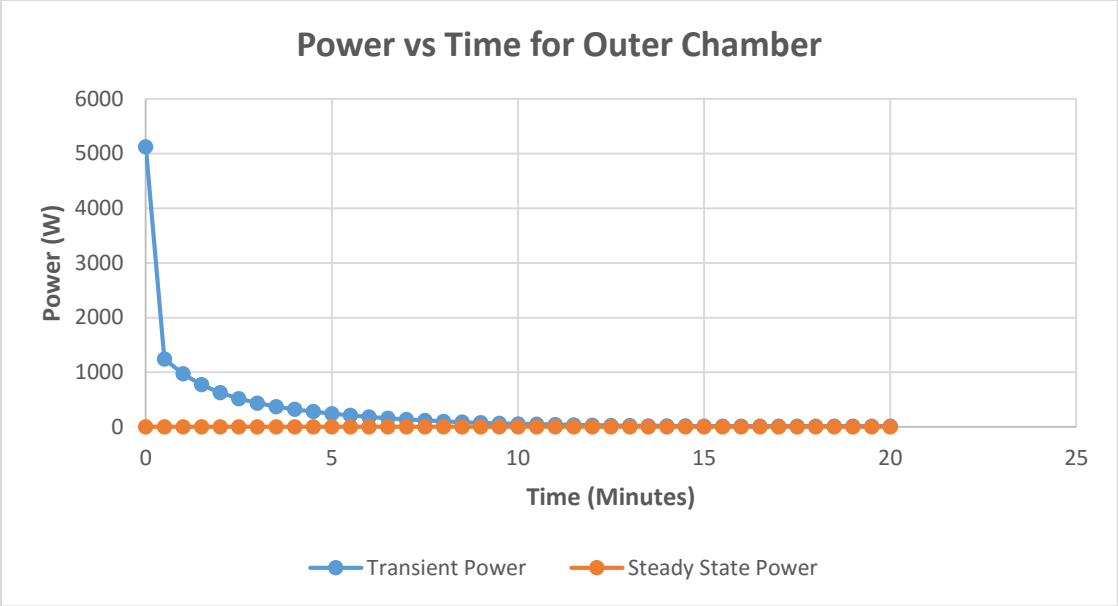

Figure 17: Instantaneous Power from the Walls and Bottom of the Outer Chamber for the Optimized model – Case 1

The final capacities are 4.6 and 6.5 liters for the inner and outer chamber with a consumption rate of 4.5 liters and 5 liters per 15-minute period respectively. They also have a steady state consumption rate of 250 ml and 70ml per hour respectively.

TEMPERATURE VS TIME

Cool down time is another important factor in the final design selection. The temperature vs time curves for the inner chamber (Temperature taken at the location of test specimen) and the outer chamber (Temperature taken at the base of the outer chamber) are shown in figures 18 and 19 respectively. The inner chamber reaches a temperature of 85 K (90% of target) and 77 K within 15 and 20 minutes of start of operation respectively. The outer chamber reaches 85 K within 7.5 minutes but it is expected to reach 77K around the same time as the inner chamber.

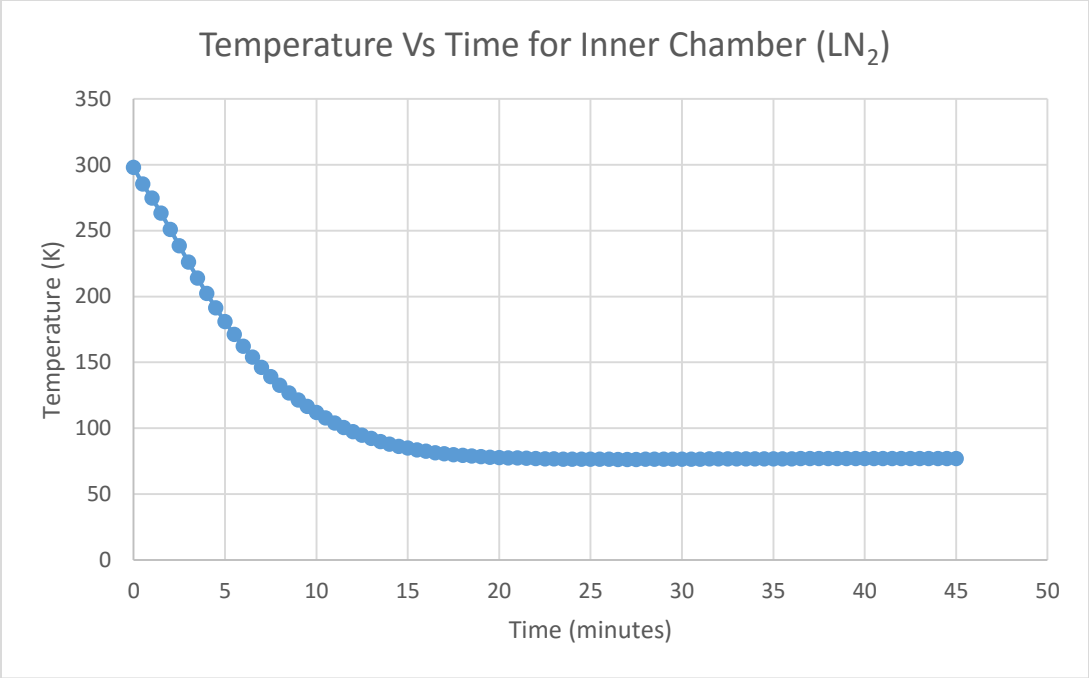

Figure 18:Temperature vs Time for Inner Chamber – Case 1

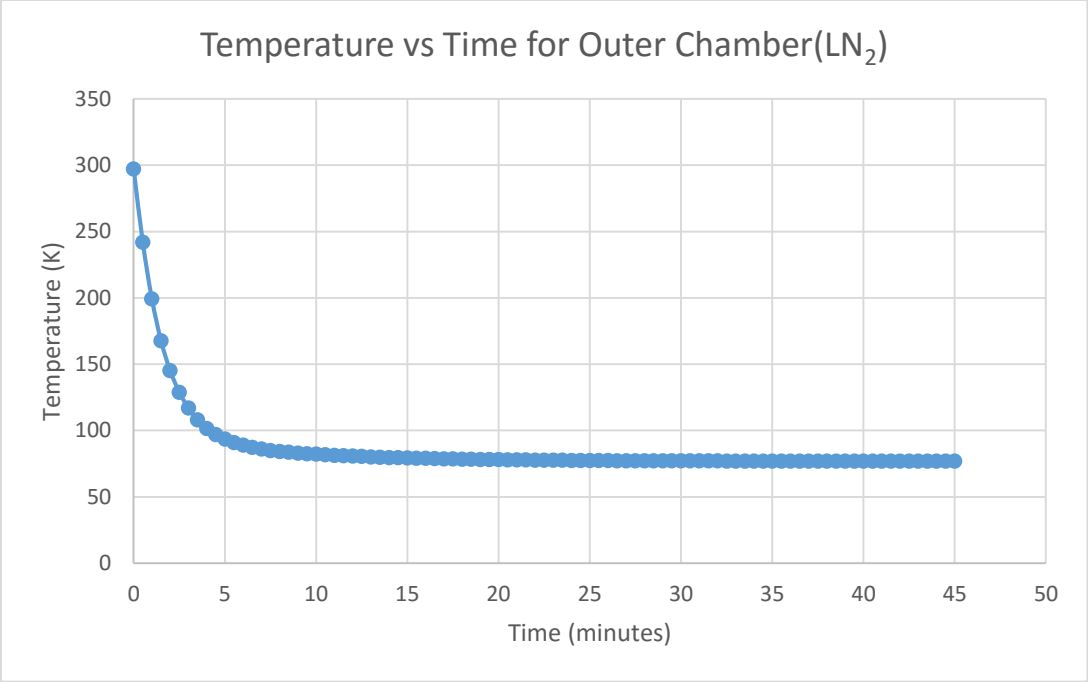

Figure 19: Temperature vs Time for Outer Chamber – Case 1

Although, reaching exactly 77 K is not possible as it requires an infinite amount of time so a realistic goal is to achieve at least 90% of the goal which is around 85 K. These results

were obtained through the transient analysis and a steady state analysis yields interesting information about the temperature of different parts of the cryostat at an infinite amount of time. The steady state results for the optimized model are shown in figure 20.

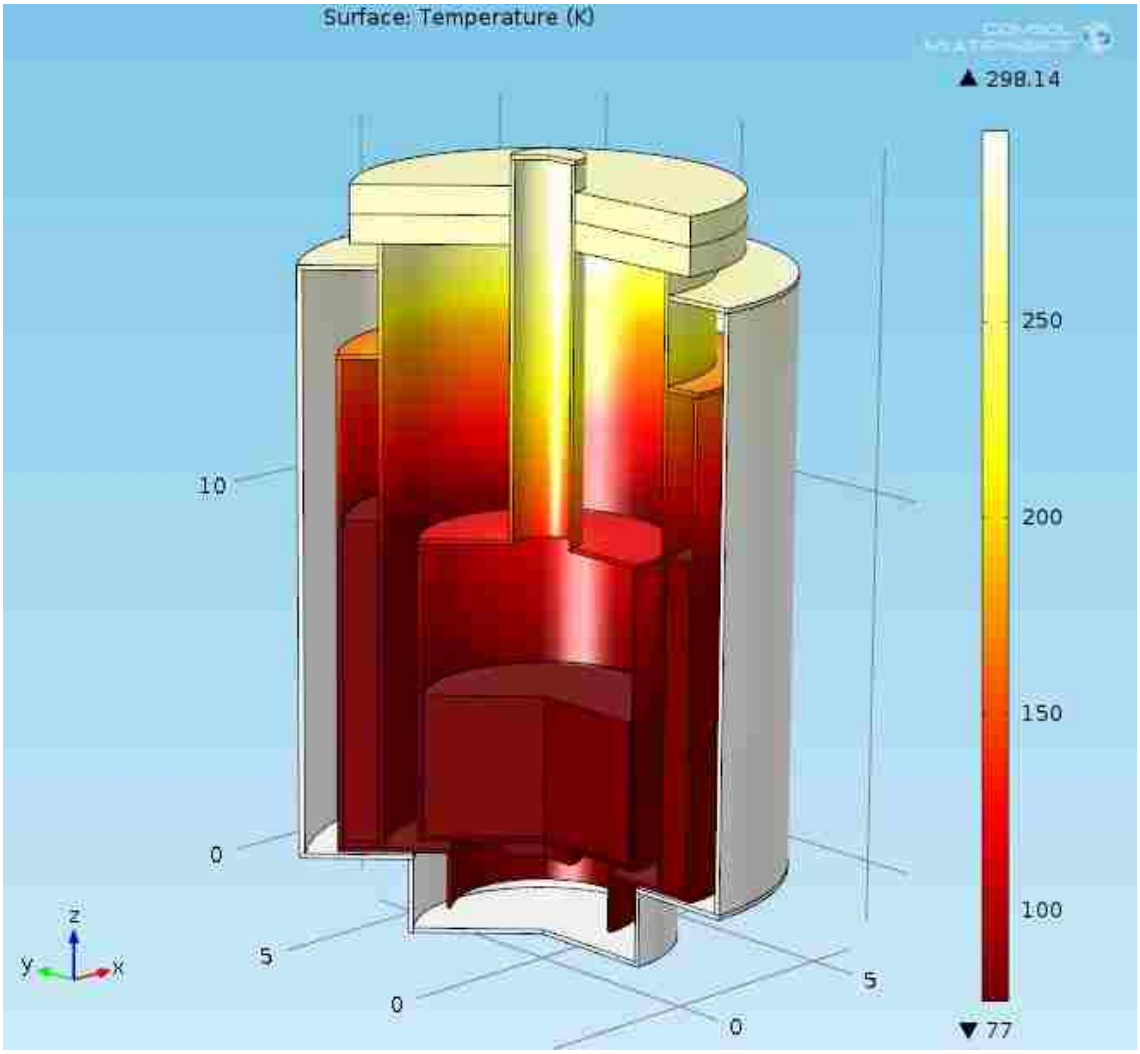

Figure 20: A steady State Analysis Showing the Temperature of Cryostat for Case-1

2.6.2 CASE 2: OPERATION FROM 77 K to 4.5 K

The second phase of operation begins after the inner and outer chambers reach their steady state temperatures. The liquid nitrogen in the outer chamber is left untouched so the chamber is completely assumed to be at 77K. By this time the inner chamber has also attained a uniform temperature of 77K. The temperature of the outer jacket and parts

directly in contact with the atmosphere are largely at room temperature. Afterwards the liquid nitrogen is removed from the inner chamber through a suction pump. This is done quickly in order to avoid any unnecessary heat gains. The inner cavity is then filled up with liquid helium using a special vacuum insulated tube.

INITIAL CONDITIONS, BOUNDARY CONDITIONS & LOADS

Initial conditions of temperature are placed on various parts of the cryostat based on the results from the steady state simulation of case 1. As shown in figure 21. The same technique is applied to simulate liquid helium boiling as liquid nitrogen in the previous case. The liquid inside the inner chamber is given liquid helium properties, an initial temperature of 4.5 K and a fixed temperature boundary at 99% of the volume. The heat source is still the inward heat flux on the outer surface with h=10 W/inch^2 and $T_{ambient}$ = 300K.

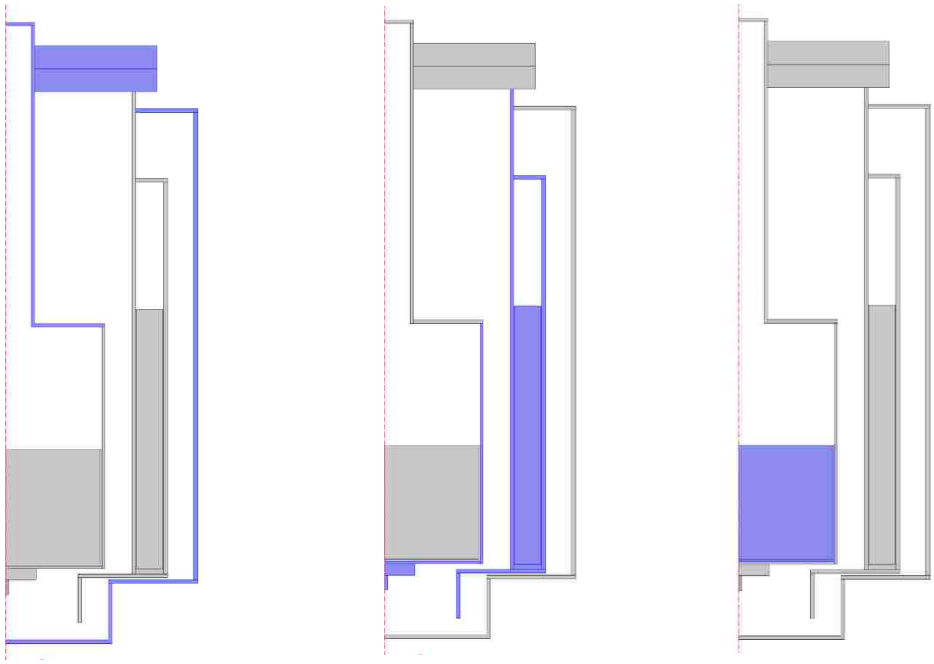

Figure 21: Initial Conditions for Case-2, (Left to Right)

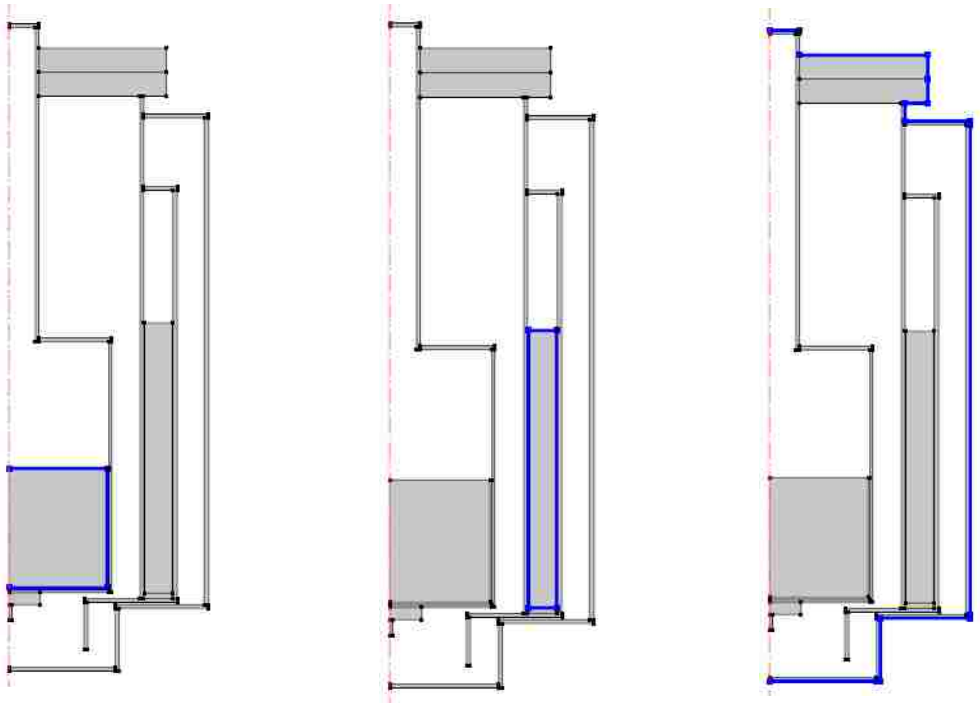

Figure 22: Boundary Conditions for Case-2, (Left to Right) a) Fixed Temperature boundary of 77 K at 99% volume, b) Fixed Temperature boundary of 4.5 K at 99% volume, c) Inward Heat Flux of 10 W/inch2 and Tambient =300K

Case 2 is still using the dimensions carried forward from case 1. The new power drawn from the inner chamber is shown in figure 22.

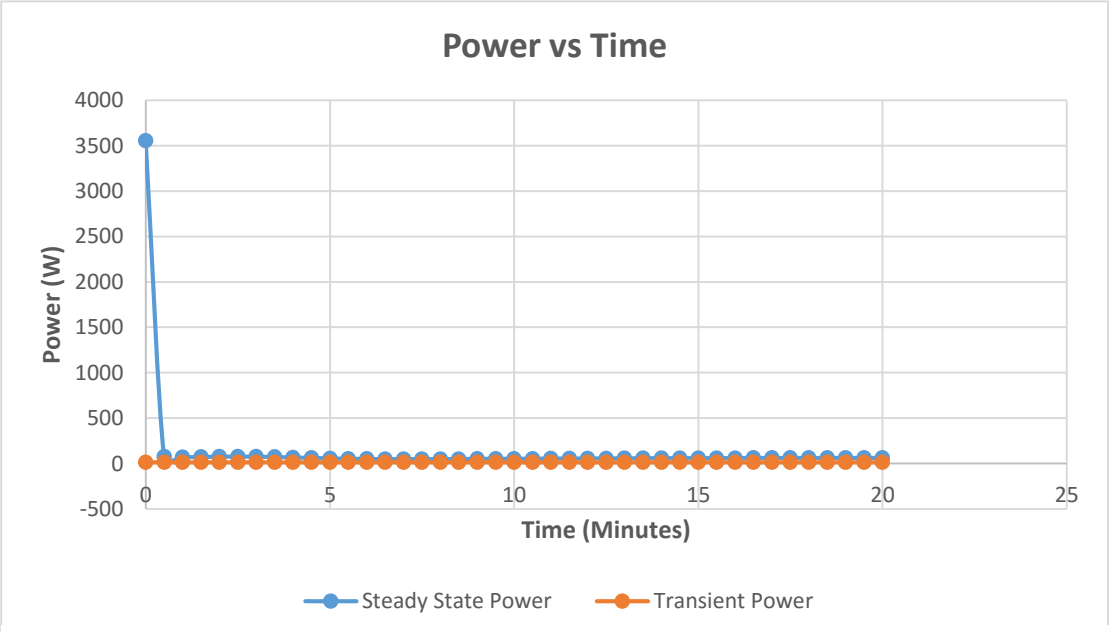

Figure 23: Instantaneous Power from the Inner Chamber for Case-2

So in the first 15 minutes it would have consumed 15 L of liquid helium and its steady state consumption is projected to be 250 mL.

TEMPERATURE VS TIME

The following plot has been made to capture the change in temperature at the test specimen sight over the course of operation.

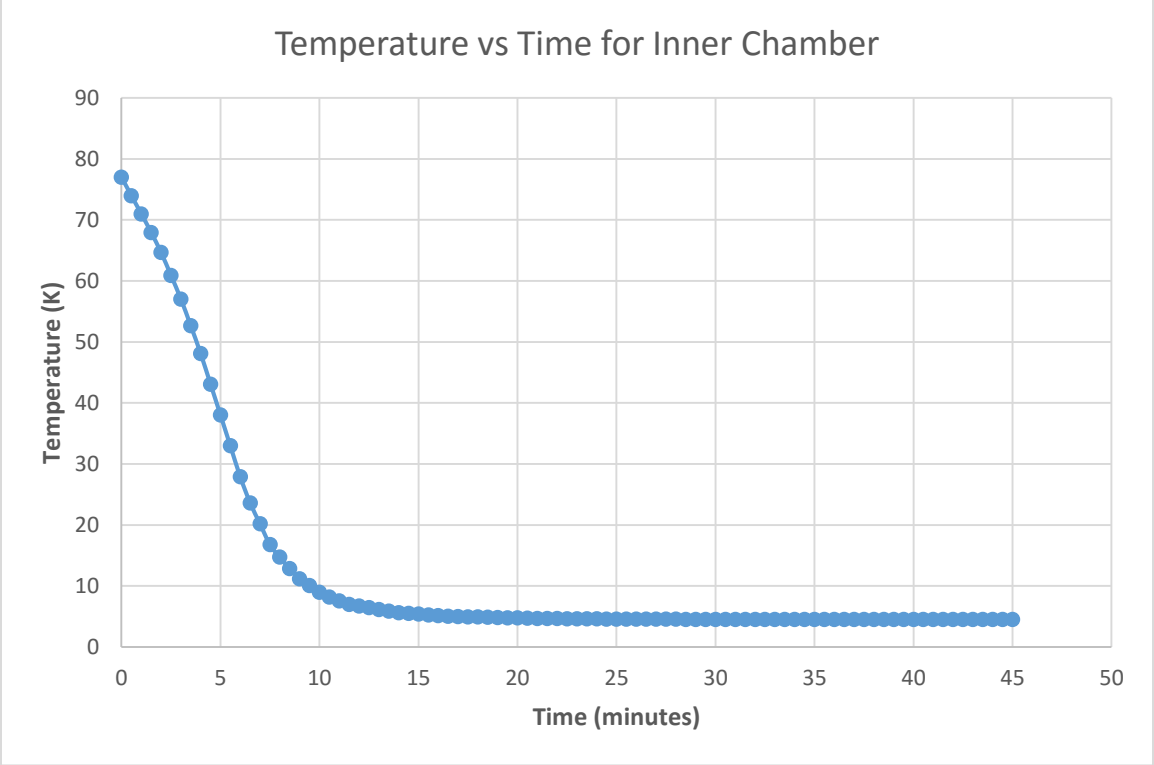

Figure 24: Cool Down Curve for the Inner Chamber, Case-2

So, it reaches 10 K in about at about 12 minutes and starts to settle down around 4 K after about 20 minutes. The temperature of the outer chamber is assumed to remain constant at 77K. Similar to case 1, figure 24 shows the steady state temperature distribution for case2.

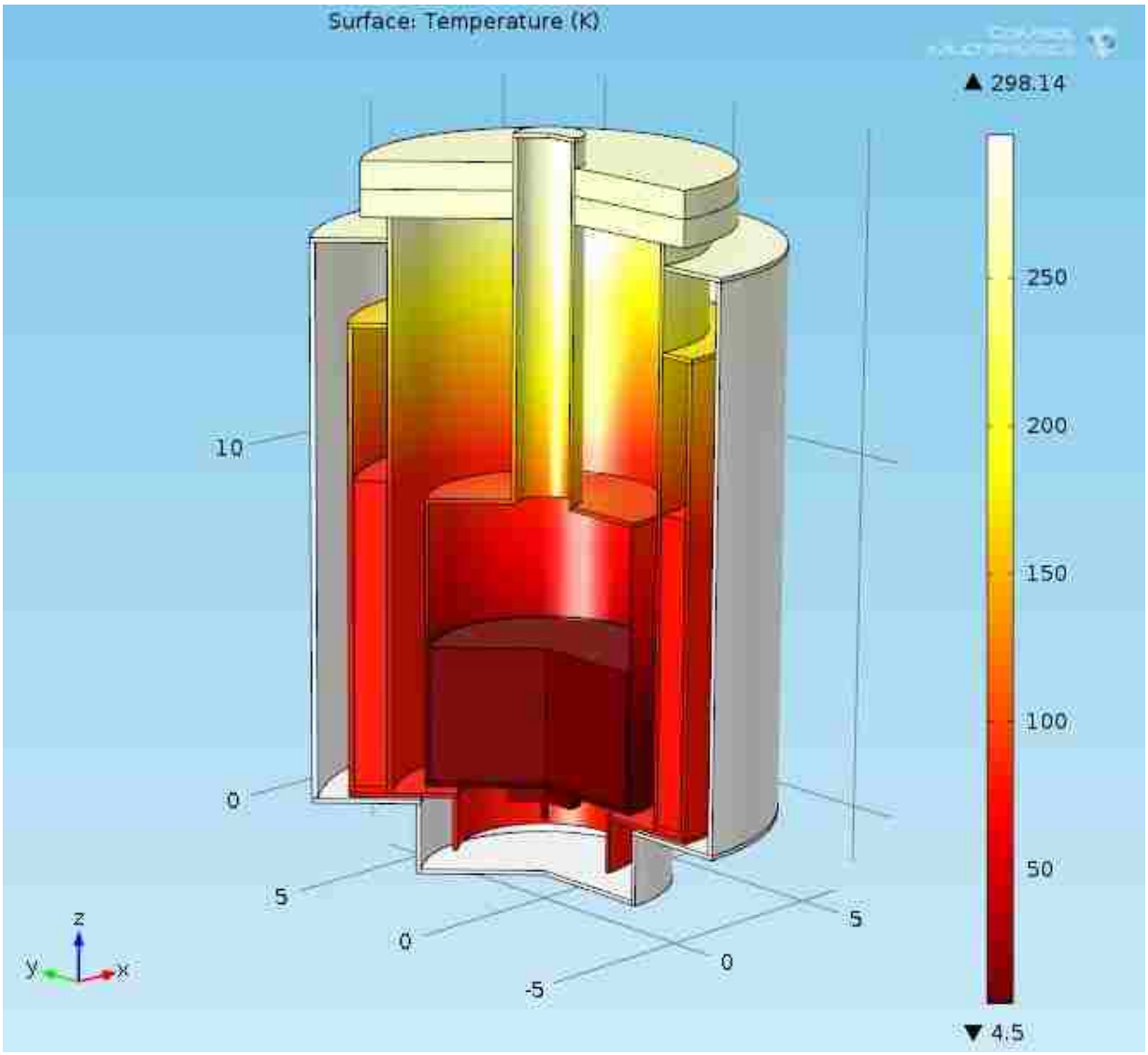

Figure 25: A steady State Analysis Showing the Temperature of Cryostat for Case-2

This concludes the design optimization process for the cryostat as per the design criteria laid out earlier. The next chapter takes these design recommendations into consideration and focuses on designing the cryostat for manufacturing using a CAD model.

Chapter 3

CRYOSTAT MANUFACTURING

3.1 CAD DESIGN

The cryostat design has finally been optimized and the next step is to set up a CAD model for making engineering drawings and getting the finer details finalized. SolidWorks 2015-2016 is used to set up the model. The CAD model thus setup is shown in figure 25.

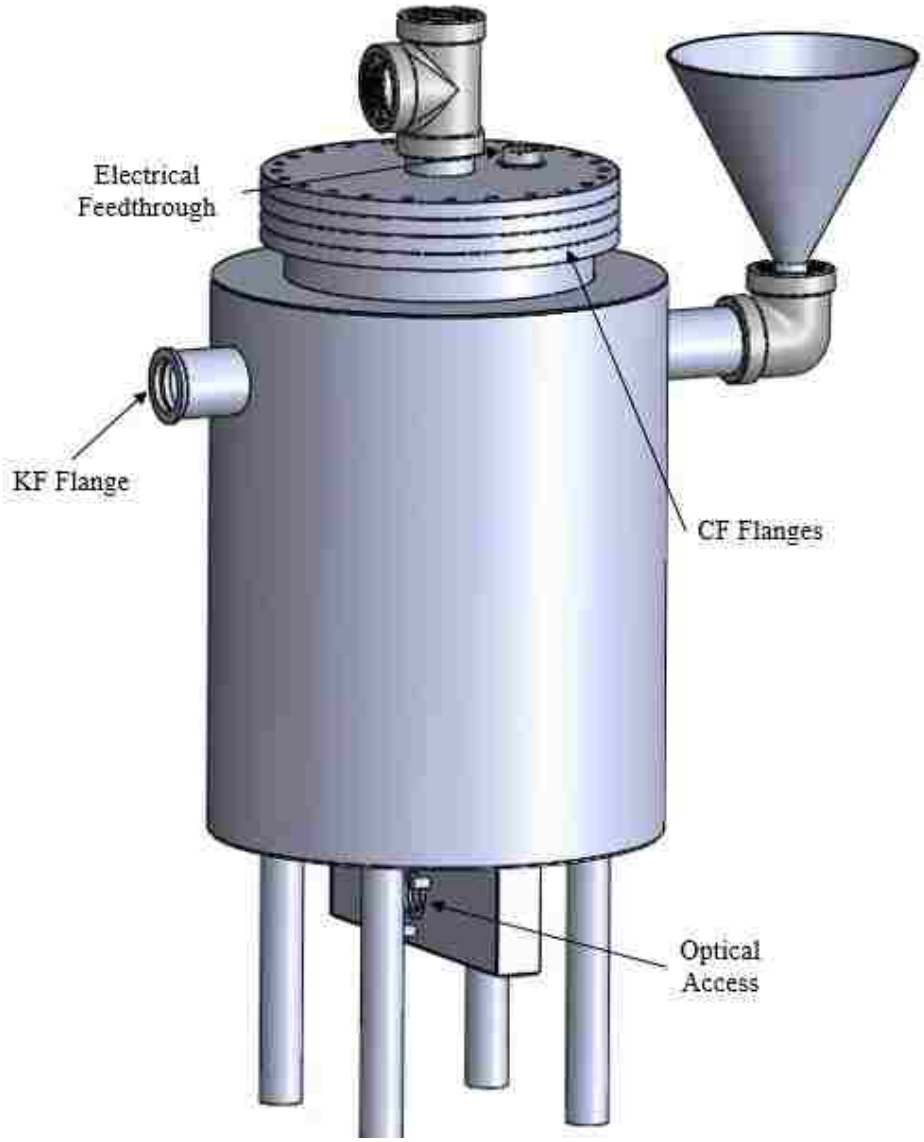

Figure 26: Cross Sectional View of Cryostat

More Importantly, the cross sectional view of the cryostat showing its different parts is shown in figure 26.

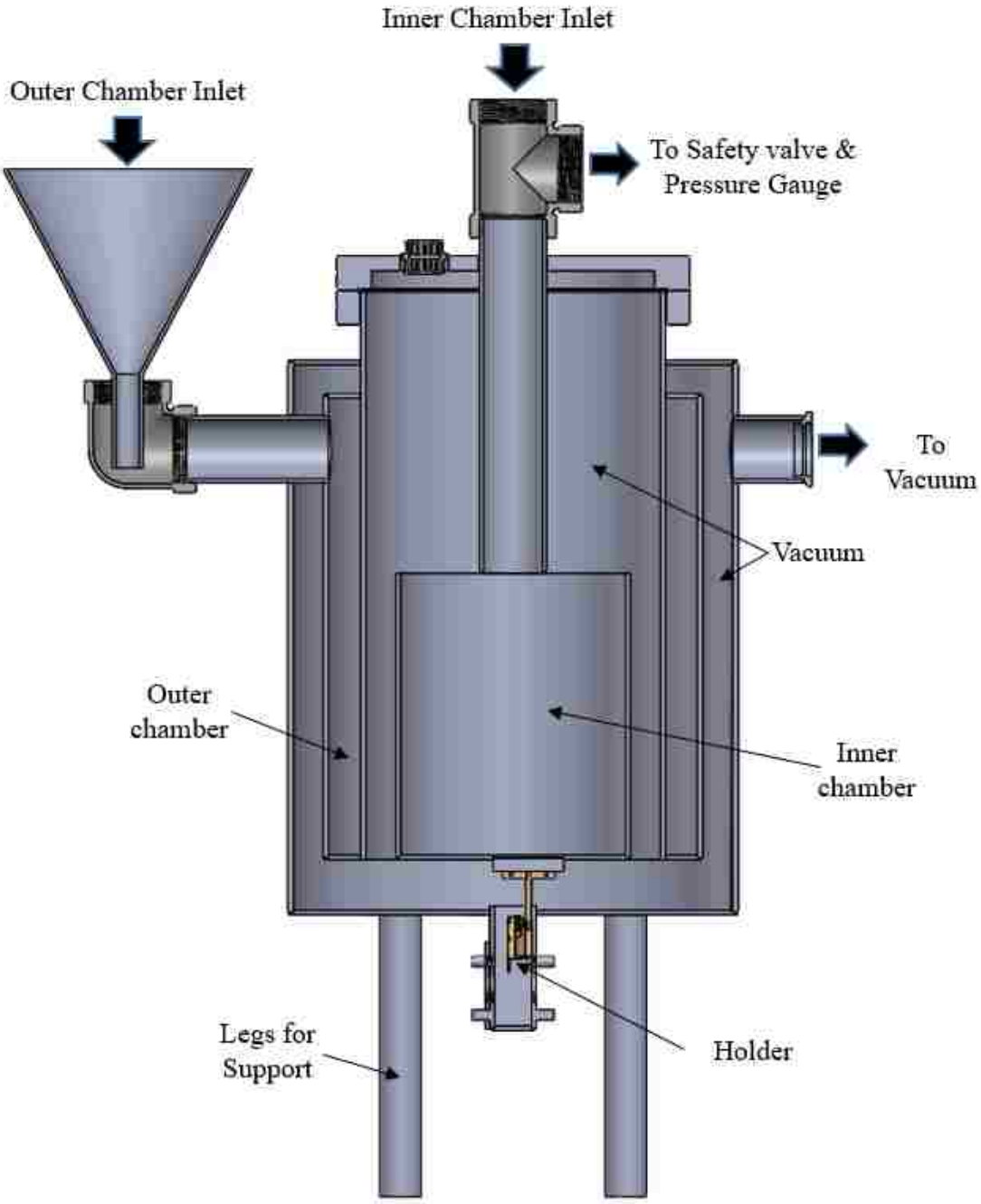

Figure 27: Cross Sectional View of Cryostat

CF FLANGES

Two CF flanges with a copper gasket are being used in this design to create a seal for vacuum jacket. CF flanges have a knife edge which bites into the malleable copper gasket, making an excellent vacuum seal. The two separable sections of the cryostat along with the CF flanges and the copper gasket are show in figure 27.

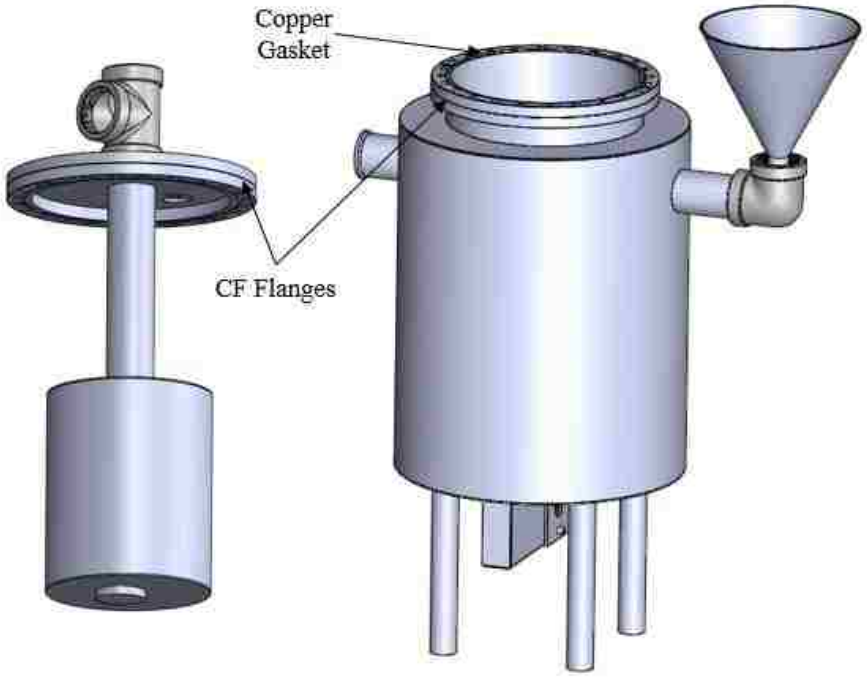

Figure 28: Separable Parts for the Cryostat

KF FLANGE

A standard KF 50 flange is used in this design to make a easily removable connection between the vacuum jacket and the vacuum pump.

ELECTRICAL FEEDTHROUGH

To enable electrical connectivity with the test specimen a vacuum grade 32 pin connector is used. These pins have been plated with Gold to prevent any out gassing.

OPTICAL ACCESS

Optical access is one of the most important requirements for a successful cryostat design. It is also one of the biggest challenges because of close packing space for the holder and it being surrounded by walls directly in contact with the environment.

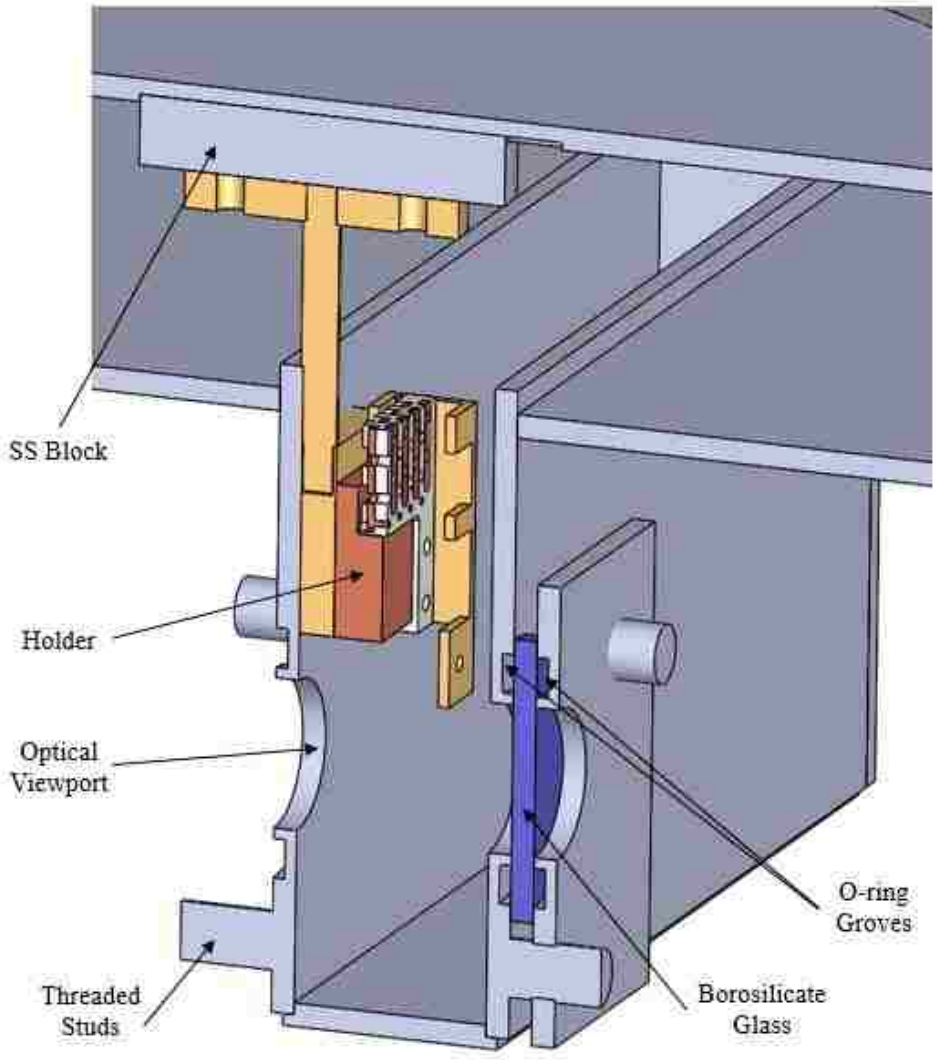

Figure 29: Optical Access for Cryostat

3.2 MANUFACTURING

Detailed engineering drawings are obtained from the CAD model for manufacturing the cryostat. These drawings can be found in Appendix A. Figure 29 shows the actual cryostat after being built.

Figure 30: Actual Cryostat

Figures 30 and 31 show the 32-pin connectors used as electrical feedthroughs and the copper gasket used to form the seal for the CF flange respectively.

Figure 31: (Top) 32 Pin Connectors for Electrical Feedthrough

(bottom) Copper Gasket for CF Flange

Lastly pressure relief valves have been added for safety if the pressures were to build up in the inner and outer chambers. A regulatory value of 150 psi has been used for the valves.

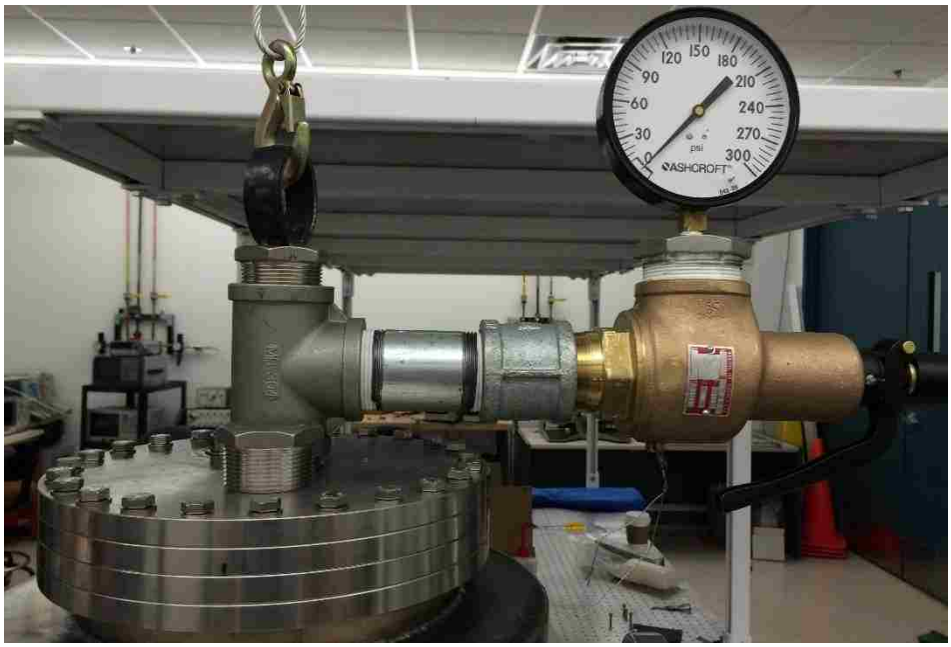

Figure 32: Relief Valves (150 psi) added to the Inner and Outer Chamber Inlets

Chapter 4

EXPERIMETAL SETUP & TESTING

4.1 EXPERIMENTAL SETUP

A copper arm such as shown in figure 33 is pressed down against the bottom of the inner chamber with screws. A Silicon diode temperature sensor is installed at the end of this arm to measure the temperature over time. The diode is connected to a current source and a voltmeter through the electrical feedthrough as shown in figure 34. A steady current of 10 μm is given to the diode and the voltage is read through the voltmeter. Based on a calibration curve provided by the manufacturer [13], the voltage is translated into temperature and plotted against time and presented as figure 35. All the time a pressure of 10 mtorr is maintained through a turbo pump connected to the vacuum jacket.

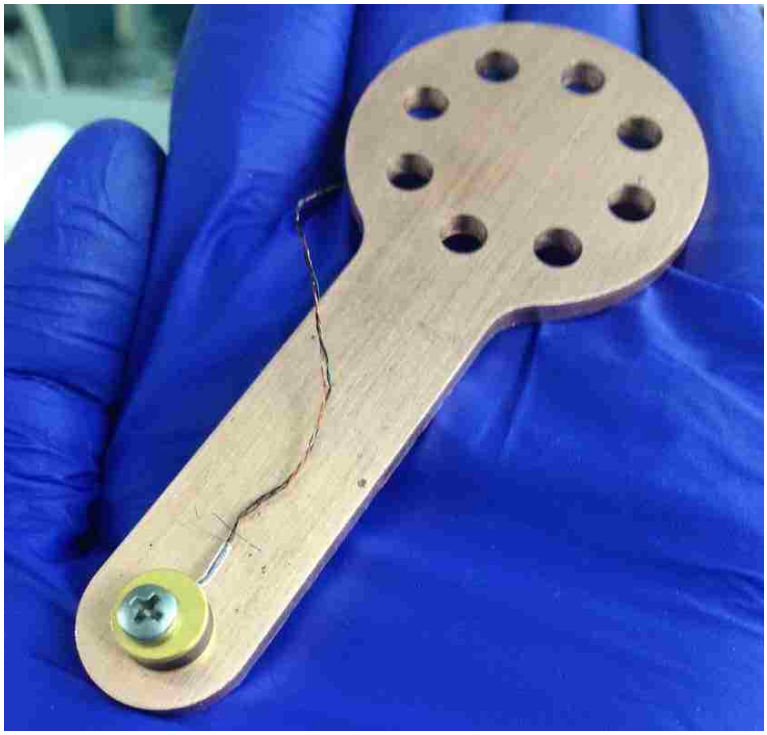

Figure 33: Copper Arm with Silicon Diode Temperature Sensor

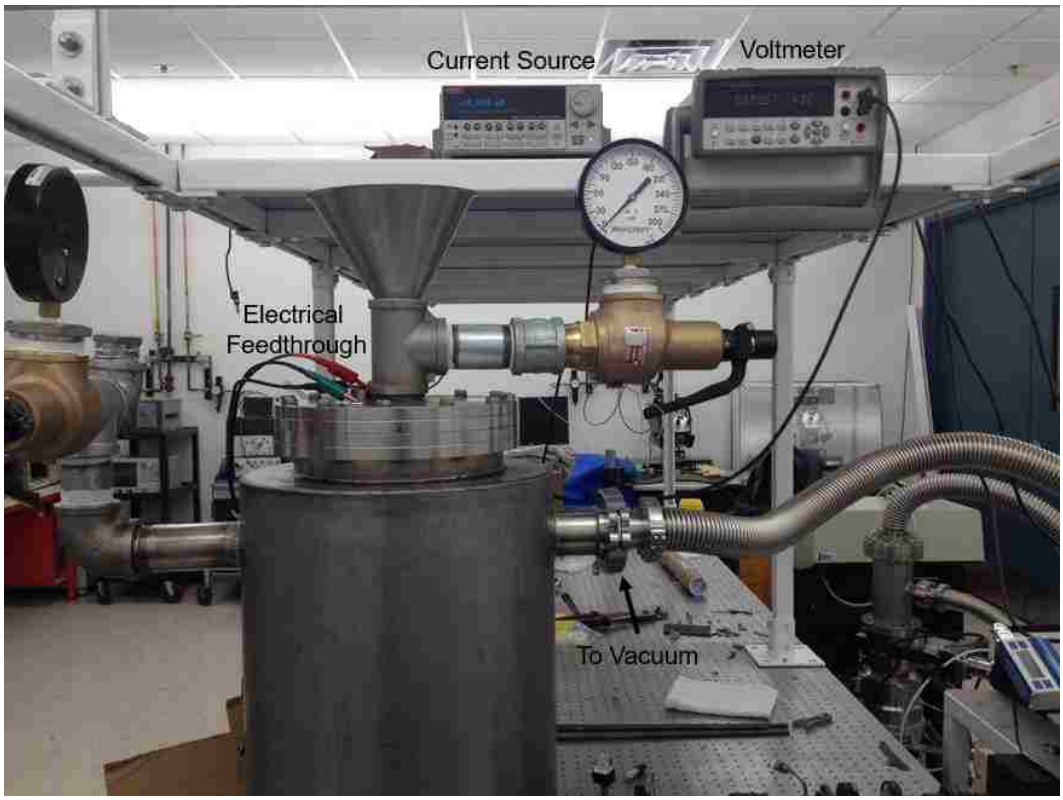

Figure 34: Experimental Setup for Testing of Cryostat

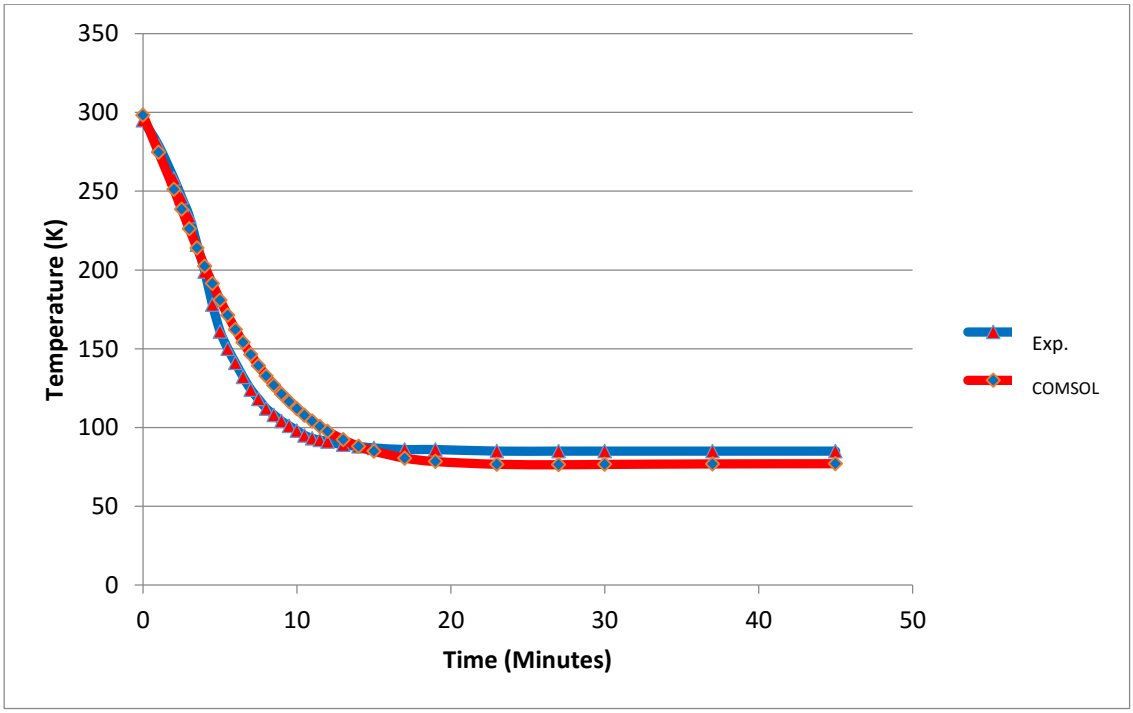

Figure 35: Temperature vs Time for Simulation and Experiment

The simulated curve shown in figure 35 is exactly the same as the COMSOL generated temperature vs time curve shown in figure 18 and contains the experimental curve super imposed on it. As seen in figure 35, the experimental result matches the simulated result almost exactly as predicted with the minimum temperature being 85 K instead of 77 K. This temperature can be further reduced by pulling a better vacuum on the vacuum jacket and also by creating a suction force on the inner chamber inlet. This outward flow of gas takes away the evaporated nitrogen on top on the liquid nitrogen reservoir thus enabling force evaporation. This forces the molecules with energy levels slightly below the evaporation point to be drawn out thus reducing the temperature of the parent liquid further. This experiment was performed by using an ordinary vacuum cleaner at the mouth of the inner chamber which resulted in a decrease of further 1-2 K.

This concludes the cryostat part of the thesis and in the following chapters the sample holder used for actual experimentation on the MEMS devices will be discussed.

Chapter 5

HOLDER DESIGN & ANALYSIS

5.1 INTRODUCTION

The holder is an essential part of the overall cryostat setup. It provides a staging area to mount the sample. It has provisions for varying the sample height with respect to the cryostat viewport and convenient electrical connectors to allow wire bonding to the sample. It also measures the sample temperature in a noninvasive manner, making good use of the high thermal conductivity of oxygen free copper.

5.2 DESIGN CRITERIA

The following design criteria has been established for an optimized holder:

1. It should attain a temperature within 5% of the desired temperature drop i.e. from 300K to 77K (case1) or from 77K to 4.5K (case 2) in under 15 minutes
2. There should be minimum amount of temperature gradient across the test specimen
3. It should be able to heat up a sample from its steady state at 77K (case1) to 300K or at 4.5K (case2) to above 77K in under 15 minutes while using a maximum 10 $W/inch^2$ thin film heater

5.3 HOLDER FINFITE ELEMENT ANALYSIS

The following model has been set up considering the design criteria. The stainless steel block acts as a ‘Thermal Capacitor’ and stores the cooling power coming from the cryogenic liquid in the inner chamber through conduction, before giving it to the sample below. This block plays a major role in the temperature patterns and the time constants of the assembly below it. The next part is the holder base which takes away the heat through

the narrow neck and gives it to the SS block. The neck is made thin and narrow to 'kill' the temperature gradients before they reach the sample stages. One stage is fixed to the neck and the other is removable and the sample is put onto its top surface with silver paste or carbon tape (to promote conductivity). The insulator is placed around the test specimen to provide wire bonding sites to the test specimen for the electrical connections. A window has been provided to enable test specimens with over hangs to be visible to the optical window of the cryostat.

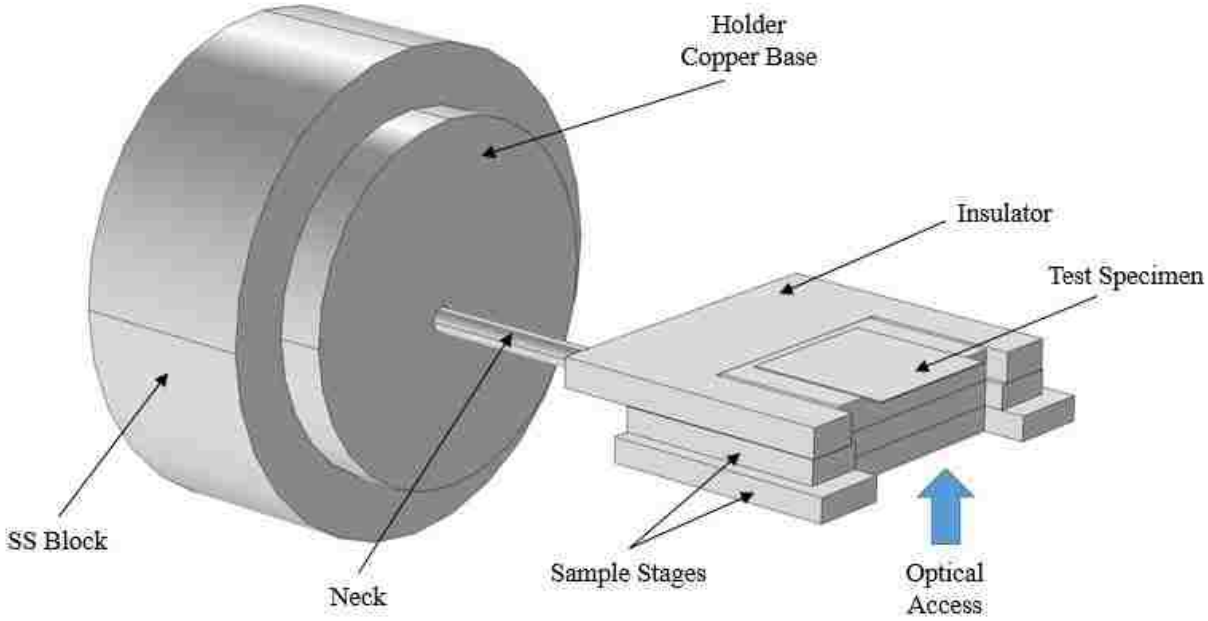

Figure 36: FEA Model for the Holder

MATERIAL PROPERTIES

Similar to the cryostat the temperature varies drastically over time for this holder. Thus thermophysical properties such as the thermal conductivity and specific capacity have to be provided as a function of temperature from 4K to 300K.[9]

As high conductivity is essential for the body of the holder thus Oxygen Free Copper (OFC) has been chosen. It has a very high thermal conductivity and low heat capacity, making it ideal for heat transfer applications. The SS block is of course made up of Stainless Steel 304 and the properties are readily available in the cryostat section. The properties of Teflon, a nonconductive plastic have been given to the insulator part of the holder. The figures below show these materials being assigned to their respective parts in the model.

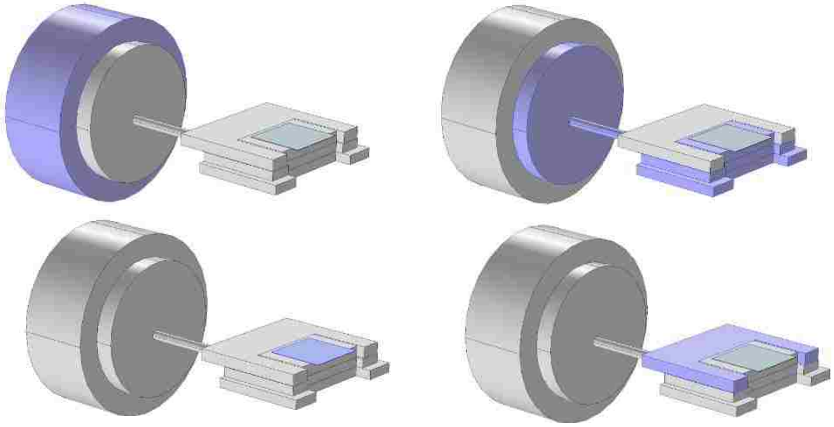

Figure 37: Highlighted Portions show (Clockwise from Top Left) a) SS304, b) OFCu, c) Teflon, d) Si

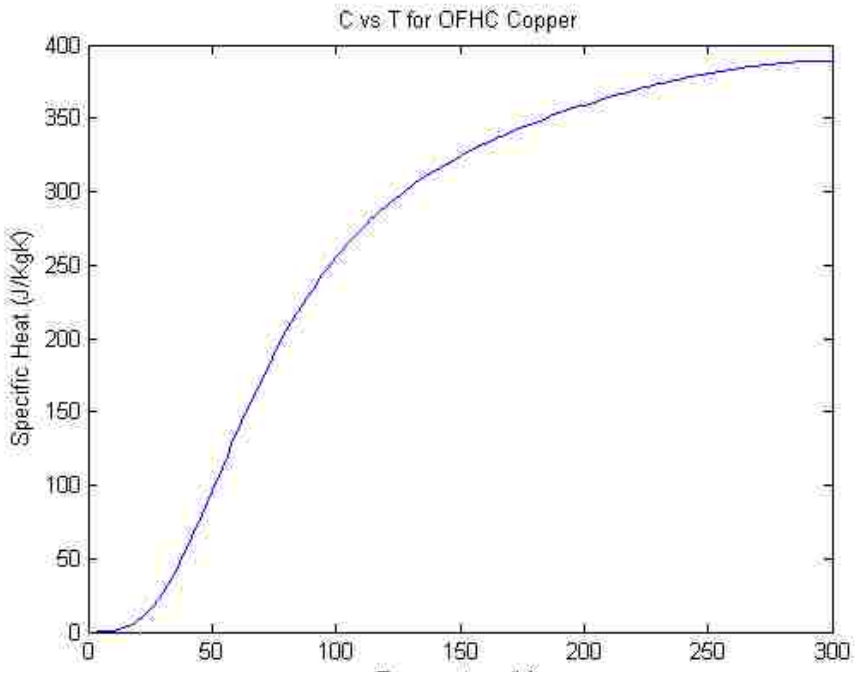

Figure 38: Thermal Heat Capacity vs Temperature for Oxygen Free Copper

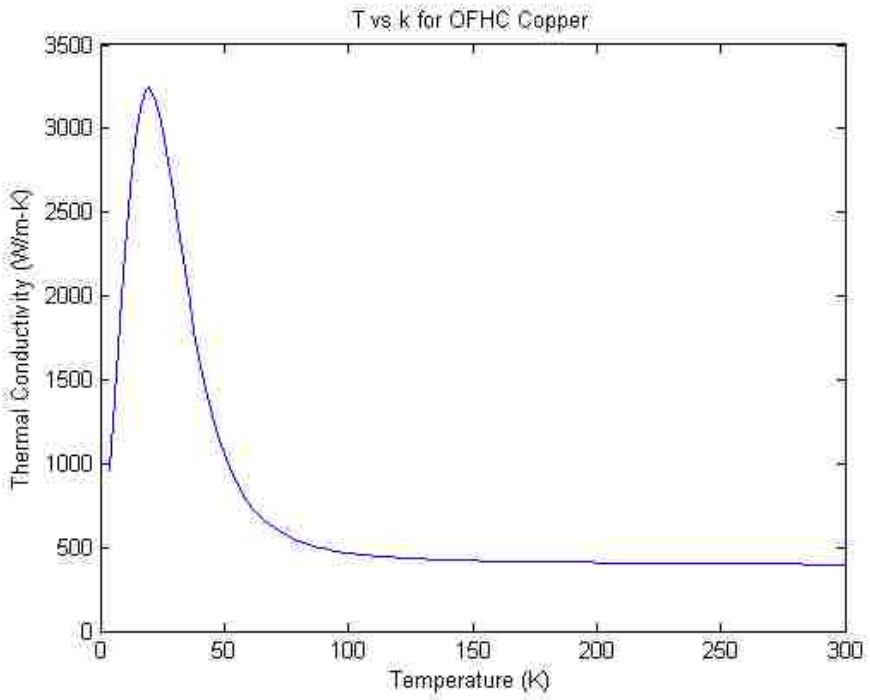

Figure 39: Thermal Conductivity vs Temperature for Oxygen Free Copper

OPTIMIZATION PROCESS

The design criteria demands that the test sample should cool down and heat up within a fixed maximum allowable time. Thus it is important to satisfy both criteria in order. First the design is optimized for cool down test for case-1 and then the design is refined for the heat up test.

CASE-1, COOL DOWN

Case-1 involves cooling down the entire structure from an initial temperature of 300K to a final steady state temperature of 77K. This has to be with 5% of the desired temperature drop which puts the maximum temperature to be at 88K. Thus the following initial and boundary conditions have been set up:

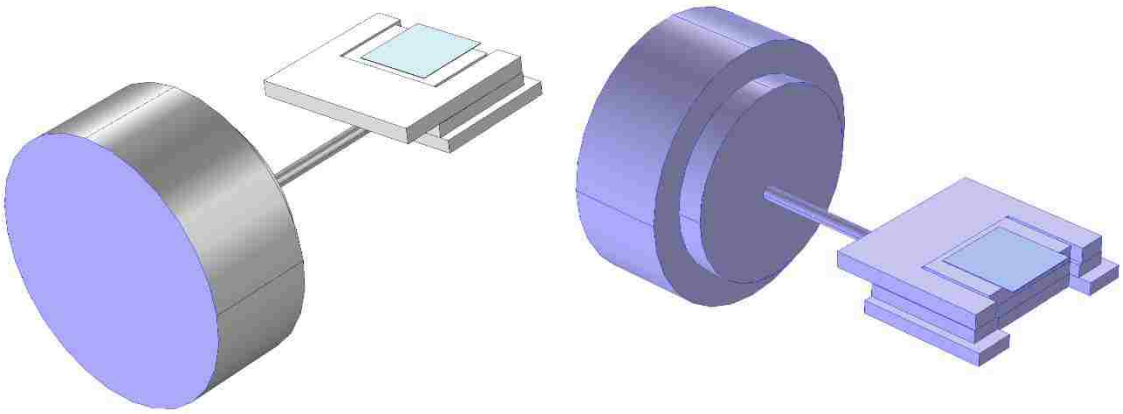

Figure 40: (Left) 77K Boundary Condition (Right) 300K Initial Condition for Cool Down Test, Case 1

The main design variables in this design are the thickness of the SS304 block and the length of the neck. The design kicks off with the block thickness at 0.75” and the neck length at 1.5”. The temperature is measure at the very tip of the sample. The following temperature time curve obtained as a result is shown in figure 41.

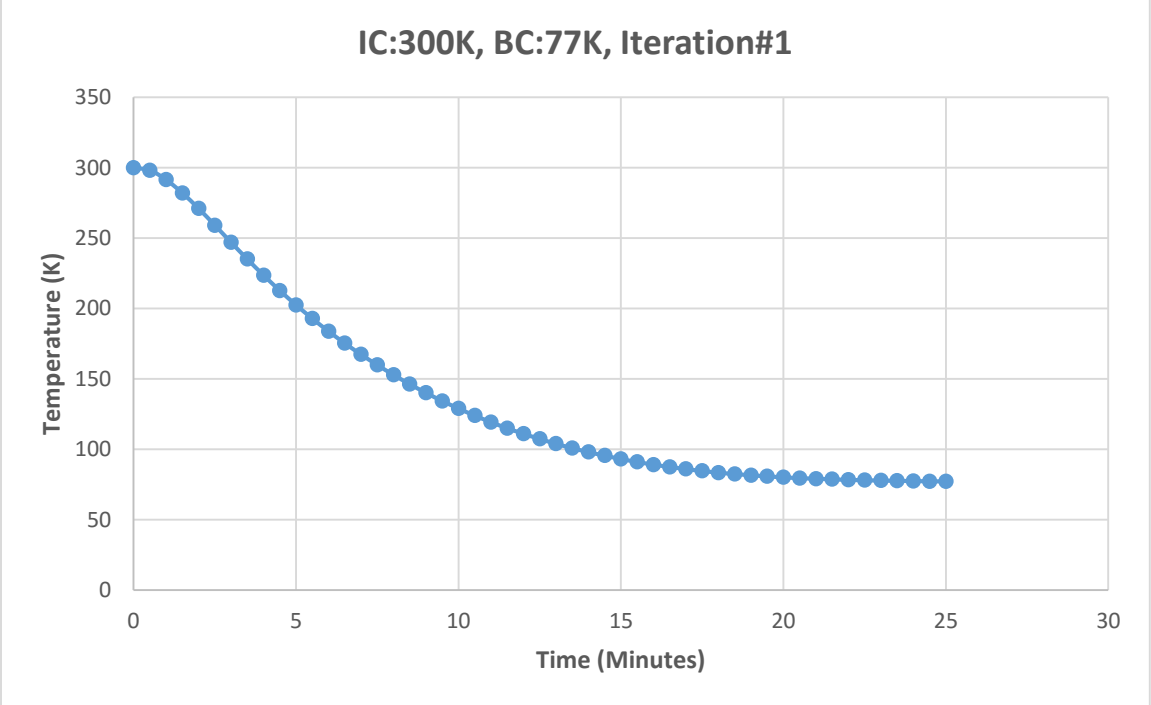

Figure 41: Cool Down Test, Case 1, tBlock=0.75”, LNeck =1.5”

The temperature at 15-minute mark is 93K which is not an acceptable temperature as per the design criteria. At 900 sec (15 min) the temperatures of various regions of the holder are shown in the figure below:

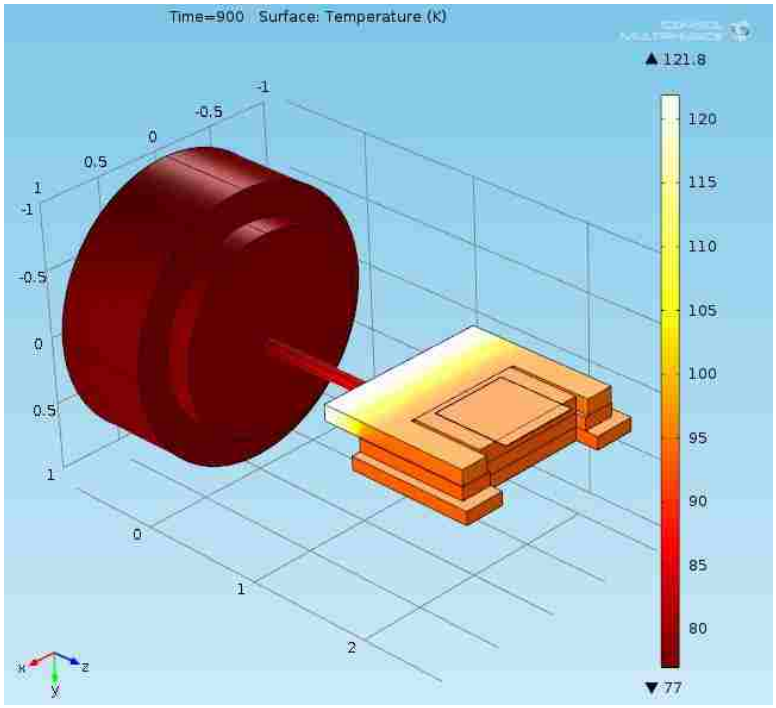

Figure 42: Temperature Distribution at 900 sec, Case 1, tBlock=0.75", LNeck =1.5"

It can be seen in figure 42 that the copper stage area and the holder base is at a uniform temperature. The insulator around the copper stage has not achieved a uniform temperature due to its poor thermal conductivity and low heat capacity. As a result of these two properties, the insulator does not influence the sample.

The long neck seems to be delaying the heat transfer from the sample assembly to the SS304 block. The maximum gradient with regards to the conduction path is along the neck. For iteration#2 the block thickness is kept fixed at 0.75" and the neck length is reduced to 1". The following temperature time curve obtained as a result is shown in figure 43.

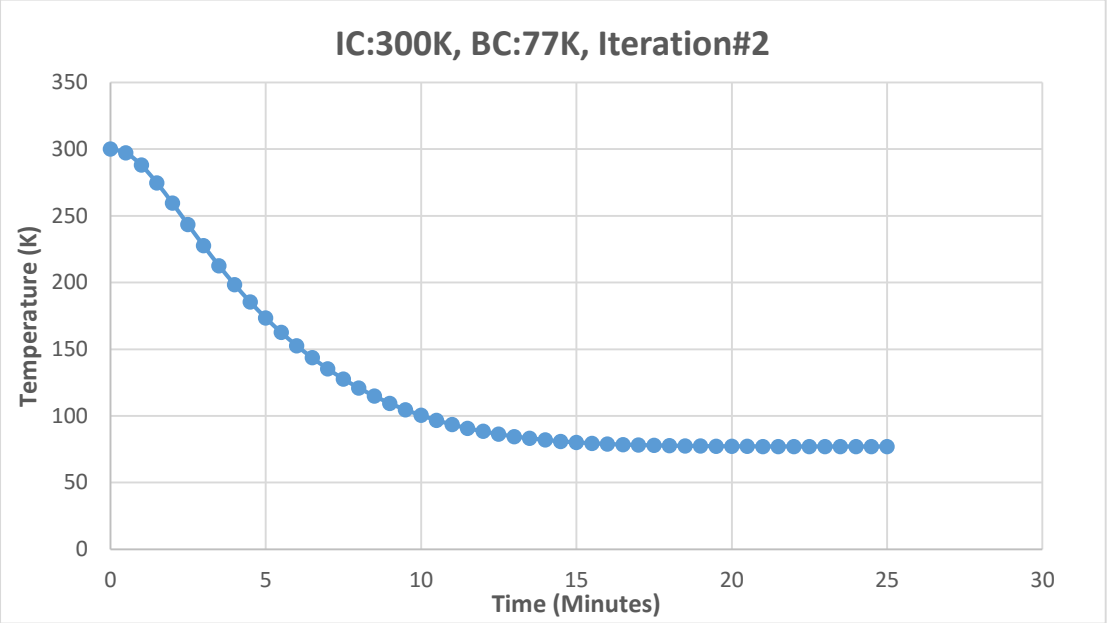

Figure 44: Cool Down Test, Case 1, tBlock=0.75", LNeck =1"

The graph indicates that at 15 minutes the temperature is 80K which is within acceptable bounds. The new temperature distribution is shown in figure 44.

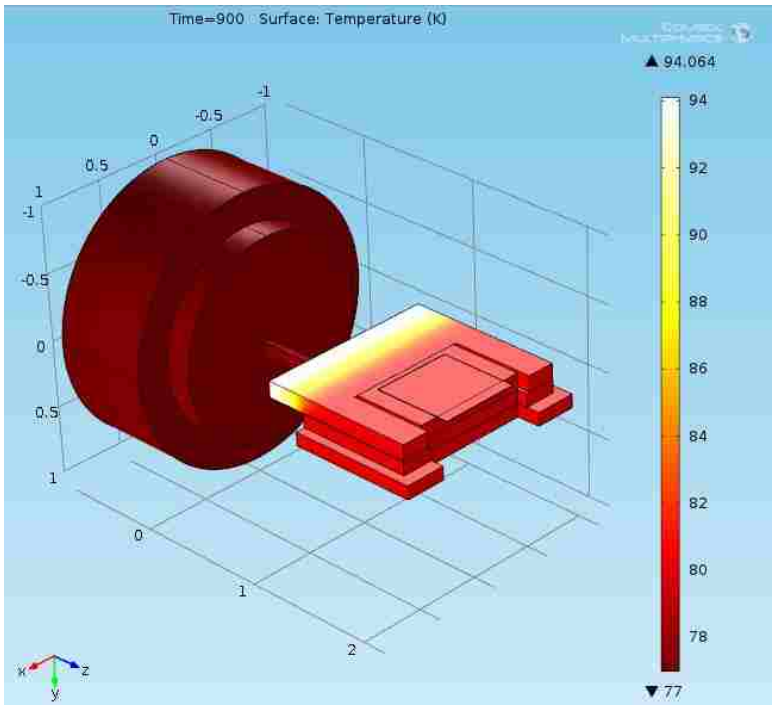

Figure 43: Temperature Distribution at 900 sec, Case 1, tBlock=0.75", LNeck =1"

The design passed the cool down test and if forwarded to the heat up test for case 1.

CASE-1, HEAT UP

The next step is to heat up the sample from the steady state temperature of 77K to 300K in under 15 minutes using a 10W/inch^2 heater. The heater is to be placed on the back of the sample stage. The stage is made up of highly conductive copper, so it should transmit the flux in a very short amount of time. So by the time the flux reaches the test specimen, it is able to heat up the stage uniformly. The following initial and boundary conditions have been applied to simulate this scenario:

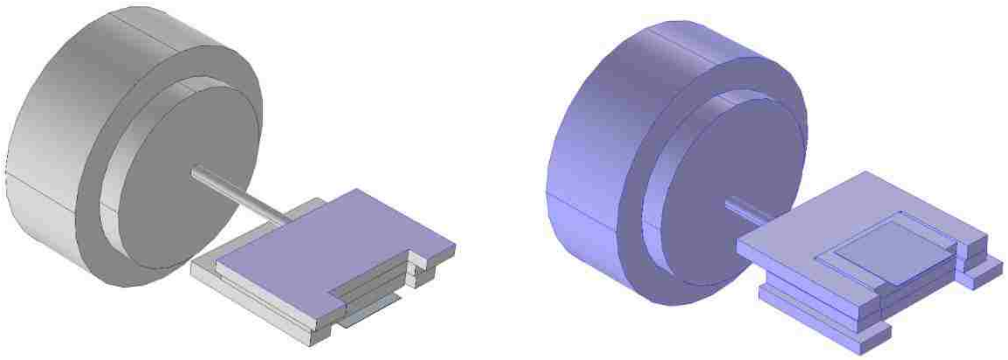

Figure 45: (Left) 10 W/inch2 Boundary Condition (Right) 77K Initial Condition for Heat Up Test, Case 1

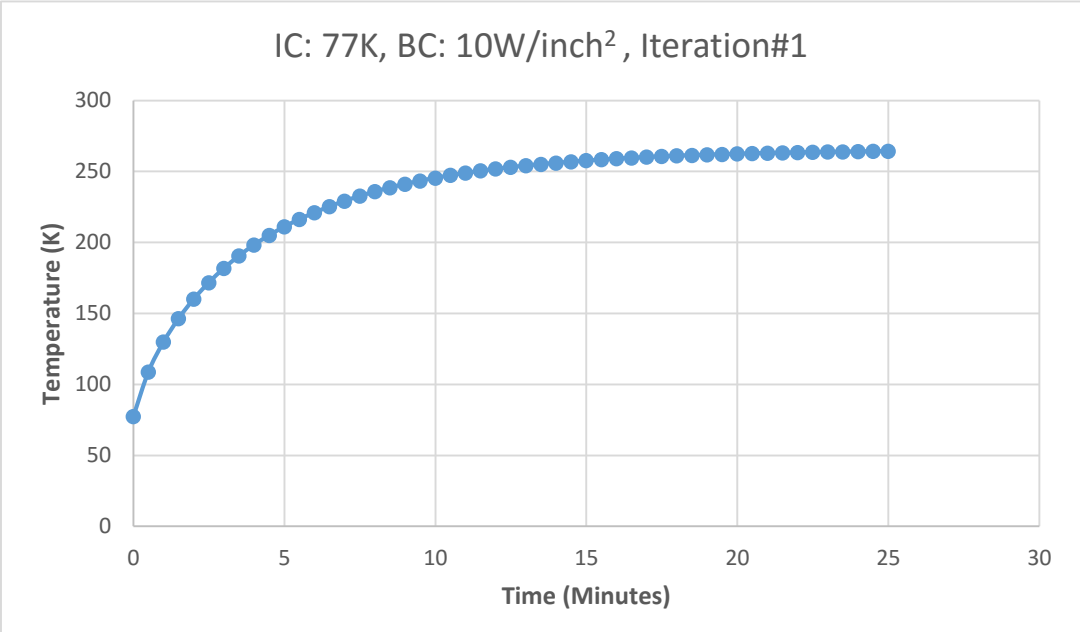

Figure 46: Heat Up Test, Case 1, tBlock=0.75", LNeck =1"

At the 15 min mark the temperature is 257K, far from the desired temperature of 300K. The corresponding temperature distribution is shown in figure 47.

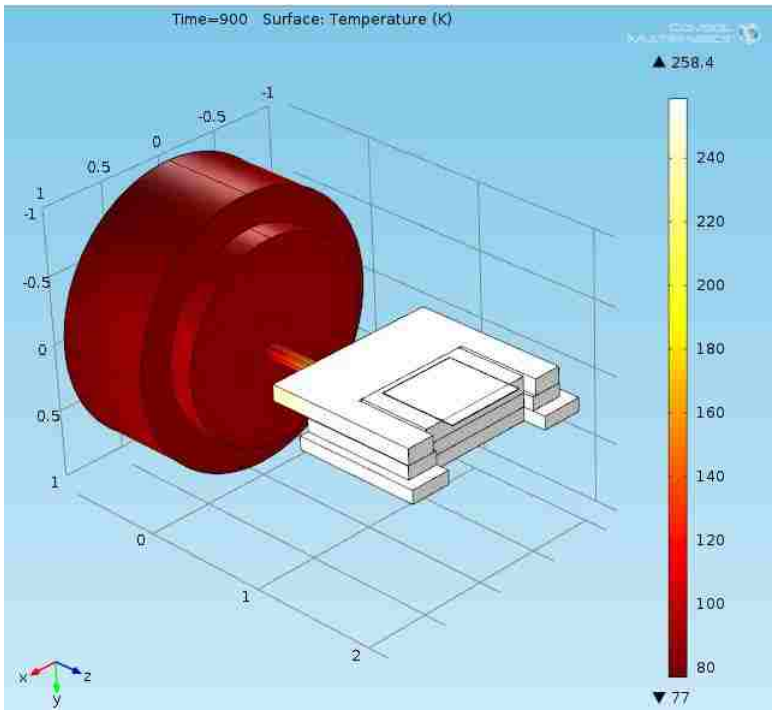

Figure 47: Temperature Distribution, Heat Up Test, Case 1, tBlock=0.75", LNeck =1"

The length is too short and the heat is escaping too fast to allow for higher temperatures. But if we increase the length the cool down time will dramatically increase. Thus along with making the length longer the block thickness is also reduced to allow for faster cooling. The design parameters are finally set to the block thickness at 0.375" and the neck length at 1.4". Figure 48 is a temperature vs time plot for this special case.

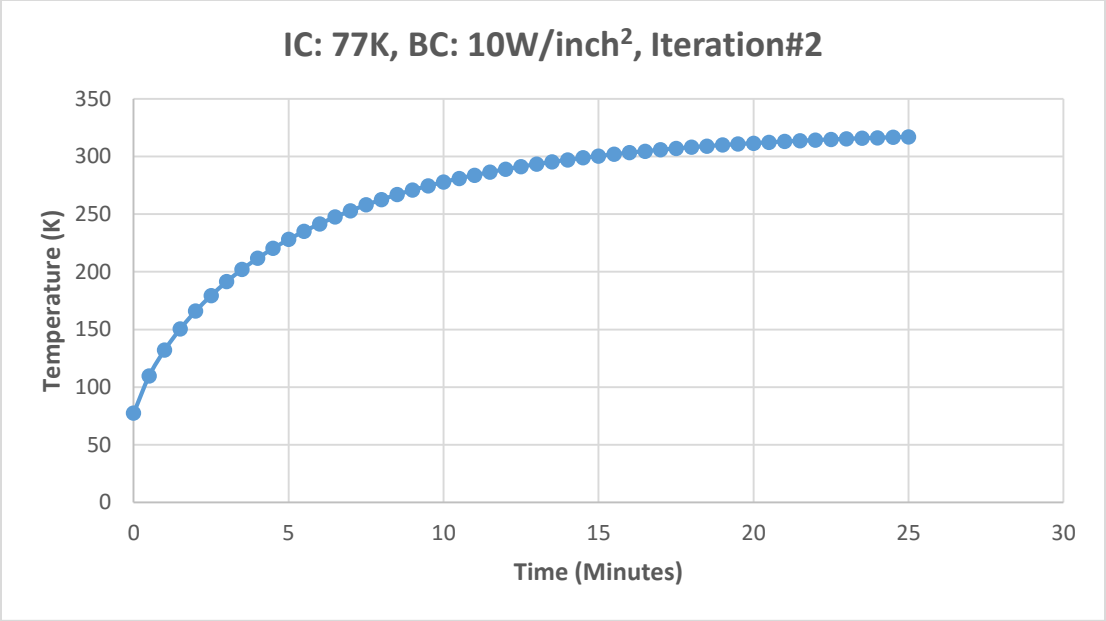

Figure 49: Heat Up Test, Case 1, tBlock=0.375", LNeck =1.4

The temperature profile hits the 300K mark beautifully at 15 minutes' time. The temperature distribution for this optimum case is shown in figure 49.

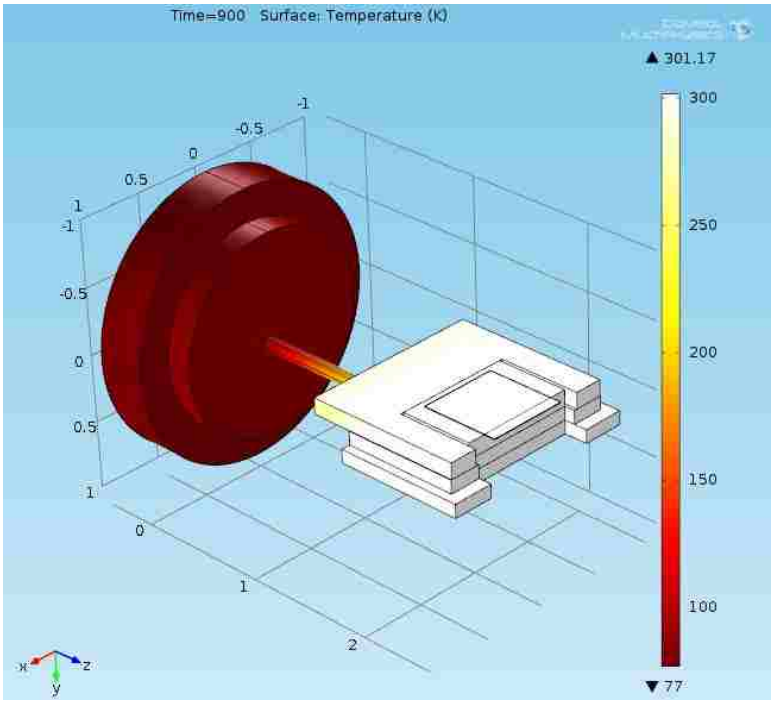

Figure 48:" Temperature Distribution, Heat Up Test, Case 1, tBlock=0.375", LNeck =1.4"

To check if this change in dimensions disturbed the cool down time, a simulation is performed with the initial condition at 300 K and the boundary condition as 77K similar to the previous section.

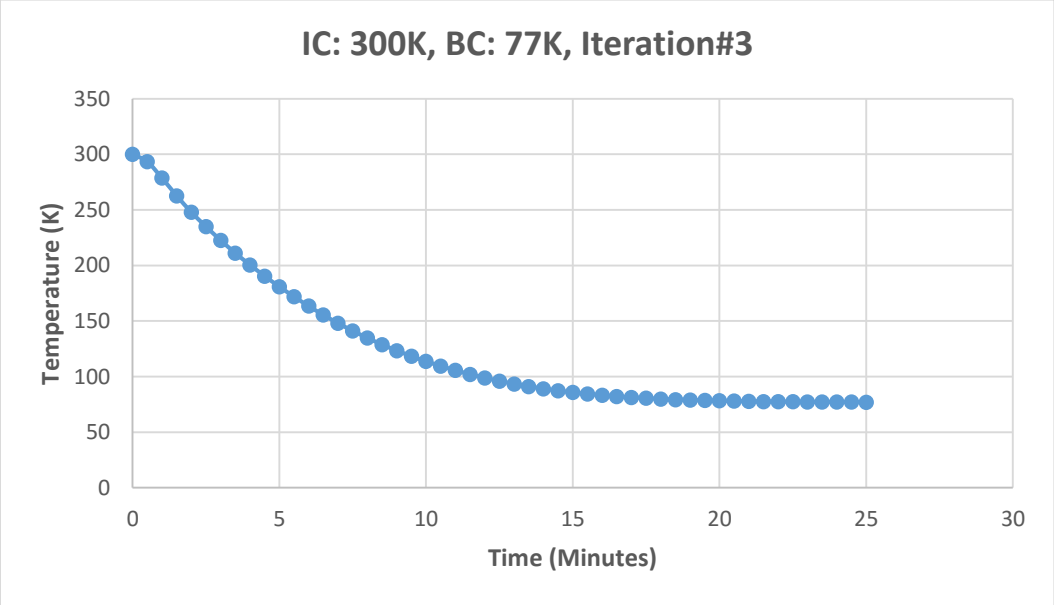

Figure 50: Cool Down Test, Case 1, tBlock=0.375", LNeck =1.4"

So at 15 minutes mark the temperature in the cool down test is 86 K which is acceptable.

The two criteria compete with each other to decide the dimensions for a finalized design. For a shorter cool down time the length of the neck and the thickness of the block should be small while the opposite is to be done for a shorter heat up time. The thickness of the SS304 block has to be kept above a certain minimum to hold the cooling power and minimize temperature fluctuations. In spite of all these challenges the final design parameters come out to be 0.375" for the block thickness and 1.4" for the holder neck. The design moves on to case-2.

CASE-2, COOL DOWN

Case-2 deals with the cool down of the test specimen from 77K to 4.5K which is to be achieved well before 15 minutes. The following initial and boundary conditions have been set up for this simulation. The dimensions are the ones finalized after the case-1 heat up test. The resulting temperature profile is shown in figure 52.

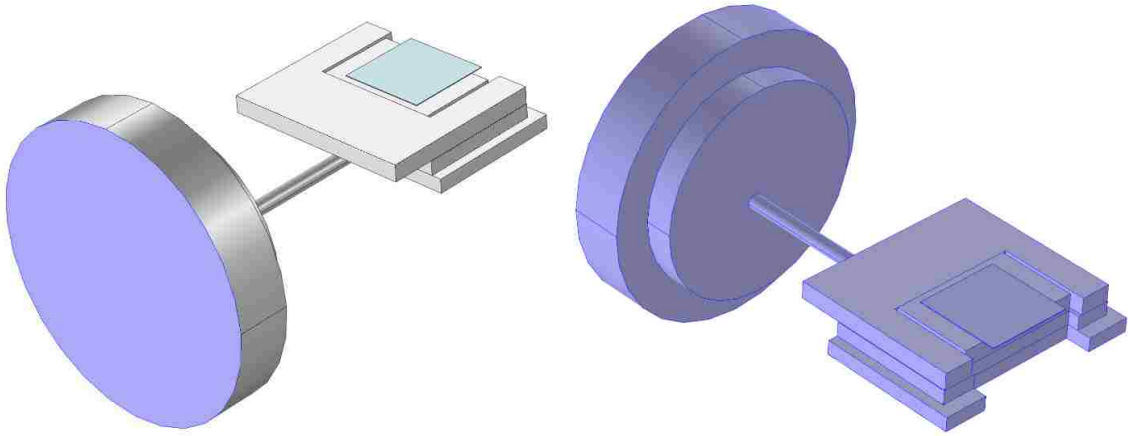

Figure 51: (Left) 4.5K Boundary Condition (Right) 77K Initial Condition for Cool Down Test, Case 2

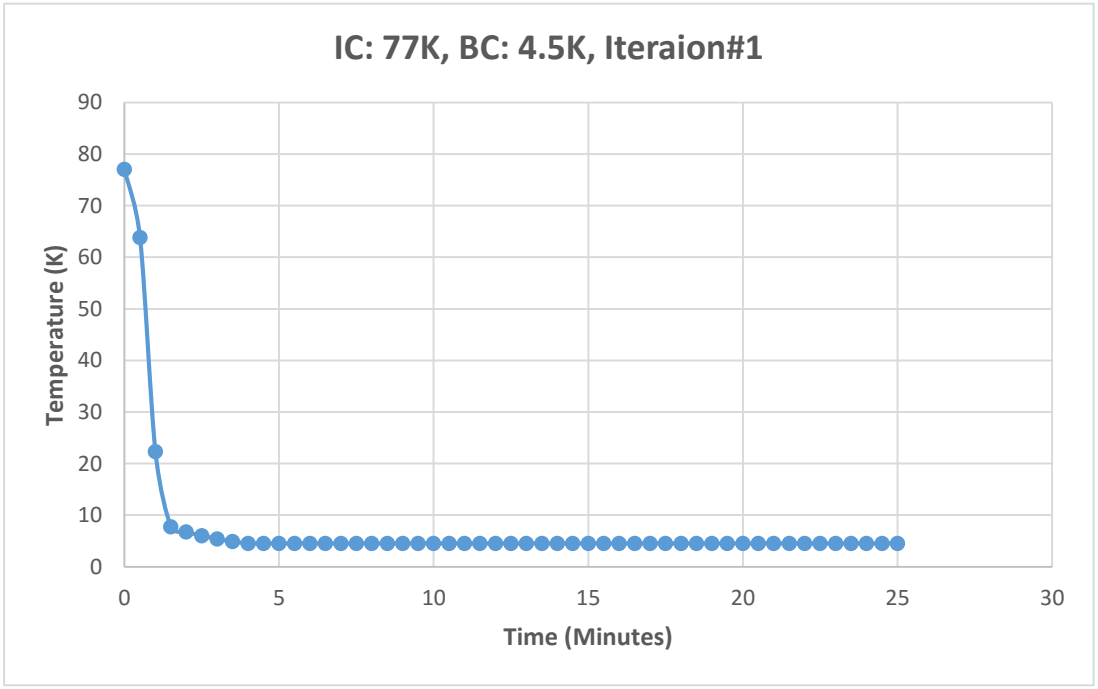

Figure 52: Cool Down Test, Case 2, tBlock=0.375", LNeck =1.4"

So it cools down much faster that case-1. Reaching 4.5K in less than 2 minutes. The temperature at 300 seconds (5 minutes) is shown below:

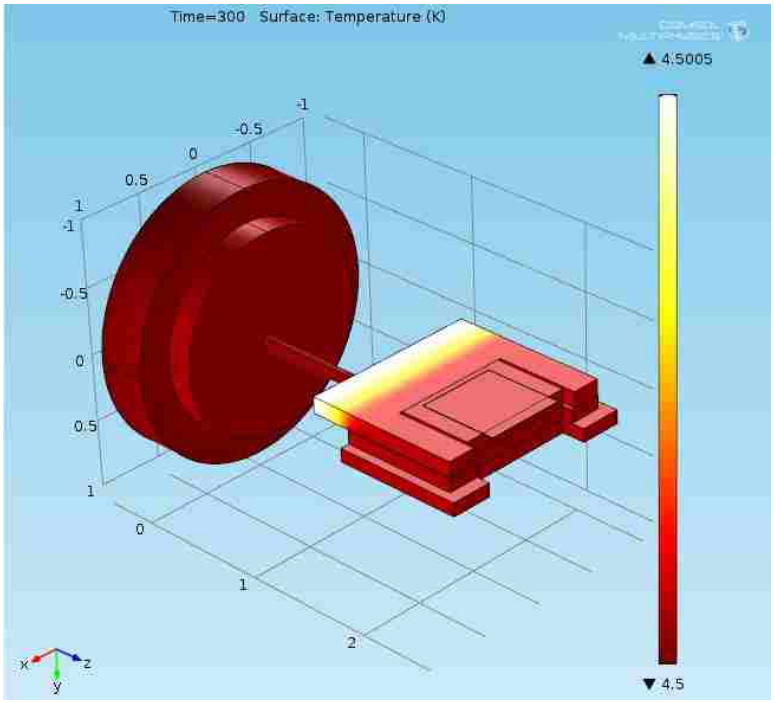

Figure 53: Temperature Distribution, Cool Down Test, Case 2, tBlock=0.375", LNeck =1.4"

The simulation is showing an almost uniform temperature of 4.5K but it is highly unlikely it will be achieved considering the losses in the system. In any case the design checks out for case-2 cool down.

CASE-2, HEAT UP

Similar to case 1, the initial and boundary conditions shown in figure 54 are simulated for a heat up test from 4.5K to 77K using the same 10 W/inch^2 thin film heater attached to the back of the holder stage.

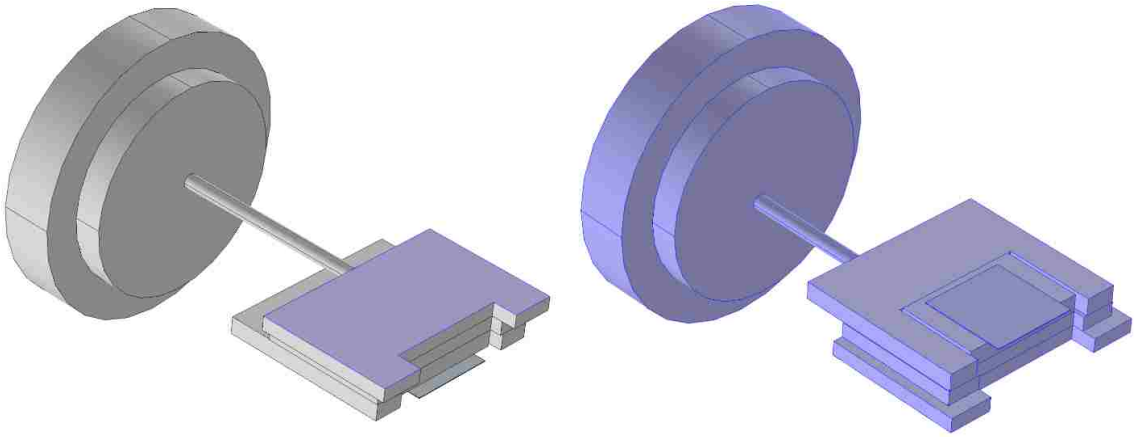

Figure 54: (Left) 10 W/inch2 Boundary Condition (Right) 4.5K Initial Condition for Heat Up Test, Case 2

This results in the temperature profile shown in figure 55.

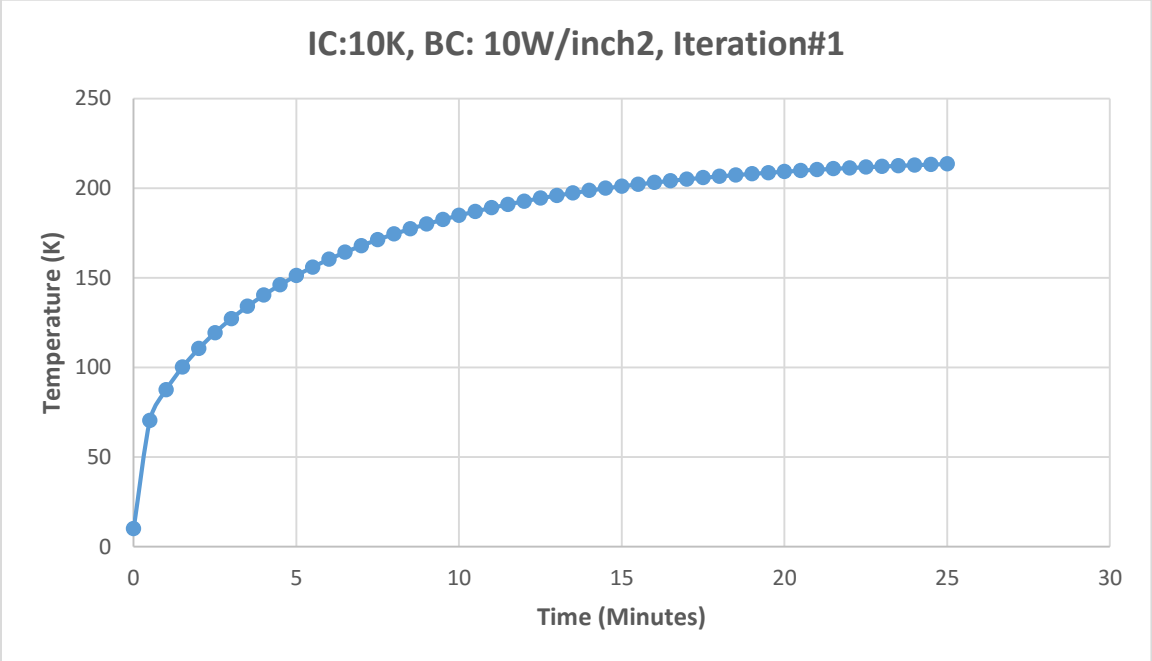

Figure 55: Heat Up Test, Case 2, tBlock=0.375", LNeck =1.4"

It is an over efficient design and shoots for 192K at the 15-minute mark. So it is more than capable of achieving 77K with less power than 10W/inch^2. The temperature distribution at 300 seconds for this model is shown in figure 56.

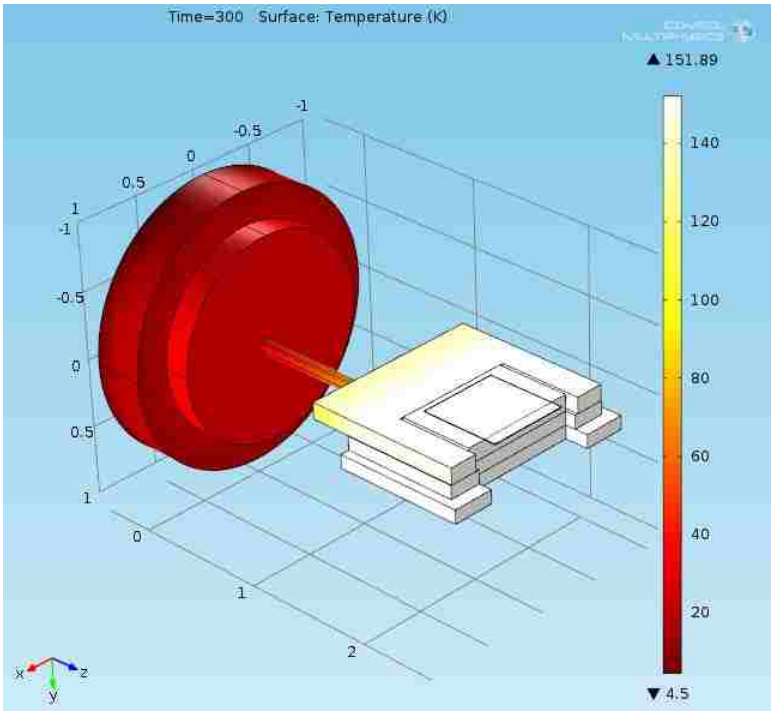

Figure 56: Temperature Distribution, Heat Up Test, Case 2, tBlock=0.375", LNeck =1.4"

With all the criteria satisfied the holder design has been optimized and is approved for manufacturing.

Chapter 6

HOLDER MANUFACTURING & TESTING

6.1 CAD DESIGN

A CAD model has to be set up for vigorous designing of the holder for manufacturing. The model is shown in figure 57.

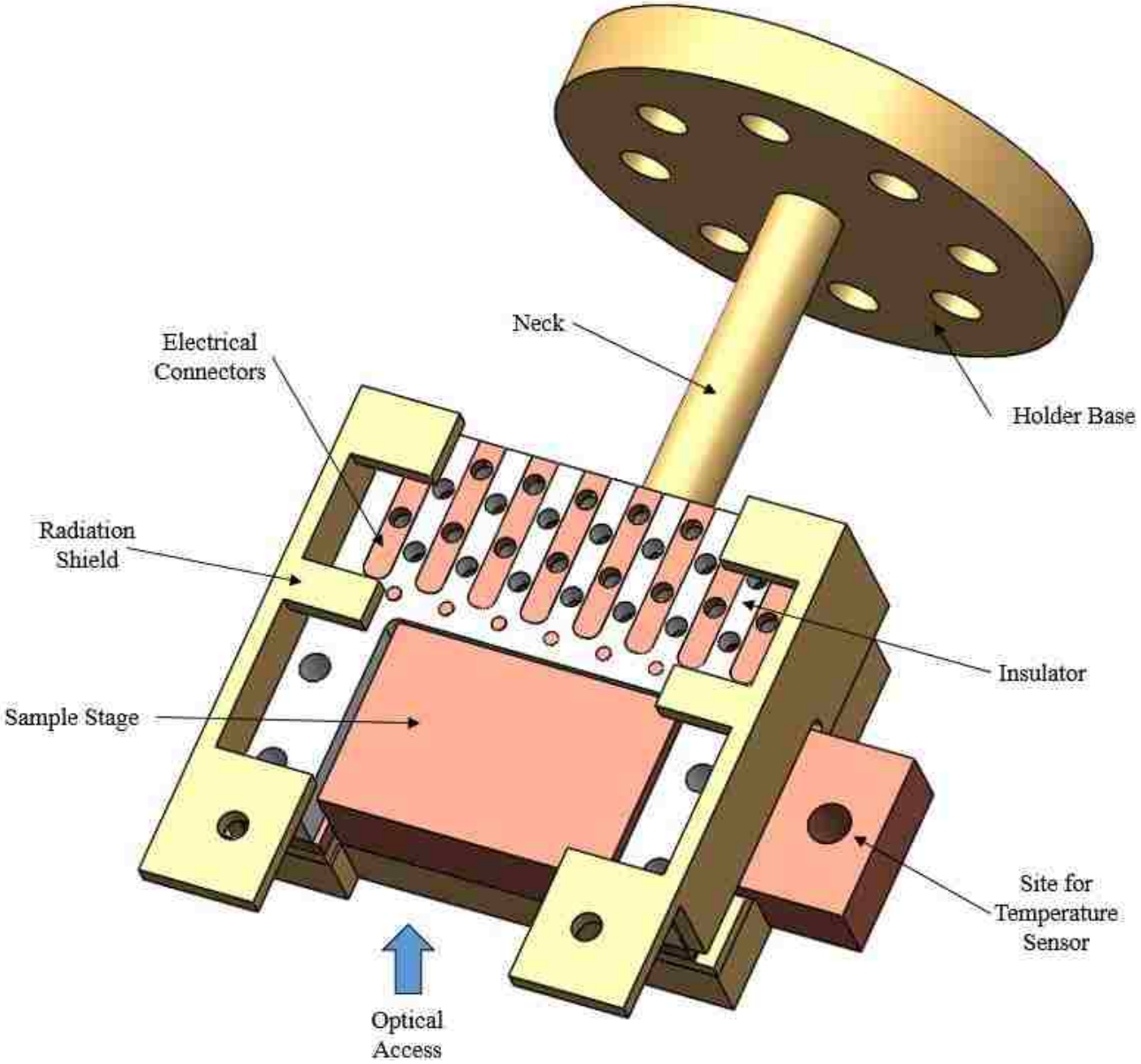

Figure 57: CAD Model for Holder

TEMPERATURE SENSOR

The CAD design incorporates the findings of the COMSOL simulation. It was seen in the simulations that the two copper stages always have the same uniform temperature because of the high thermal conductivity of the oxygen free copper. Thus an extension has been made to the side of the copper stage to allow installation for the temperature sensor. The samples are usually delicate and cannot be probed directly for a temperature measurement so that reading is taken indirectly as the extension for the temperature sensor and the sample are effectively at the same temperature. When mounting the sample on to the stage, silver paste or carbon tape should be used to promote heat transfer by reducing the interface resistance as much as possible.

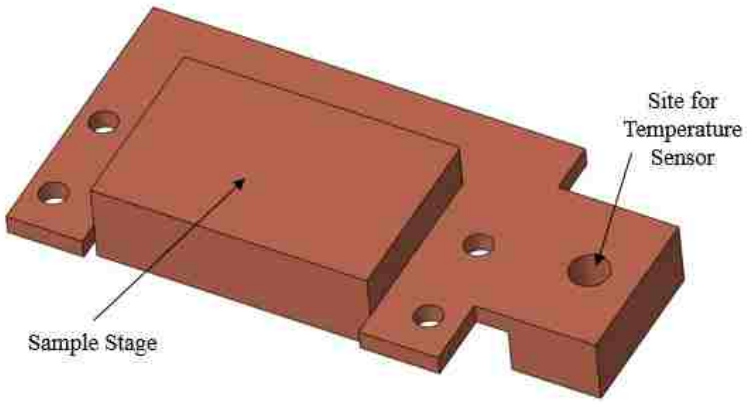

Figure 58: Copper Sample Stage

ELECTRICAL CONNECTIVITY

Another design requirement is the provision of electrical connectivity to the sample. The insulator has been especially designed for that purpose. It has slots to receive and hold down small copper connectors. The sample can be wire bonded to these small copper

connectors and then wires can be drawn out, grouped together and connected to the 32 pin electrical feedthrough of the cryostat.

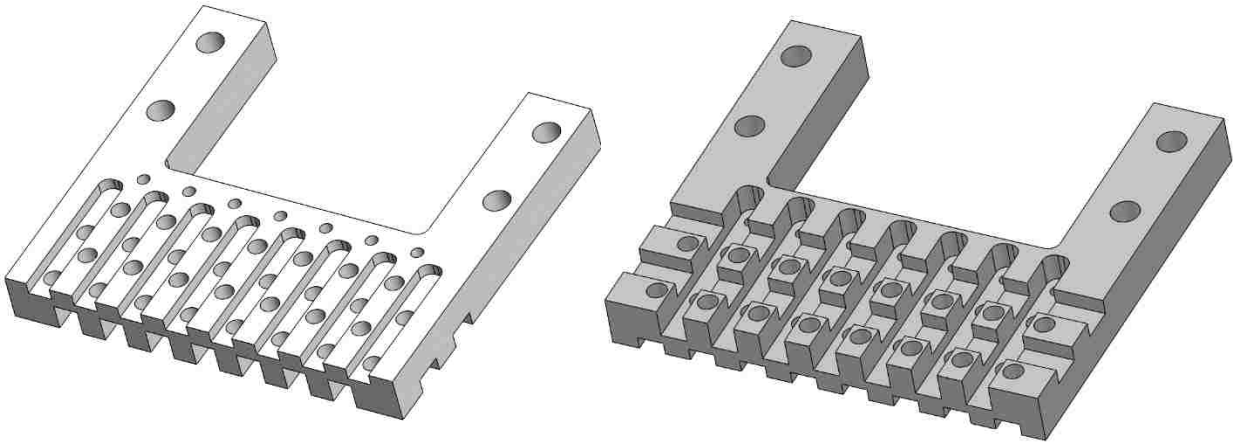

Figure 59: Ceramic Insulation for Electrical Connectors (Left) Top View, (Right) Bottom View

PROTECTIVE SHIELD

Although the simulation showed that the temperature varies by less than 0.1% by the addition of radiative losses in the model so they were ignored altogether. But as a precautionary measure a shield consisting of protective side walls and an upper cover have been designed. They are all cooled directly from the sample stage so they are at the same temperature as major portion of the sample. Another useful purpose of these shields is to physically protect the sample during loading and unloading from the cryostat. These shields are all made from the same oxygen free copper but can be Gold plated if required to minimize radiation and out gassing.

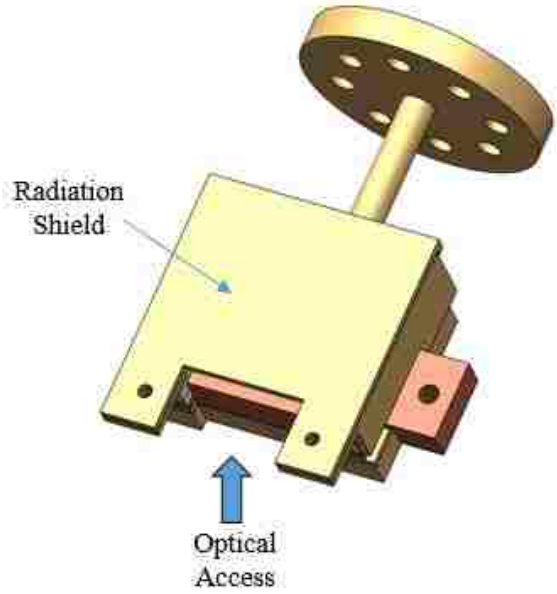

Figure 60: Protective Cover for Sample

VARIABLE LENGTH

The holder neck is separately manufactured and has threaded ends which screw into the holder base and holder stage. Thus the length can easily be varied by using different neck sizes. An isolated view of the neck is shown in figure 61.

Figure 61: Separated Holder Neck for Variable Length

6.2 MANUFACTURING

After the CAD model has been finalized, engineering diagrams are generated as shown in Appendix B. Figure 62 shows the different parts of the holder pending assembly.

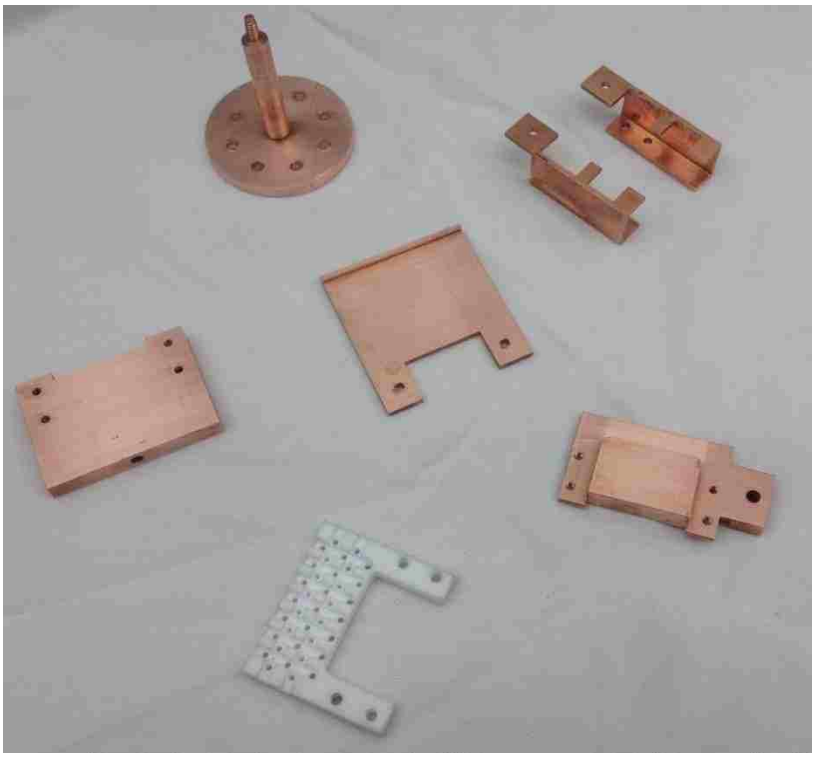

Figure 62: Different Parts of Holder before Assembly

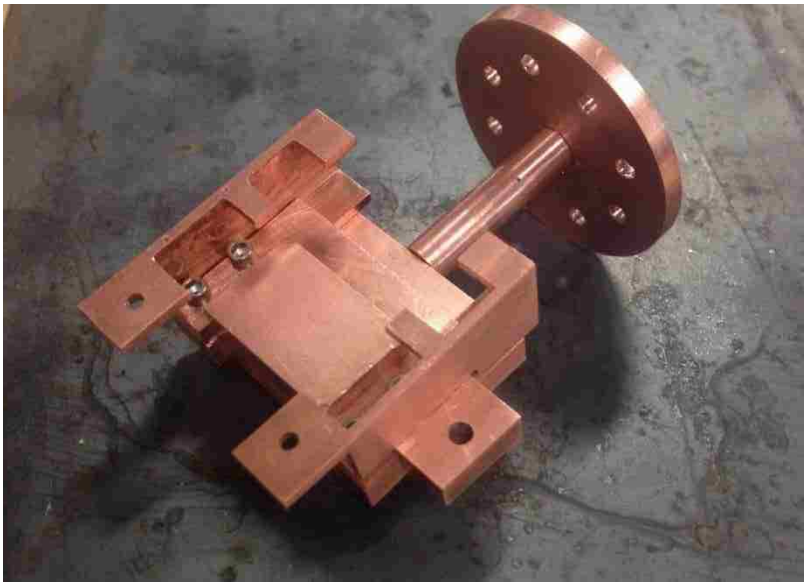

Figure 63: Assembled Copper Structure of Holder

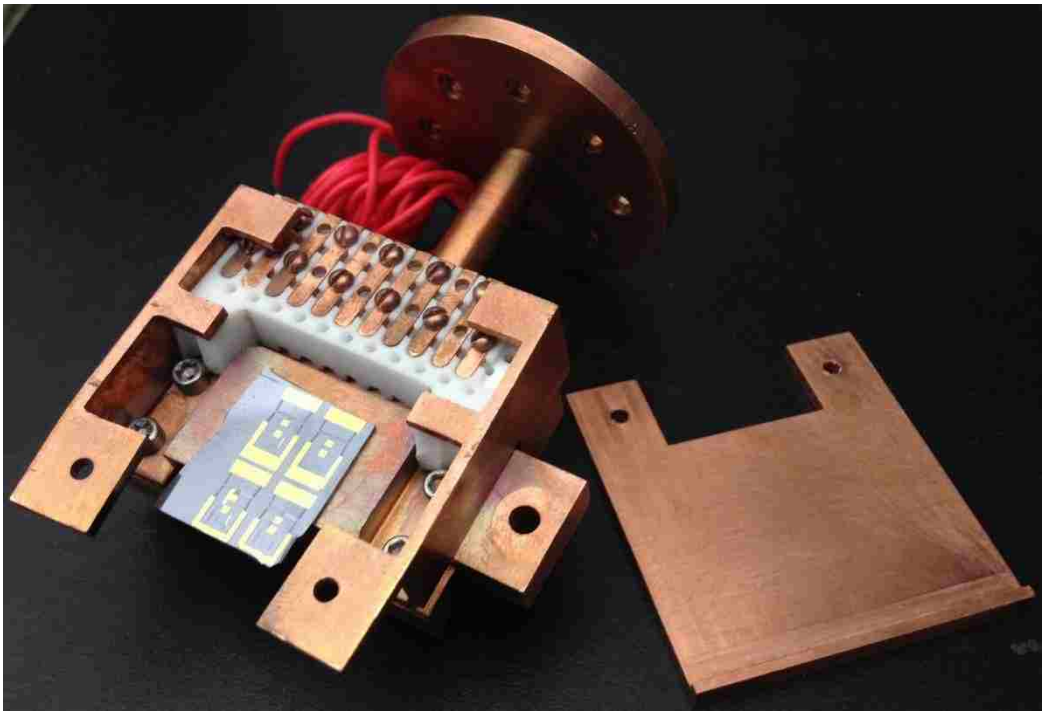

Figure 64: Final Assembly of Holder

6.3 TESTING

Similar to figure 33, the same temperature sensor is mounted on to the holder as shown in figure 65. The sample and the temperature sensor are mounted onto the same oxygen free copper piece so theoretically they should always be at the exact same temperature, although a delay of a few spit seconds is to be expected. The holder is put in to the cryostat and an experimental setup exactly as shown in figure 34 is employed. The current source produces a steady current of 10 μA and the voltmeter reads the voltage which is in turn converted into temperature with the help of a calibration curve provided by the manufacturer.[13] The experimental results from this experiment are shown in figure 66. As the holder has a delay of its own so the minimum temperature achieved was 104 K.

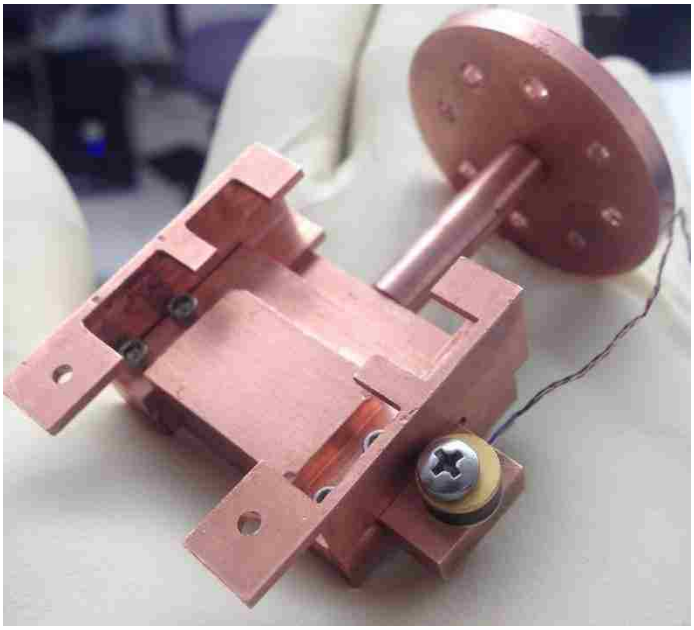

Figure 65: Copper Infrastructure for Holder along with a Temperature Sensor

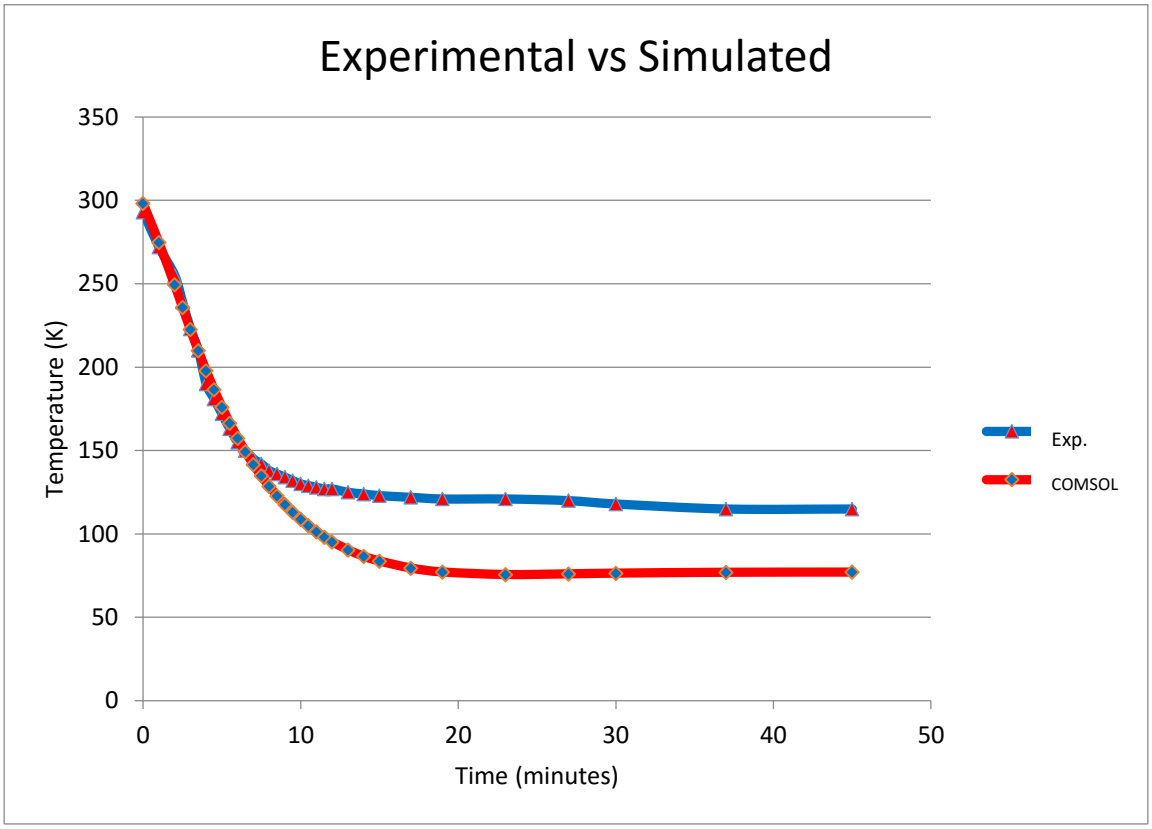

Figure 66: Temperature vs Time curve for Holder Cool Down

The delays in temperature response from the cryostat combined with the delays of the holder led to a large divergence of the experimental results from the simulated results in figure 66. Better vacuum and decreased temperature in the cryostat can possible push the two curves together. Although the major problem seems to be coming from the radiative heat gains as the holder is surrounded by the outer most wall at 300K unlike the cryostat inner chamber which is surrounded by the outer chamber around 85K. Thus the solution seems to lie in building extensions of the inner chamber around the holder. These extensions would be cooled by the lower chamber and thus drastically reduce the deviation.

Figure 67 has been created to test out the response of the holder in a heat up test. As the lowest temperature achieved was 105 K so the experimental graph starts at that temperature. This graph was obtained partially through actual experimentation and partially through extrapolating data keeping in mind the behavior of the thermophysical

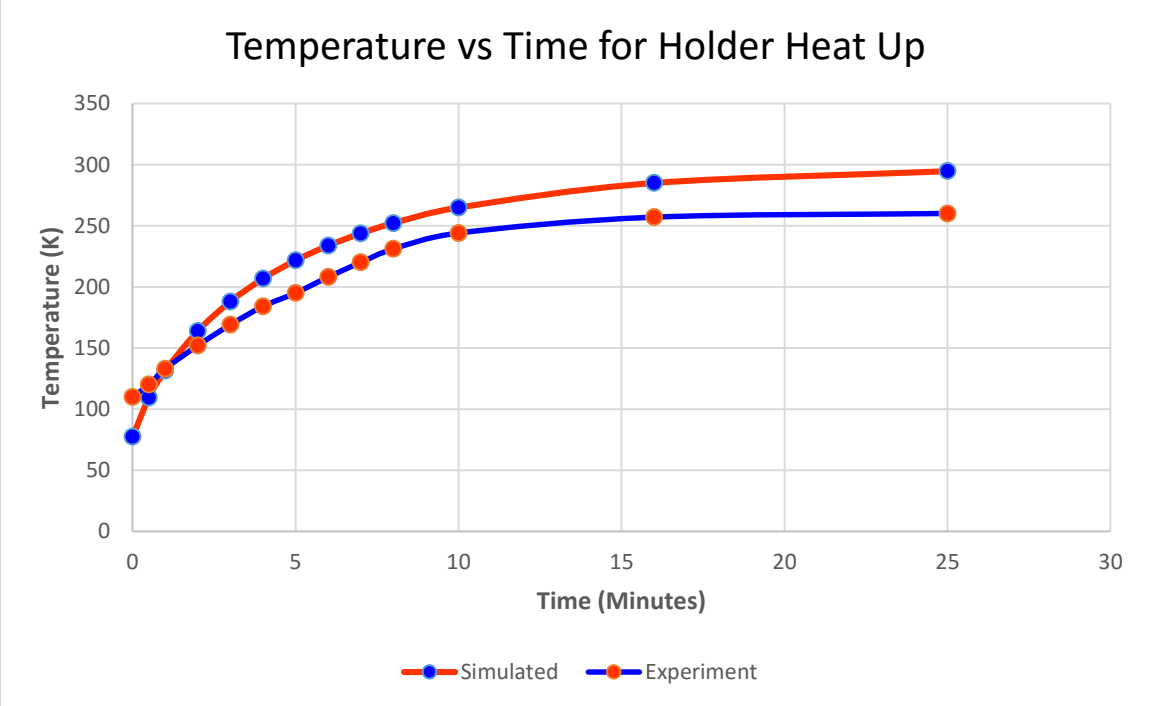

Figure 67: Temperature vs Time curve for Holder Heat Up

properties of the Oxygen Free Copper. The experiment was performed using a power supply connected to the thin film heater. The current and voltage were adjusted to produce a power of 10 W spread over the 1 square inch area of the heater. The initial temperature was higher than 105 K and thus lead to a final temperature much higher than 300 K. These results were then manually adjusted keeping in mind the variation of the thermal conductivity and specific heat capacity of the OFC used to make the holder. The author is much less concerned about the deviation in the results of figure 67 than of figure 66 because of the ease at which power input can be manipulated. If the temperature achieved is lower than expected or requires a time much greater than anticipated, the power can easily be increased by adjusting the current and voltage inputs. Thus there is a one-time need to make a custom calibration curve for temperature to power correlation for future needs.

Although the cool down and heat up results were not as good as expected but the design still managed to achieve 87% of the target temperature difference between 300 K and 77K alongside a satisfactory heat up response which can be improved with higher power.

This concludes the holder design part of the thesis. With the low temperature testing capability in place, the following chapters move on to the actual design, fabrication and testing of the MEMS actuators need for the tensile testing of independent samples.

Chapter 7

CASCADED THERMAL ACTUATORS

& INDEPENDEDNT SAMPLES

7.1 INTRODUCTION

Thermal actuators are valued for their thermal stability and large displacements. Usually mechanical testing of thin free standing films requires a large enough force and displacement which can only be possible by using thermal actuators. The greatest drawback that these types of actuators have is with their large temperature gradients, which is understandable due to the fact that high thermal gradients are responsible for the thermal expansion of the Silicon structures and in turn the displacements they provide. Khawar et al [6]addresses this problem by using a cascaded structure where one type of actuators provide amplification to a set on another while maintaining a very low thermal gradient across the test sample. The limitation of [6] is that the sample is co fabricated with the actuators and the test can only be performed one time with the same actuator setup. Thus there is a need to have independently made samples which are transferred to the test site so that the same load cell can be used repeatedly with varying samples. This gives rise to great precision and reliability. Gold has a recrystallization temperature of 320 ^{0}C [14] and requires a displacement of at least 2.5% to undergo tensile failure for a 250nm thick film [15]. So that translates to an actuator deflection of 12.5 µm plus a 4 µm tolerance value which puts the temperature difference across the sample at 45 ^{0}C. Although for a 50 µm sample the deflection required would be 1.25 µm plus the 4 µm tolerance value. Figure 68 shows the actuator mechanism along with the removable sample followed by an introduction to some of its important features.

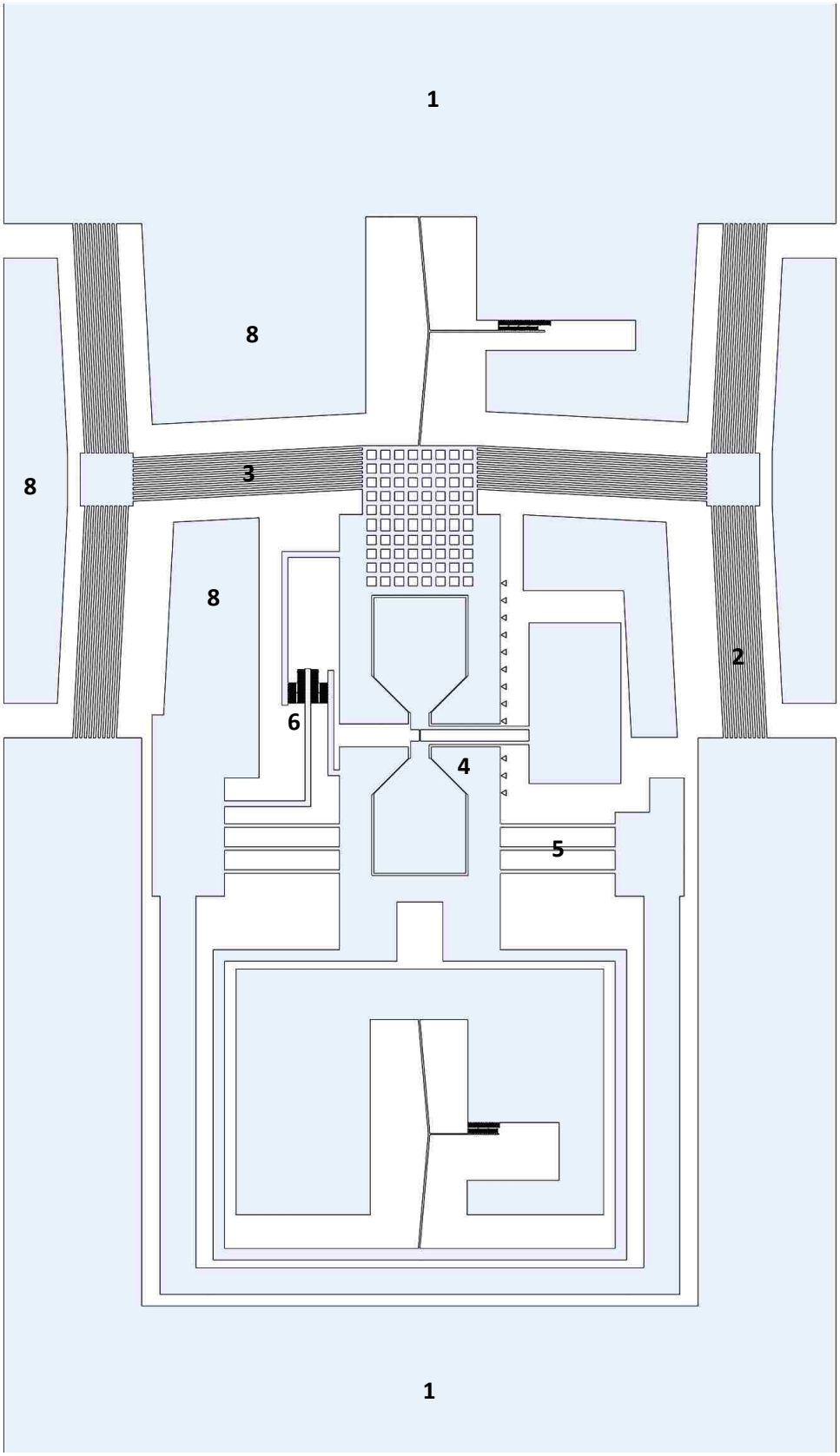

Figure 68: Cascaded Thermal Actuators with Interchangeable Sample

1. Site for bonding pads. These also act as an anchors for the actuators so it is imperative that they do not release. Also it is convenient to have large areas for wire bonding and the testing.
2. Chevrons for producing horizontal displacements.
3. Chevrons for producing vertical displacements. These chevrons have their deflections magnified due to the chevrons producing the horizontal deflection.
4. Jaws for holding the sample during tensile test. Care has been taken to make then stiff enough so that no extension is added to the sample due to their compliance.
5. These springs provide the restoring force to the lower jaw and are also responsible for providing the tensile force on the lower end of the sample. These fixed-fixed beam should have a linear displacement throughout the operation of these thermal actuators. For that purpose, these beams have been designed such that they will have perfectly linear within the test range with a deflection of one fourth of the thickness for a text deflection of 20 μm.
6. These Vernier calipers measure the relative displacement of the lower and upper jaw with respect to a stationary reference. These calipers have a least count of 0.5μm due to fabrication limitations.
7. These buckling beams have been added to amplify the displacements of the lower and upper jaw. As these beams only work under a compressive load so a cage has been added to the lower beam. A COMSOL simulation was run and found that these beams have an amplification factor of 5.6 and take less than 0.05% of the force applied to break the sample for a maximum deflection.

8. These stationary structures are added to limit the open areas for a more uniform etch rate and release rate during the fabrication process.

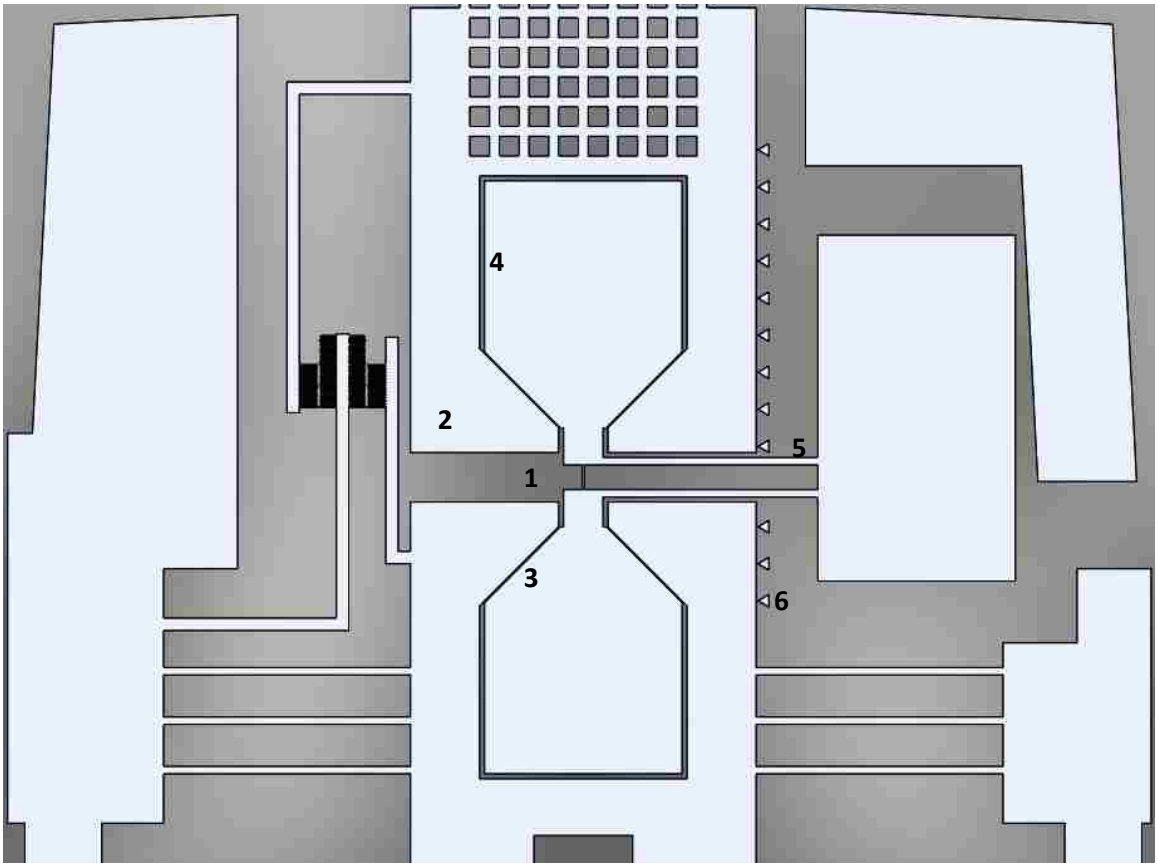

Figure 69: Zoomed In view of Sample

1. The actual Gold sample.
2. Clamps for holding the sample in the actuator jaws for tensile test.
3. A 45-degree surface with 2 µm play has been designed to center the sample.
4. 10 µm clearance for easy positioning of the sample.
5. Arms to hold the sample with pad. These arm can then be cut with a laser to avoid disturbing the sample when it is properly placed. These arms are minimum 500 µm long to have minimum impact on the sample due to the energy put in by the laser.
6. Stops to limit the horizontal motion of the actuators during sample loading.

7.2 MASK DESIGN

The next step after a CAD design is to implement it on another 2D design software for producing a photolithography mask. Several features are conveniently added at this stage rather than at the CAD stage due to ease of using a layered approach. Figure 70 shows the mask design for the thermal actuators with added electrical pads for wire bonding and a sample net to hold the sample while it is being transferred into the actuator clamps for a tensile loading. Without these nets the sample would just fall right through the structure.

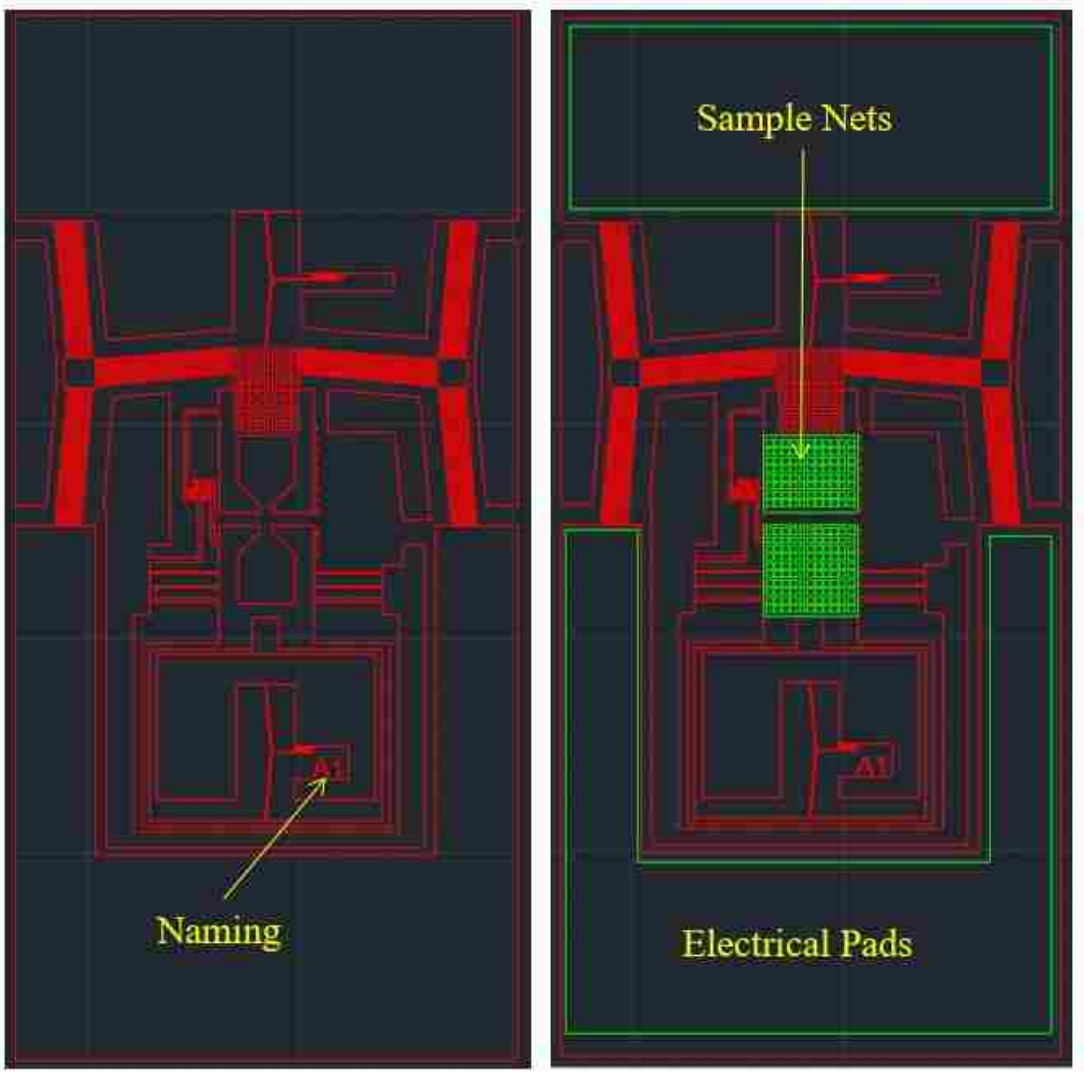

Figure 70: Thermal Actuators with Electrical Pads and Sample Nets

Mask polarity is of great importance. The polarity depends upon the type of photoresist the user plans to use. Positive photoresist retains the areas which are unexposed to UV radiation. For that purpose, it is important to have all the close form, 'wanted' features on the photolithographic mask to be 'Dark', which means they will be make out of chrome or iron oxide. The open area on the other hand will be transparent and will be made from quartz or soda lime glass. Thus an overall view of the mask will show a 'Clear Field'. The opposite is true for the mask bearing the bonding pads where the majority of the area will be covered by metal and the mask ordered will be 'Dark Field'. Lastly some alignment markers are added to both masks to align them during fabrication of devices.

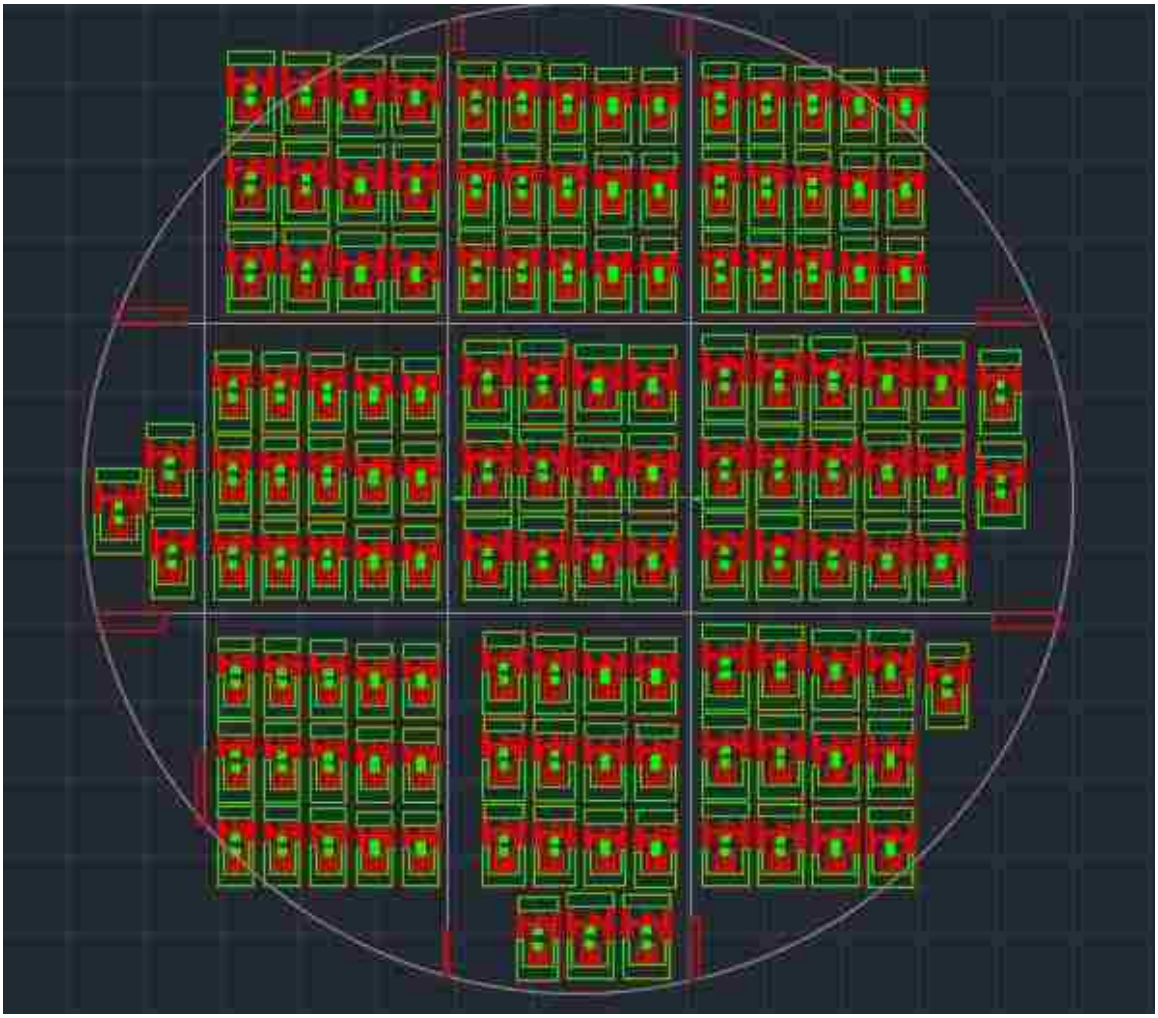

Figure 71: Photolithographic Masks for Thermal Actuators and Bonding Pads

One additional feature that is added to the samples is a large area bearing iron or any other ferromagnetic material for easy transfer of the sample, before and after the test. Electromagnetism can be used with the micromanipulators to easily pick up and drop these pieces. The concept is shown in figure 72. This is an experimental concept not tried before so even if it does not work suction or a small amount of weak adhesive can be used.

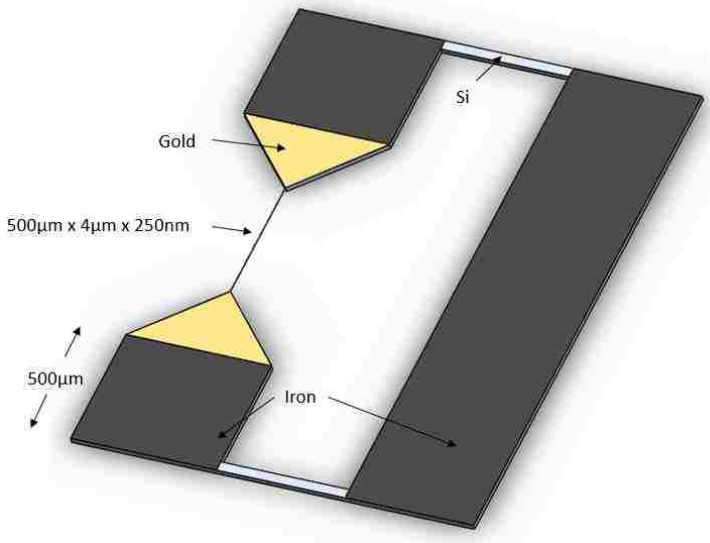

Figure 72: Novel Concept for Transferring Samples through Electromagnetism

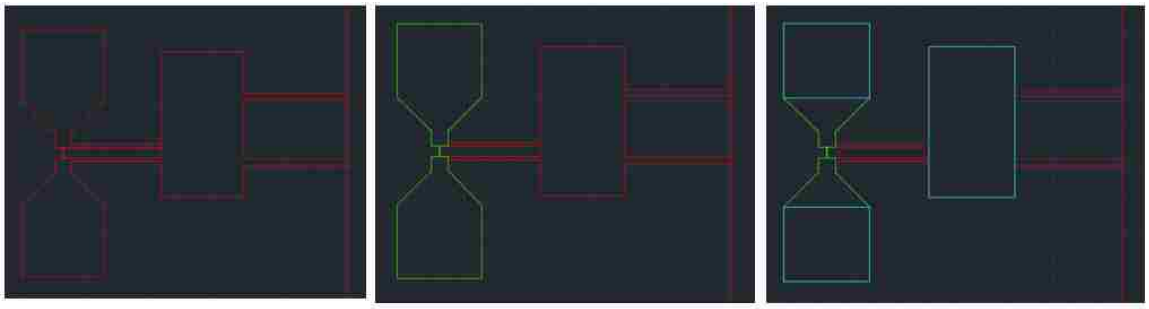

Figure 73: Masks showing Individual Sample

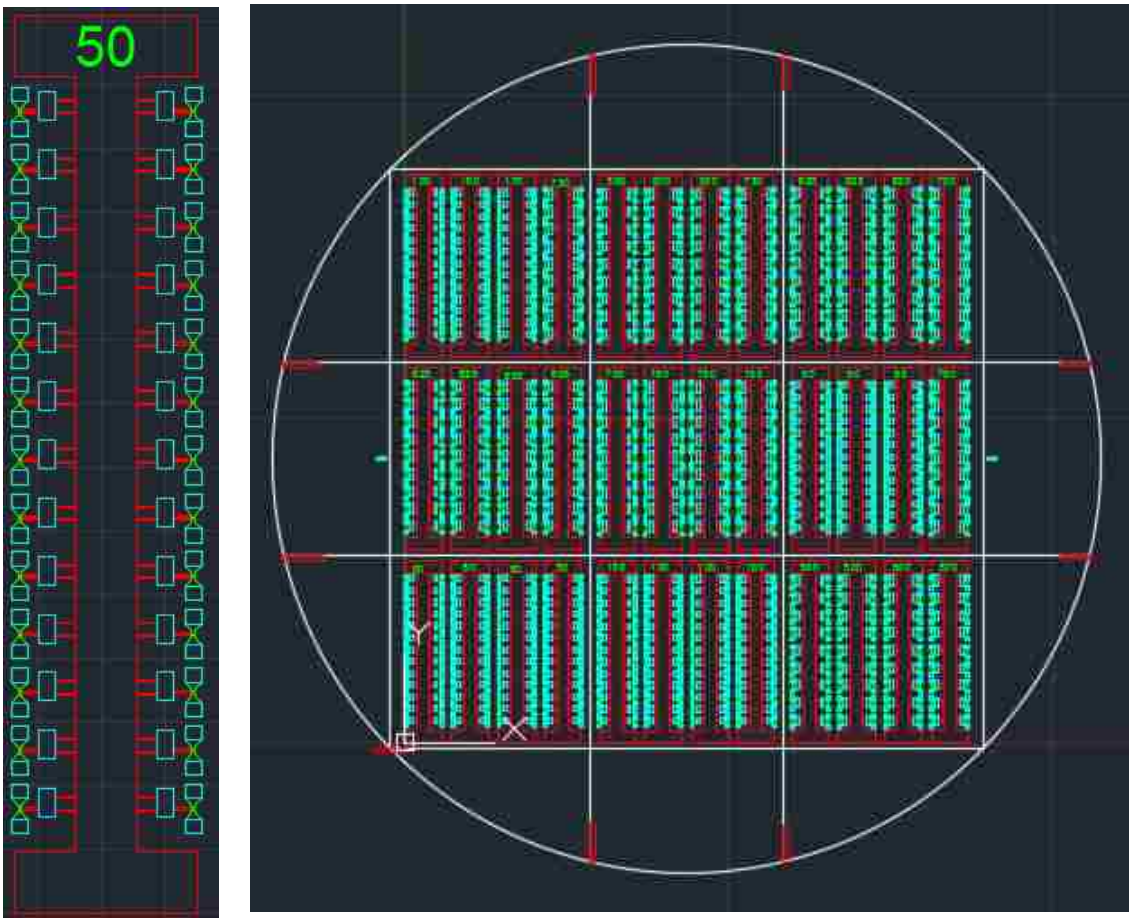

Figure 74: Masks showing a 'Sample Tree' (Left) & a 'Sample Forest' (Right

Different sample materials with desired thickness can then be deposited using this method to independently produce hundreds of samples of varying length at a time. Figure 74 shows these samples being held together in the form of a 'Tree' with respect to these lengths as the central structure does on release and holds the samples till they are finally released and ready to be transferred after being cut from the tress with a laser. These trees collectively form a 'Sample Forest'. Afterwards these geometric files were sent to a company specializing in making photolithographic masks with the specification of critical dimension 2 µm and a maximum deviation of +/- 0.25 µm.

Chapter 8

FABRICATION

8.1 STEPS INVOLVED

STEP 1: DESIGN MASK

The first step in the fabrication process of any MEMS device is the implementation of the intended design on a CAD software. The details of the mask design work for this project has been presented in the previous chapter.

STEP 2: MANUFACTURE MASK

The CAD data is then shipped off to a mask manufacturing company where they convert it into a physical photolithography mask. Most manufacturers accept only .DXF and .DWG formats so care should be taken that the final CAD file is compatible. Various configurations of the base and feature materials are available but the author preferred Chrome features on Soda Lime glass. The features were requested to be on the underside of the glass to enable sharp focus. The critical dimension being 2.0 microns with a tolerance of +/- 0.25 microns. The mask for the actuators is a clear field mask and the one for the pads is a dark field mask so that the same positive photoresist can be used for both the masks.

STEP 3: COAT HMDS

The prime SOI wafer is first coated with Hexamethal DiSilazane to promote bonding between the inorganic silicon substrate and the organic photoresist. The substrate is heated up to 100 ^{o}C to promote bonding.

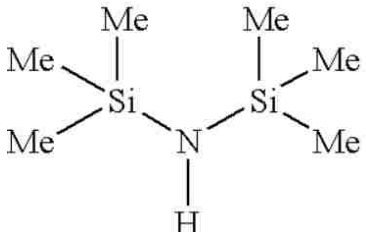

Figure 75: Chemical Structure of HMDS showing Groups for Organic & Inorganic Bonding

STEP 4: SPIN PHOTORESIST

The wafer is then allowed to cool to room temperature and then a consistent layer of photo resist is deposited onto it. Different spin speeds and photo resists give a varying range of film thickness.

A 2-micron layer was used for the DRIE process and a 11-micron thick PR layer was used in the sputtering process. The details of steps 3-6 comprise the 'photolithographic recipe' and are presented in appendix C.

STEP 5: SOFT BAKE

The wafer is then baked at a high temperature (110^0C in this project) for varying lengths of time to bake the photoresist. The photoresist hardens and bonds strongly to the Si wafer through the HMDS layer. The soft bake initiates the linking in the PR thus making it stiffer and enhances bonding.

STEP 6: EXPOSE

The mask is then inserted into the mask aligner along with the soft baked wafer. The mask aligner is equipped with a UV source that exposes the PR layer to UV light of constant intensity over a specified length of time. The light passes through the mask and is

obstructed by the dark features on it. Thus the areas which are directly below the chrome features on the mask are not exposed to the light. The exposed regions behave differently depending upon the polarity of the PR layer. The positive PR starts delinking on exposure to the UV light and dissolves in developer. The inverse is true for negative PR. The PR thickness is the main factor in deciding the energy that should be put into it and hence the deciding factor for the time required. If the wafer already contains some features, then it is essential to alight the mask and the wafer first.

STEP 7: DEVELOP

The exposed wafer is then immersed in a developer solution compatible with the PR used. The exposure time and the thickness of the PR are the deciding factors for the immersion time. The PR clears away the exposed areas in positive PR and unexposed areas in negative PR. A few resources that the author used can be found in [16]–[19].

STEP 8: RINSE & SPIN DRY

The wafer is then put in a dump rinser which periodically immerses the wafer in water. It is then carried to a spin dryer in a boat which spins the wafer while spraying it with deionized wafer. Afterwards it increases the spin speed and starts shooting a steam of dry hot nitrogen at the wafer.

STEP 9: DRIE

Bosh process is used for Deep Reactive Ion Etching (DRIE) of the features on the Silicon device layer. The Bosh DRIE technique is a form of highly anisometric dry etching where the tool continuously releases pulses of the etchant (SF_6 for Si) and passivation agent (C_4F_8 is used to yield a product similar to Teflon). The Oxygen plasma used gives rise to the

directional component of these gasses. The machine continuously deposits the passivation layer and bombards it with the etchant. The passivation layer deposits everywhere but the portion of it clinging to the vertical walls is not etched away completely, thus it only etches the area at the bottom of the walls. A proposed recipe is also presented in the appendix 'A' but for this project the DRIE step was contracted out to the cleanroom at the University of Washington.

STEP 10: CLEAN IN PIRANAH

The etched wafer is then clean thoroughly in 'Piranha' which is one-part Hydrogen peroxide and four parts 96% sulfuric acid. The composition is given in the appendix as well. It thoroughly cleans the wafer from the remaining photoresist and the passivation layer deposited during the DRIE. Afterwards it is rinsed in water and spin dried as explained in step 8. By this step the wafers have the actuators and the Silicon substrates for the samples.

The actuator wafer is getting ready to have electrical pads and the sample net deposited onto it. The sample wafer is also ready to receive the gold sample layer and the iron magnetic layer onto the silicon substrates it already possesses. At this stage steps 1 to 10 are repeated again with a thicker PR layer and the secondary photolithography masks.

STEP 11: DE SCUM

The wafers are then put in Reactive Ion Etcher to de scum them, removing any residual PR on the deposit sites. Oxygen plasma is used for this purpose.

STEP 12: SPUTTER

Sputtering is the technique of plasma assisted metal deposition in high vacuum. Different metals have different sputter rates depending upon the metal, power input for the plasma, the gas used and pressure at which the plasma is generated. Some etch rates are presented in the appendix C along with the conditions at which the sputtering was done. Aluminum was first choice for the bonding pads on the actuator pads due to its low cost but it was replaced by gold due to its slow deposition rate and the problems faced in the release stage. Gold is notorious for its low adhesion so a layer of Titanium, 30nm thick was deposited onto silicon before gold. This Ti/Au layer was also deposited on to the sample mask for making the actual samples.

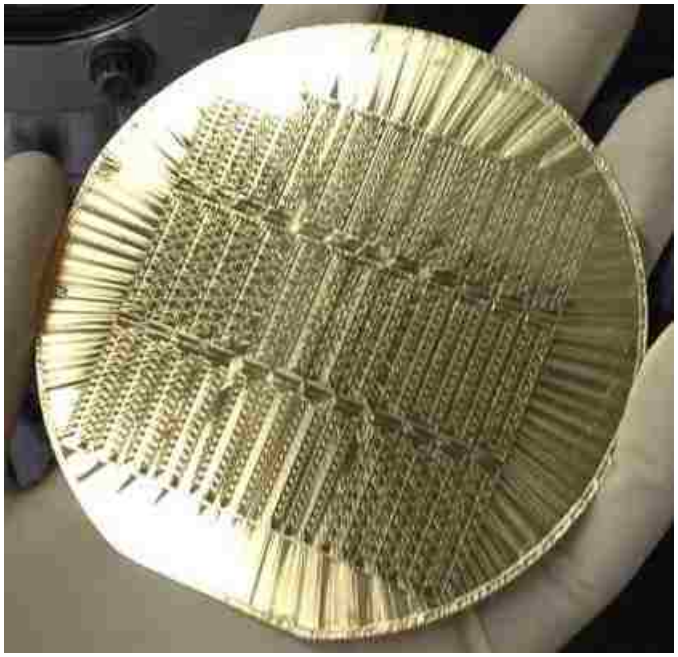

Figure 76: Sample Wafer Sputtered with Gold

Afterwards steps 1 through 12, except 9 are repeated to but a layer of iron on to the sample holders.

STEP 13: LIFT OFF

During sputtering metal is deposited on the whole wafer, irrespective of the presence and absence of the PR layer. However, the metal is directly deposited on to the Silicon device layer in the open areas where there is no PR. The areas which have PR on them do not need the metal. Thus, there is a need to lift off this option of metal from the wafer. For this purpose, the wafer is left in acetone with periodic agitation. The acetone seeps into the PR layer and dissolves it while simultaneous lifting the metal layer on top of it. Sonication can be done to assist the lift off process but that is very aggressive and may destroy the delicate features. It is highly recommended that the PR layer be thick enough to lift off the metal layer without requiring sonication if the wafer has fragile devices. The wafers should then be rinsed and spin dried.

STEP 14: RELEASE

The last step is releasing the devices from the buried oxide layer which is immobilizing the entire structure. The structures would still contain support anchors to hold it while it moves.

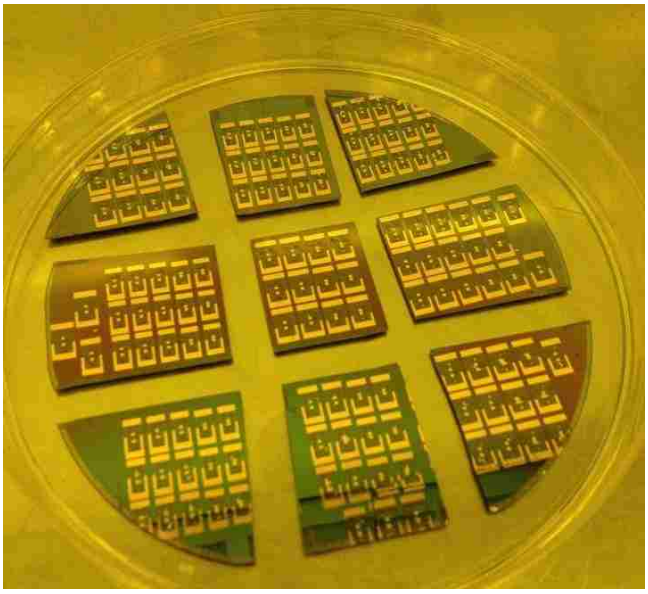

Figure 77: Diced Actuator Wafer

These anchors are large pieces of silicon which cannot be released within the time the reset of the movable structure is release. It is also highly recommended to dice out the wafer before releasing it as a lot of work has been put into reaching this point and there is no further need to have the wafer intact.

STEP 15: XeF_2 ETCH

One additional last step only for the samples is to etch out the silicon underneath the actual gold samples to make them truly free standing. The XeF_2 not only etches away the silicon underneath the tensile sample but also the titanium which was used as an adhesion layer. This ensures that the tensile sample is purely gold as initially intended. The figure 78 summarizes all the fabrication steps up till now.

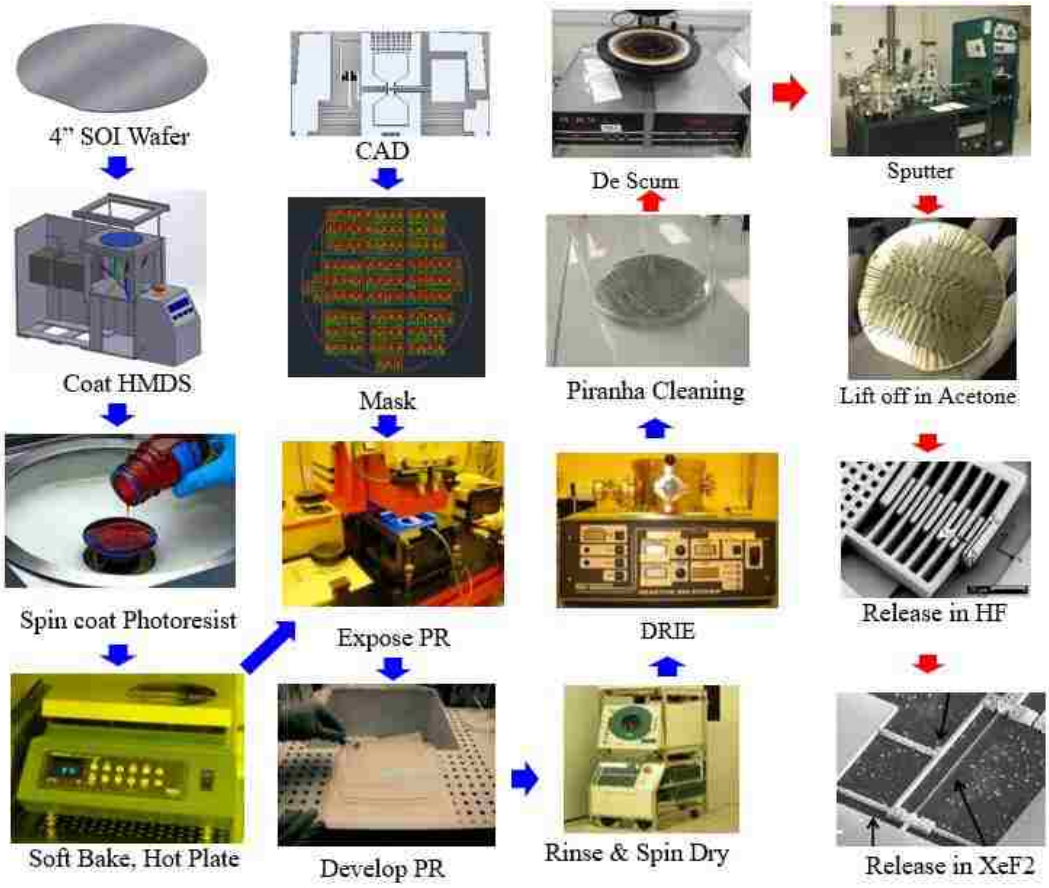

Figure 78: Summarization of Fabrication Process.

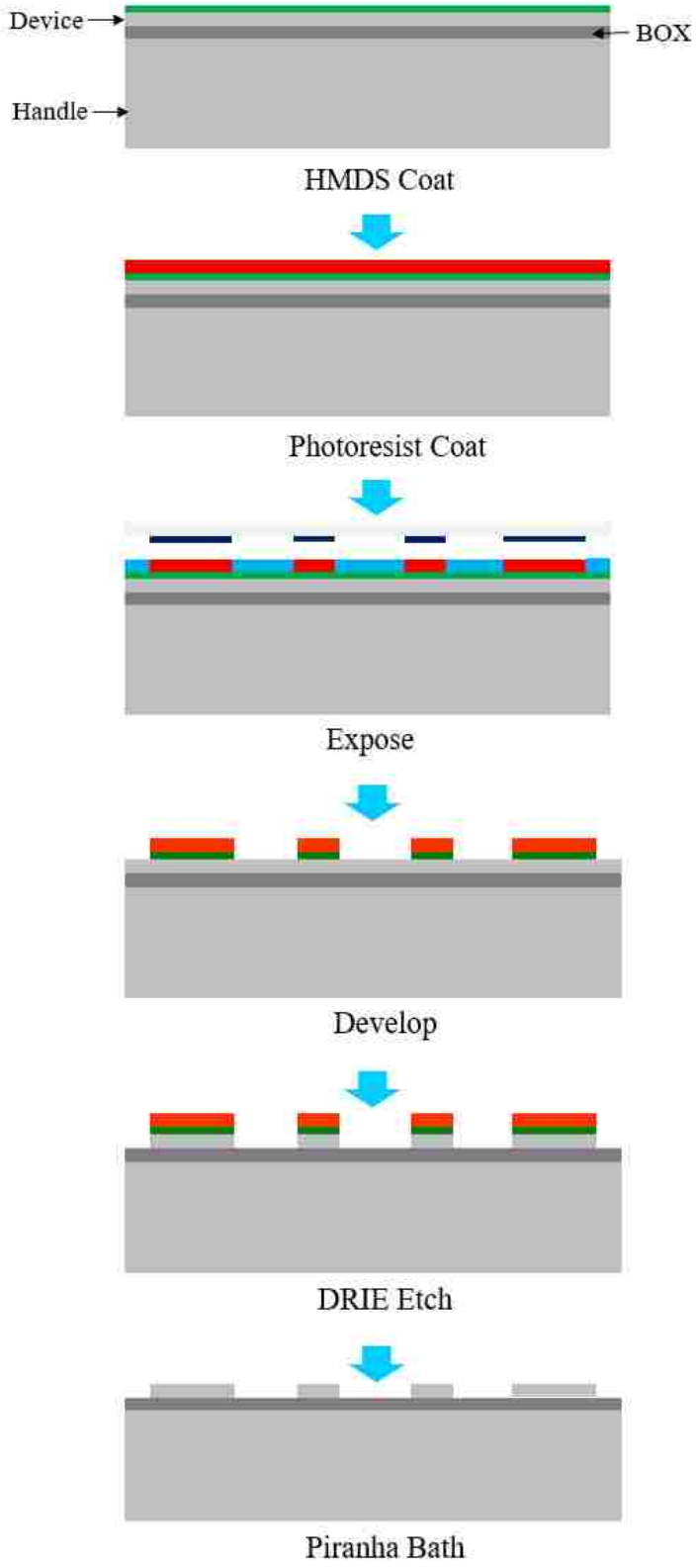
Device
BOX
Handle
HMDS Coat
Photoresist Coat
Expose
Develop
DRIE Etch
Piranha Bath

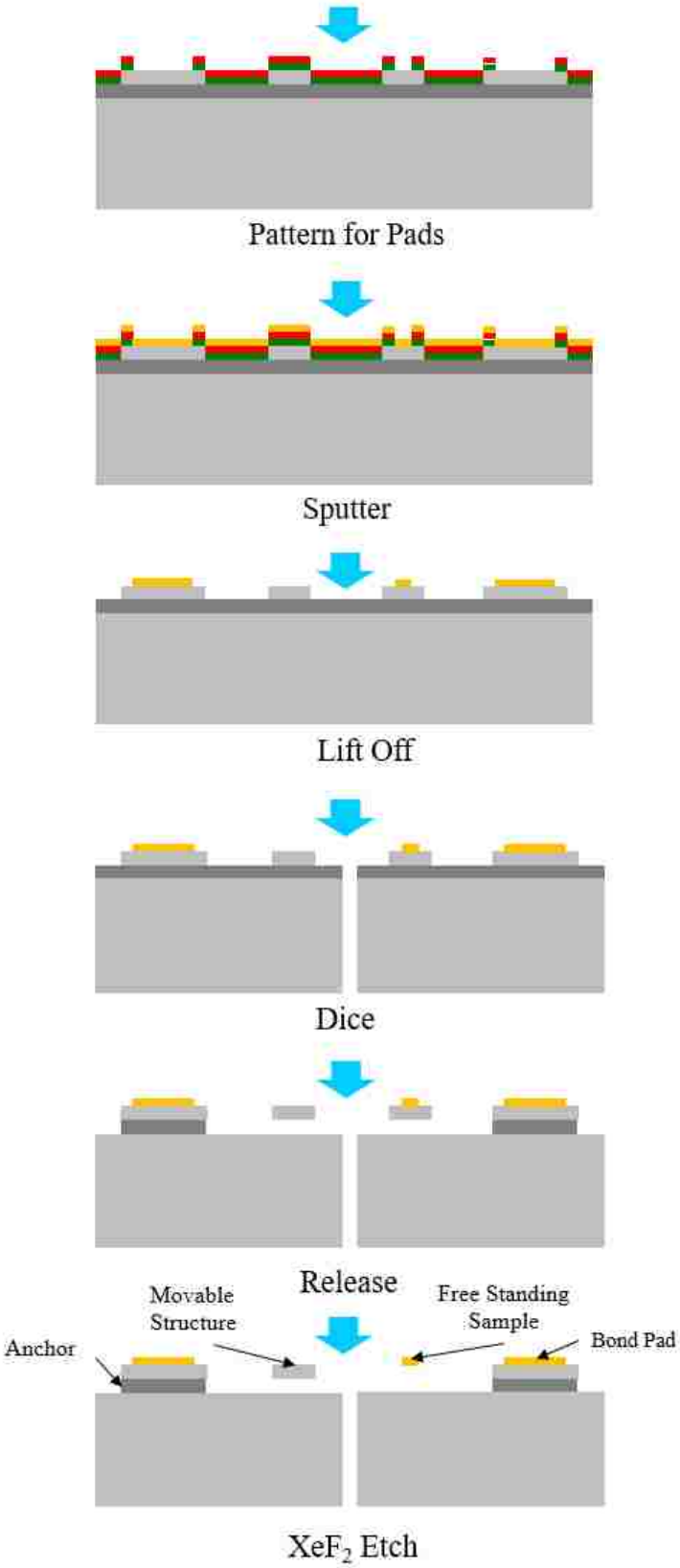

Figure 79: Fabrication Process Flow

Chapter 9

RESULTS & RECOMMENDATIONS

9.1 FABRICATION RESULTS

The following images have been obtained through a Scanning Electron Microscope (SEM) for the various parts of the thermal actuators and samples.

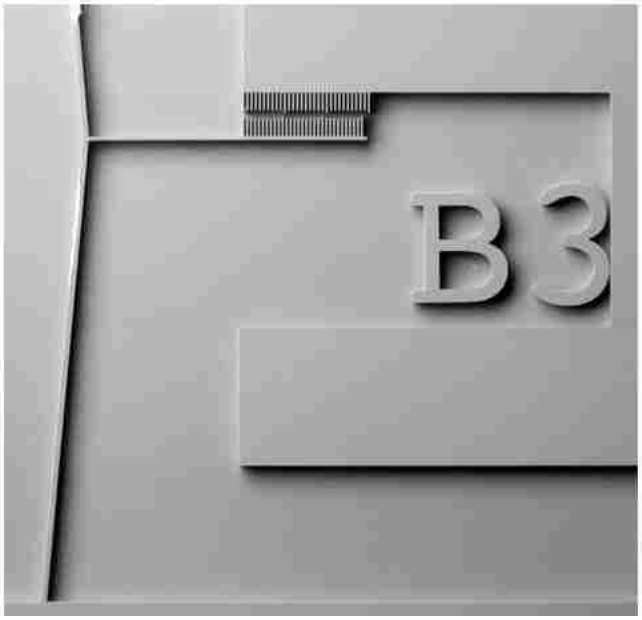

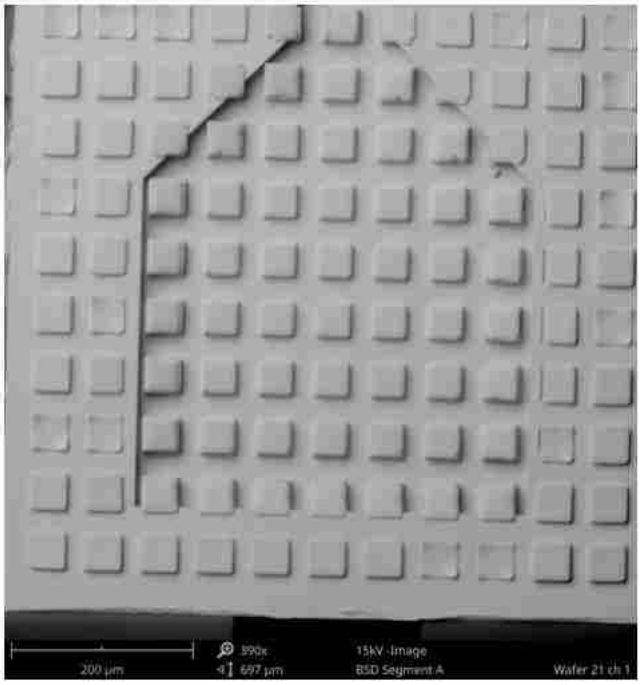

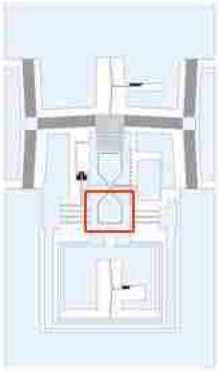

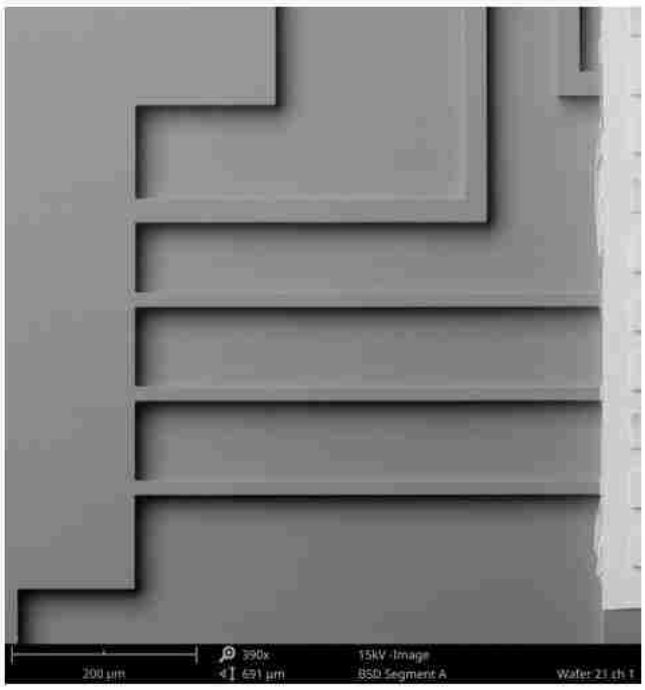
200 µm
390x
691 µm
15kV -Image
BSD Segment A
Wafer 21 ch 1

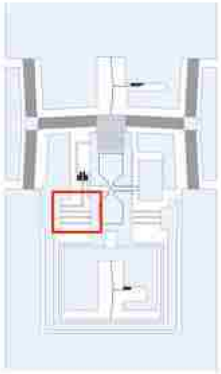

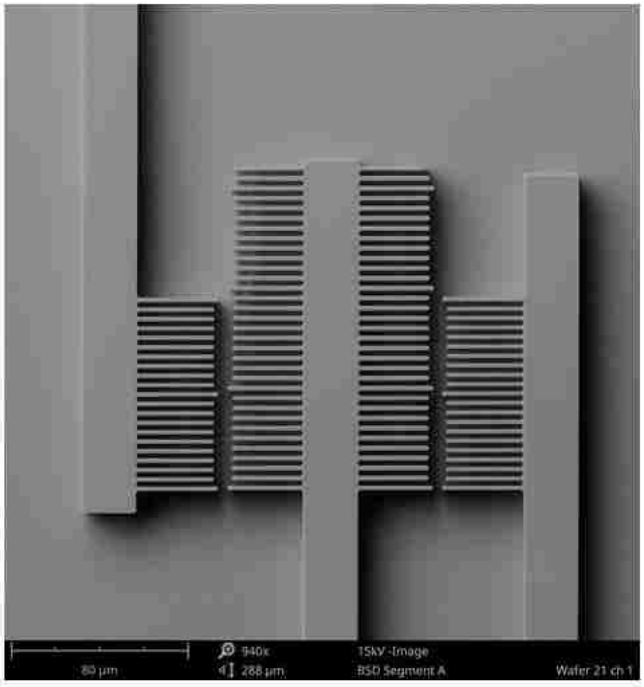
80 µm
940x
288 µm
15kV -Image
BSD Segment A
Wafer 21 ch 1

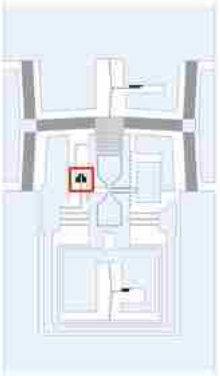

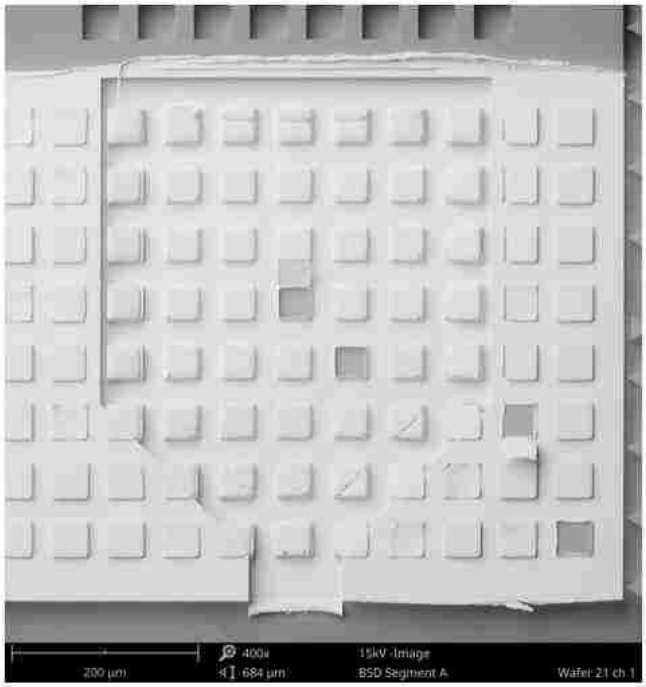
200 µm
400x
684 µm
15kV Image
BSD Segment A
Wafer 21 ch 1

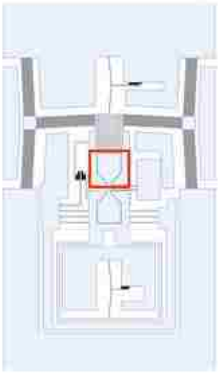

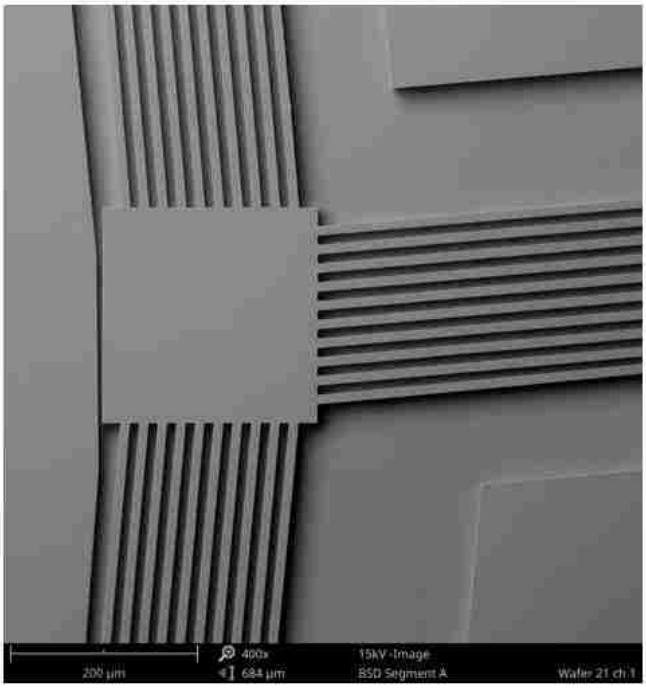
200 µm
400x
684 µm
15kV Image
BSD Segment A
Wafer 21 ch 1

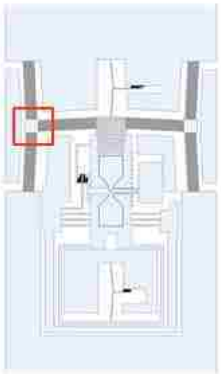

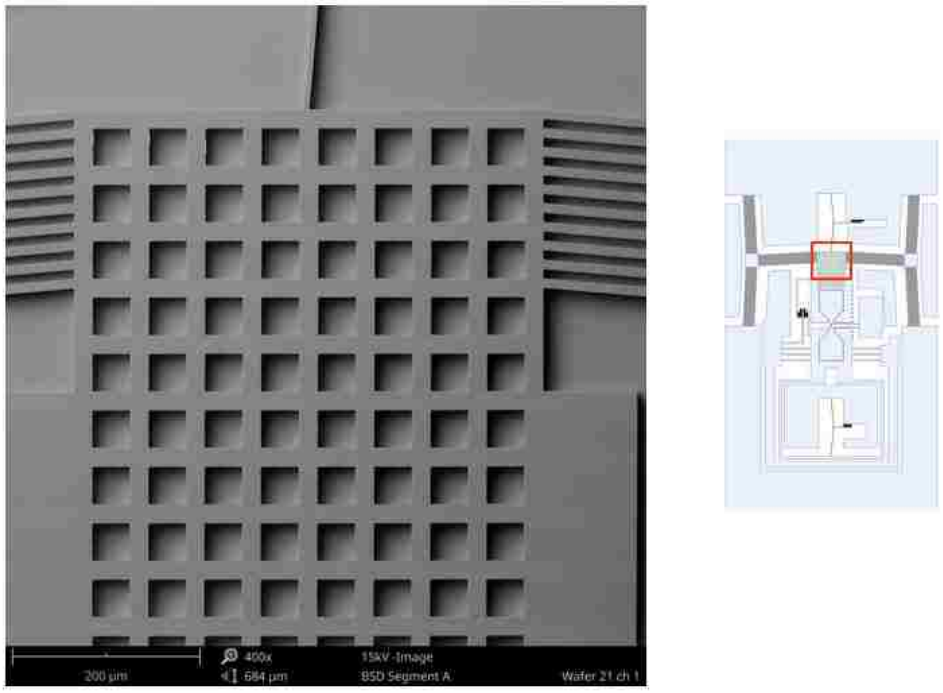

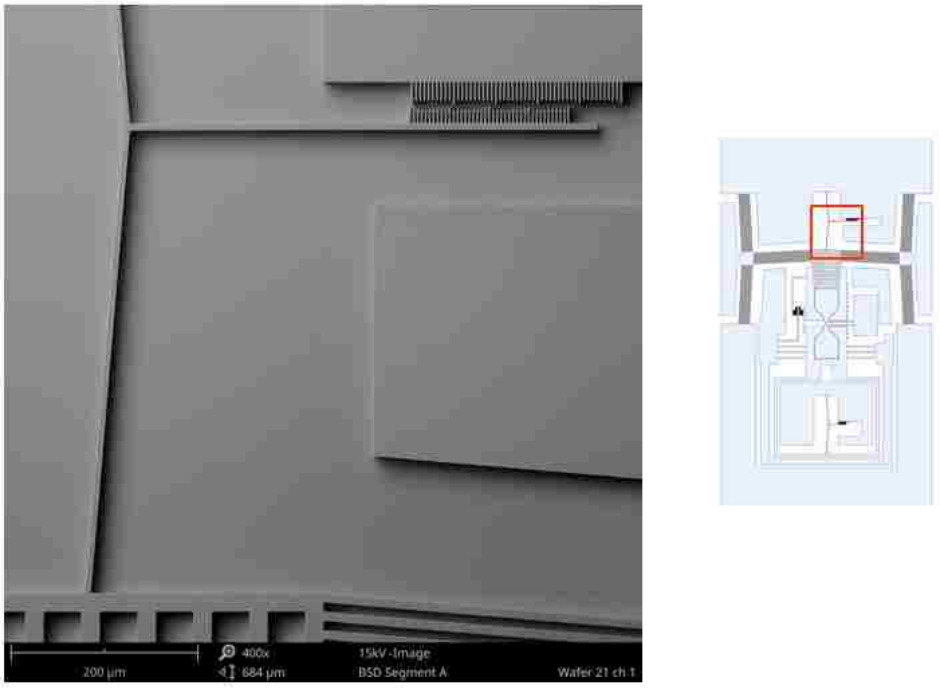

Figure 80: SEM Images for Actuator

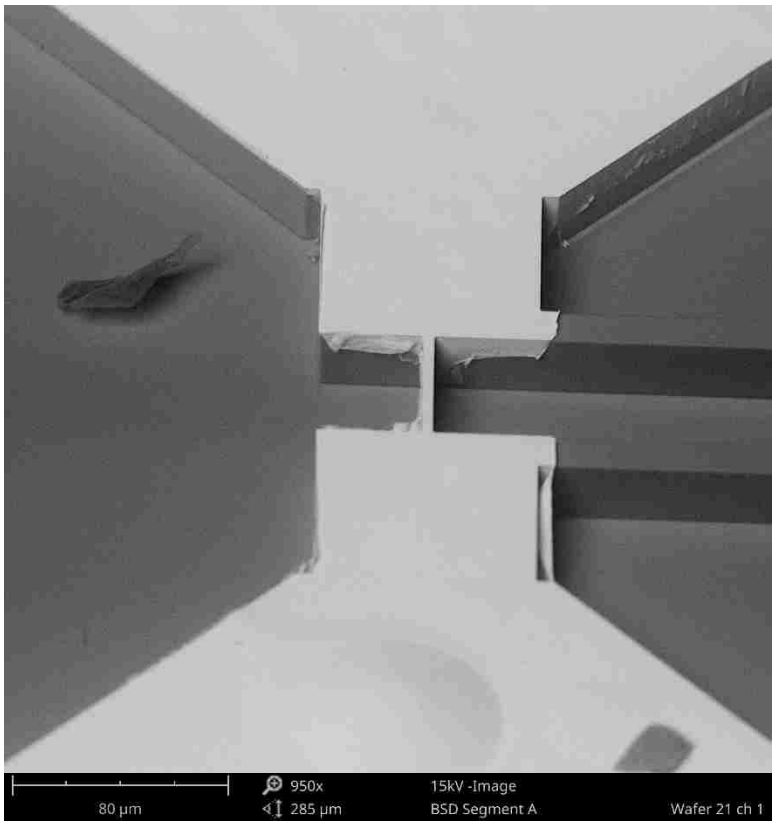

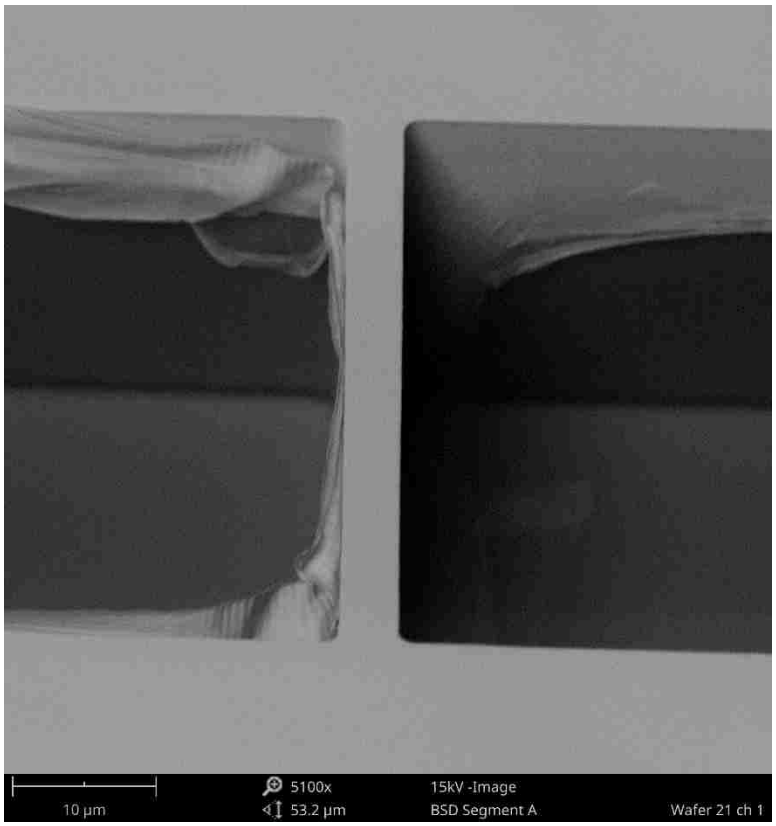

Figure 81: SEM Images for Sample

9.2 EXPERIMENTAL SETUP

The actuator samples are then placed on to the probe station as shown in figure 82, 83 & 84 where the electrical pads are supplied with a live and neutral terminal via tungsten probes. These terminals are then connected with a power supply which supplies current to actuate the devices. These probes are held in place with vacuum and are moved in space through micro manipulators with a resolution of one micron. Several objectives are also available to study the motion of the actuators with x2.5, x 10 and x 50 magnification. A CCD camera is also available to capture the motion of the devices in the form of a video which can later be broken down into its individual frames for an accurate treatment of the displacements using Digital Image Correlation.

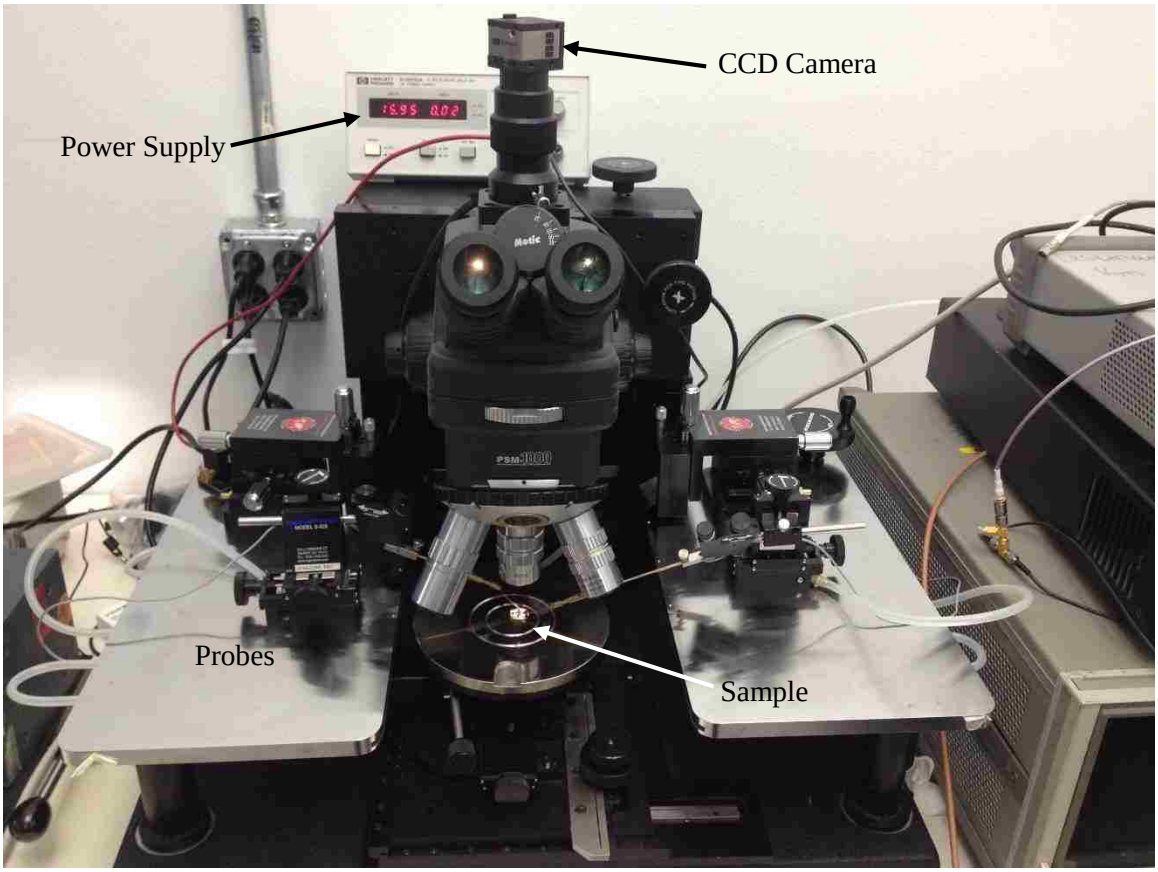

Figure 82: Experimental Setup for Thermal Actuators

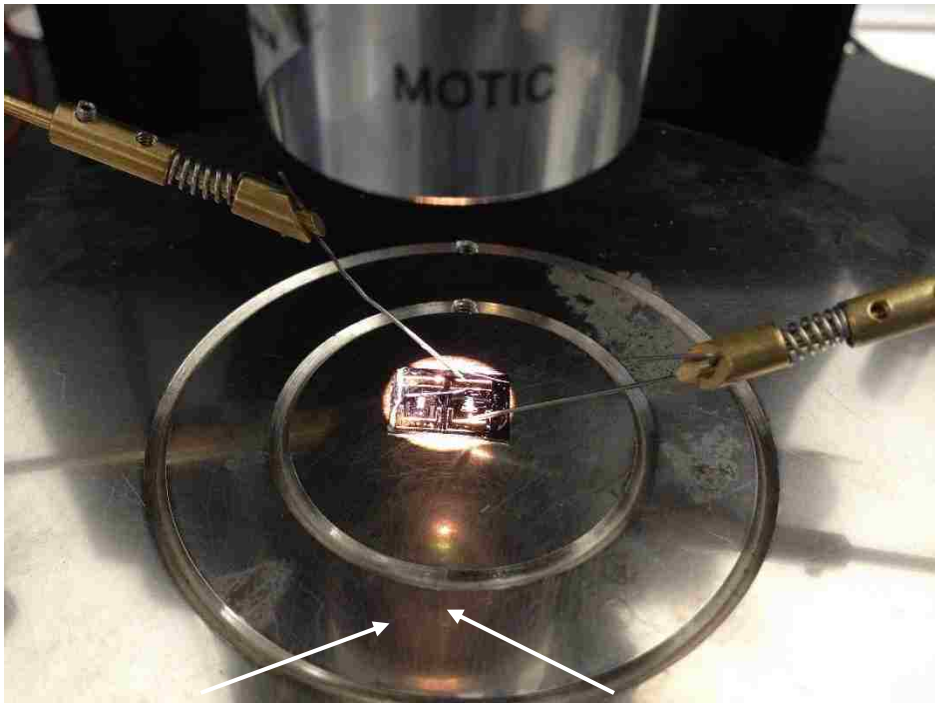

Figure 83: Sample with Tungsten Probes

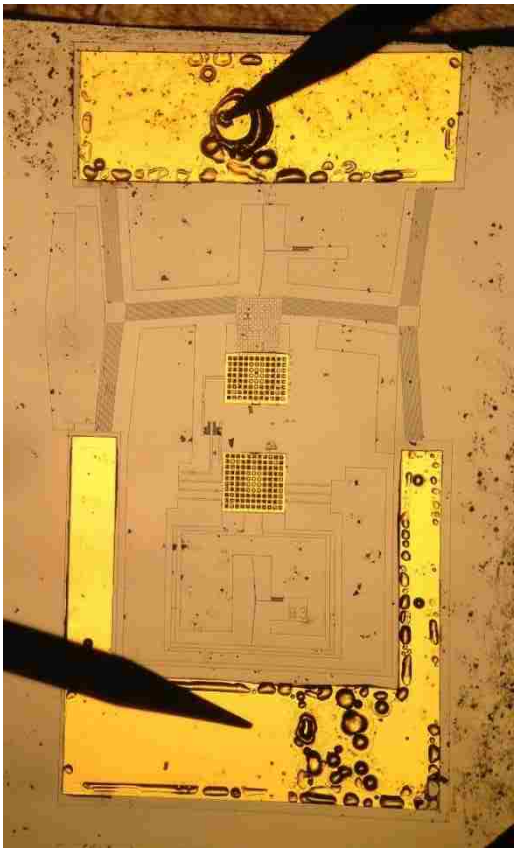

Figure 84: Thermal Actuator with Probe Needle

Unfortunately, no significant motion could be detected to characterize the response of the actuators. Several reasons exist which are hindering the motion of the actuators aside from a weak power supply. These reasons are discussed in the next section with recommendations to remedy these hindrances for an effective electromechanical response from the actuators.

9.3 RECOMMENDATIONS

The following reasons are presented to explain the immobility of the actuators and some recommendations are also given to solve these problems for future experimentation.

a) SIMILAR RELEASE TIMES

The release time required for all the movable components should be roughly the same. The junction of vertical and horizontal chevrons and the huge sections of the clamps are the last sections to release. The time is so large that the anchors might start to release as well. The

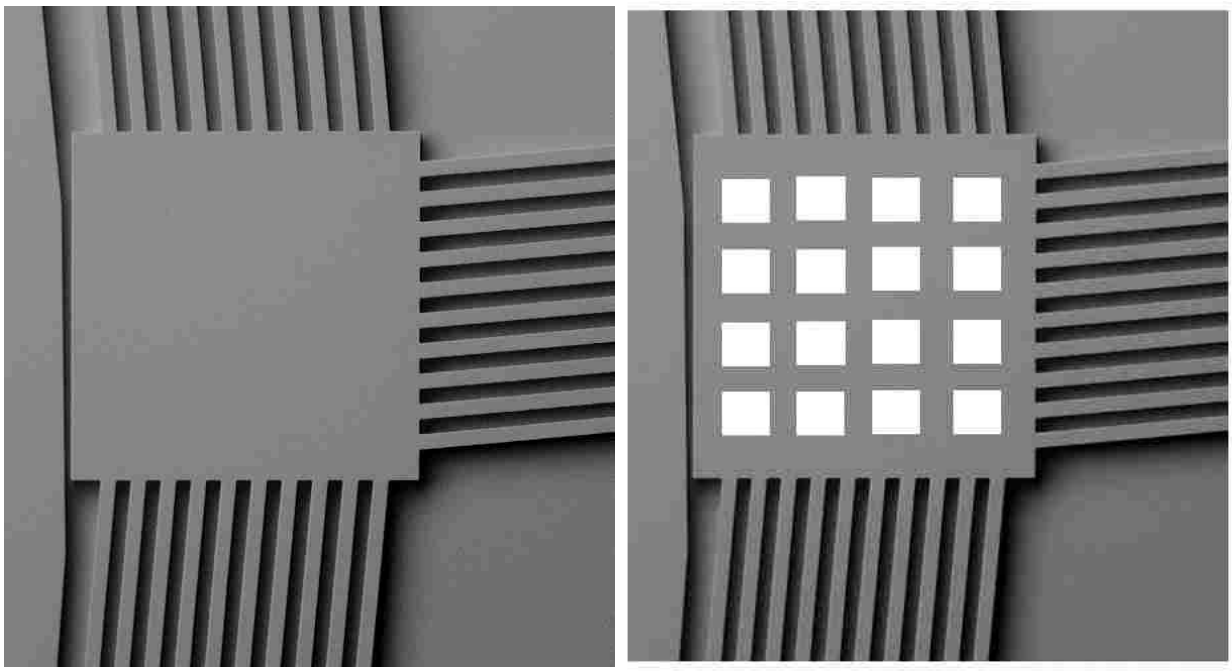

Figure 85: (Left) Present Chevron Junction (right) Improved Junction

figures below show how the chevron junction is and how it should have been. The thinner chevrons release first and wait on the bulk sections to release.

b) STICTION FAILURE

Delayed release times using liquid etchants can also lead to Stiction failure. The high surface tension of the liquid such as diluted Hydrofluoric acid or Buffered Oxide Etch (BOE) can pull on the structures causing the geometry to curve up or down. It may also cause separate sections to stick together or break.

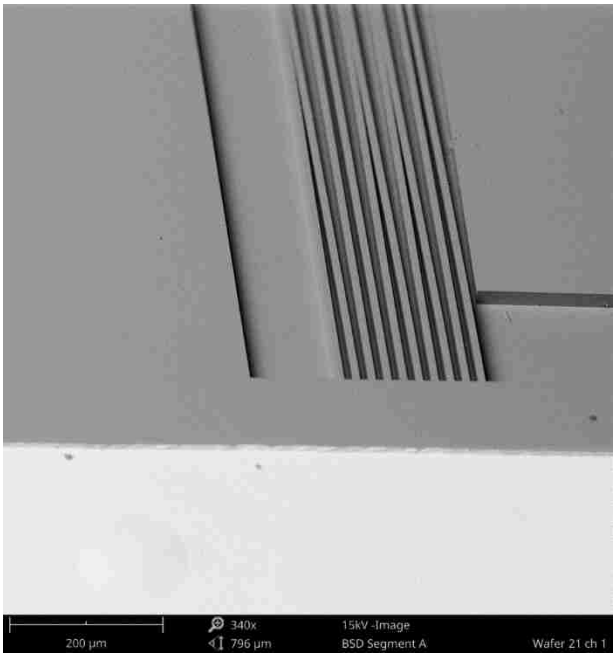

Figure 86: Stiction Failed Chevrons

c) RESIDUE

Residue from liquid etchants of wreckage from other smaller section can build up around or below the free standing movable structures and immobilize them. Such an example is shown below where a lump of silicon is stuck to the underside of the load cell beams and is hindering its motion.

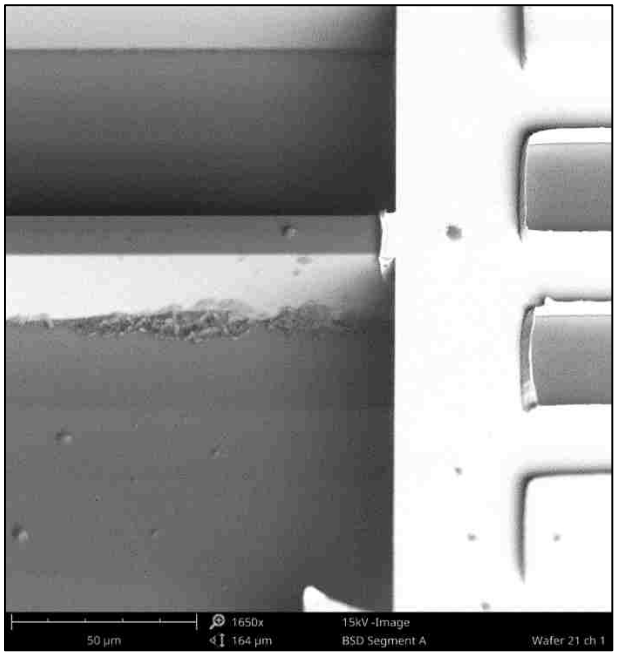

Figure 87: Residue Preventing Load Cell Motion

d) GOOD LIFT OFF PROFILE

The gold sample net is stuck to the oxide layer and is causing sever releasing problems.

The net is shown below.

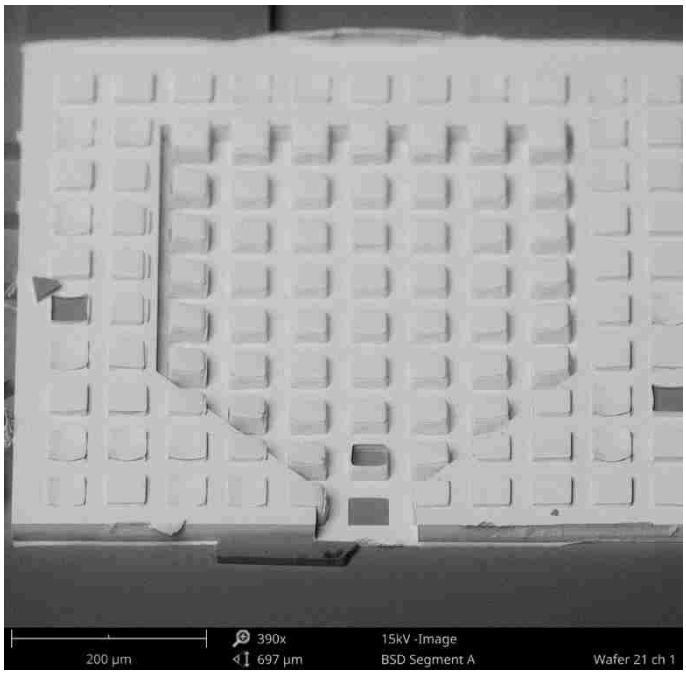

Figure 88: Gold Net (White) Stuck to BOX Layer Preventing Load Cell Motion

As it can be seen in the picture that most of the sections that should have been removed are still there, clinging to the BOX layer underneath. This is due to two strong reasons. The first reason is that the Gold layer is too thick for the acid to go in, etch away the oxide and lift off the access metal. The second reason is that the profile is not equipped to facilitate this kind of maneuver. One individual photoresist block covered with Gold is shown below.

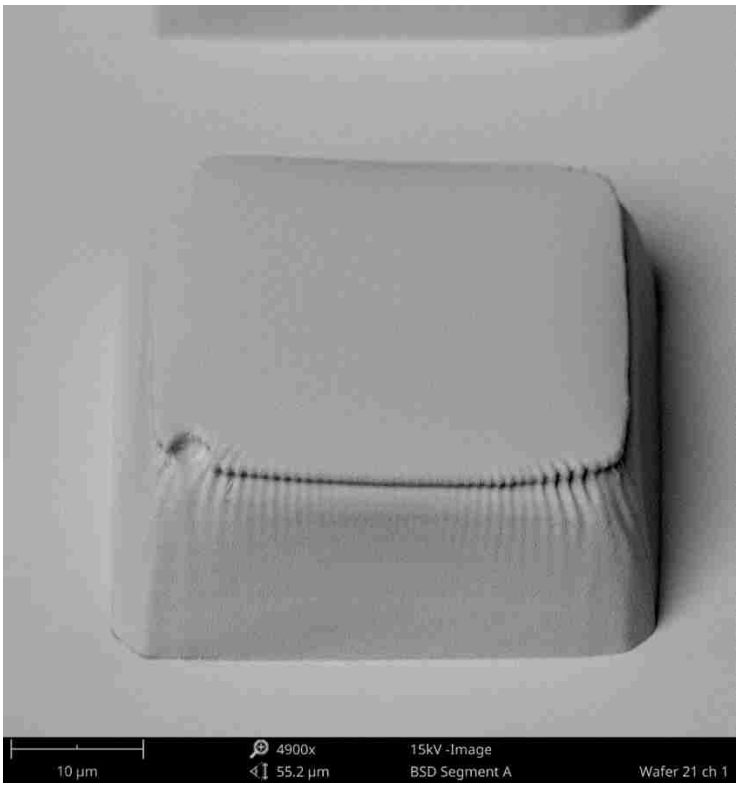

Figure 89: Bad Lift Off Profile for PR in place of Sample Net Opening

This is a very undesirable lift off profile and the Gold is encasing the entire structure firmly. There is extremely low probability for the liquid etchant to seep into the cracks and etch away the oxide. This profile would also have hindered the lift off procedure performed after deposition of Gold for the samples. But acetone is much more viscous and fast acting on photoresist than acid on PR. The comparison of good and bad lift off profiles are given in figure 90.

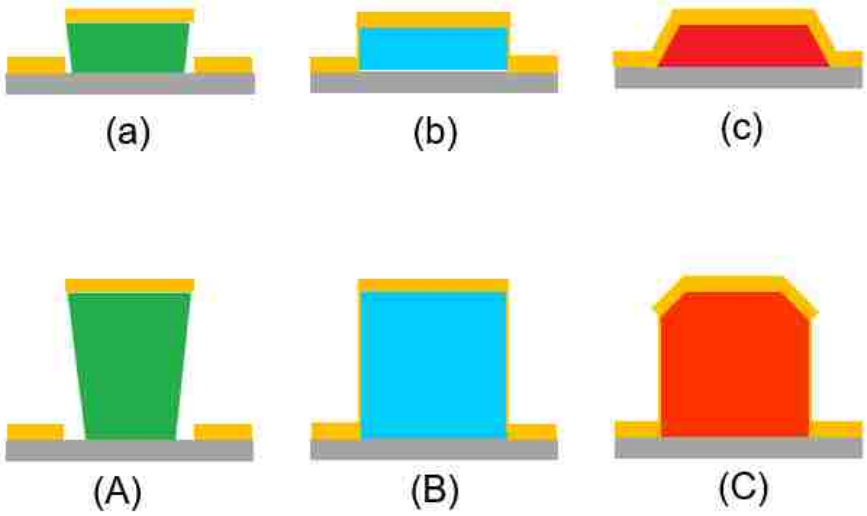

Figure 90: (Left to right) Comparison of Good to Bad Lift Off Profile

The profiles get increasingly undesirable for lift off and the correct profile can be obtained by experimenting with the exposure time for the PR used. Slightly under exposed PR layers tend to have an under cut as shown in the part 'a' of the figure which is the most desirable type of lift off profile. [20] [21]

9.4 CONCLUSION

In light of this discussion more experimentation is deemed necessary for a good lift off profile alongside perfecting the releasing techniques. The author is confident that these devices will surely produce the desired electromechanical response once fully released. Then the samples can be transferred to the test site and a tensile test can be performed. The cryostat and holder are ready to receive these devices which in turn will produce a wealth of low temperature tensile data for these free standing, independently fabricated, thin film Gold samples.

REFRENCES

[1] B. Vigna, “Future of MEMS : An industry point of view,” pp. 1–8, 2006.

[2] J. A. Walker, “The future of MEMS in,” vol. 1.

[3] K. J. Rebello, “Applications of MEMS in Surgery,” vol. 92, no. 1, pp. 43–55, 2004.

[4] A. Nisar, N. Afzulpurkar, B. Mahaisavariya, and A. Tuantranont, “MEMS-based micropumps in drug delivery and biomedical applications,” vol. 130, pp. 917–942, 2008.

[5] A. M. Y. C. R. Grayson, R. S. Shawgo, A. M. Johnson, N. T. Flynn, Y. Li, M. J. Cima, and R. Langer, “A BioMEMS Review : MEMS Technology for Physiologically Integrated Devices,” vol. 92, no. 1, 2004.

[6] K. Abbas, S. Alaie, and Z. C. Leseman, “Design and characterization of a low temperature gradient and large displacement thermal actuators for in situ mechanical testing of nanoscale materials,” *J. Micromechanics Microengineering*, vol. 22, no. 12, p. 125027, Dec. 2012.

[7] M.-T. Lin, P. El-Deiry, R. R. Chromik, N. Barbosa, W. L. Brown, T. J. Delph, and R. P. Vinci, “Temperature-dependent microtensile testing of thin film materials for application to microelectromechanical system,” *Microsyst. Technol.*, vol. 12, no. 10–11, pp. 1045–1051, Mar. 2006.

[8] Yong Zhu and H. D. Espinosa, “An electromechanical material testing system for in situ electron microscopy and applications,” *Proc. Natl. Acad. Sci.*, vol. 102, no. 41, pp. 14503–14508, 2005.

[9] E. D. Marquardt, J. P. Le, and R. Radebaugh, “Cryogenic Material Properties Database,” *11th Int. Cryocooler Conf.*, vol. 12, no. 6, pp. 1–7, 2000.

[10] J. Ekin, “Experimental Techniques for Low-Temperature Measurements: Cryostat Design, Material Properties and Superconductor Critical-Current Testing,” *Exp. Tech. Low-Temperature Meas. Cryostat Des. Mater. Prop. Supercond. Crit. Test.*,

no. May, pp. 1–704, 2006.

[11] S. S. Andrews and S. G. Boxer, “A liquid nitrogen immersion cryostat for optical measurements,” *Rev. Sci. Instrum.*, vol. 71, no. 9, pp. 3567–3569, 2000.

[12] C. Design and J. W. Ekin, “Experimental Techniques for Measurements Properties , and Superconductor Critical-Current Testing.”

[13] S. Diodes, “DT-670 Silicon Diodes,” no. 614, pp. 32–35.

[14] J.-H. Cho, H.-P. Ha, and K. H. Oh, “Recrystallization and grain growth of cold-rolled gold sheet,” *Metall. Mater. Trans. A*, vol. 36, no. December, pp. 3415–3425, 2005.

[15] C. A. Neugebauer, “Tensile Properties of Thin , Evaporated Gold Films Tensile Properties of Thin , Evaporated Gold Films,” vol. 1096, no. 1960, 2016.

[16] T. O. F. Contents, “Photolithography using AZ 1512 Photoresist STANDARD OPERATING PROCEDURE,” pp. 1–9.

[17] D. Package, “AZ 9260 Photoresist.”

[18] T. Sop, “Photolithography SOP,” pp. 1–8.

[19] A. Around, M. C. Problems, and M.- Structuring, “Lithography Trouble Shooter,” 2012.

[20] MicroChemicals, “Lift-off Processes with Photoresists,” *Web Broch.*, 2013.

[21] L. Fuller, M. Filmer, and N. Liotta, “Lift-Off Metal Patterning,” pp. 1–18, 2012.

APPENDIX A

ENGINEERING DIAGRAMS FOR CRYOSTAT

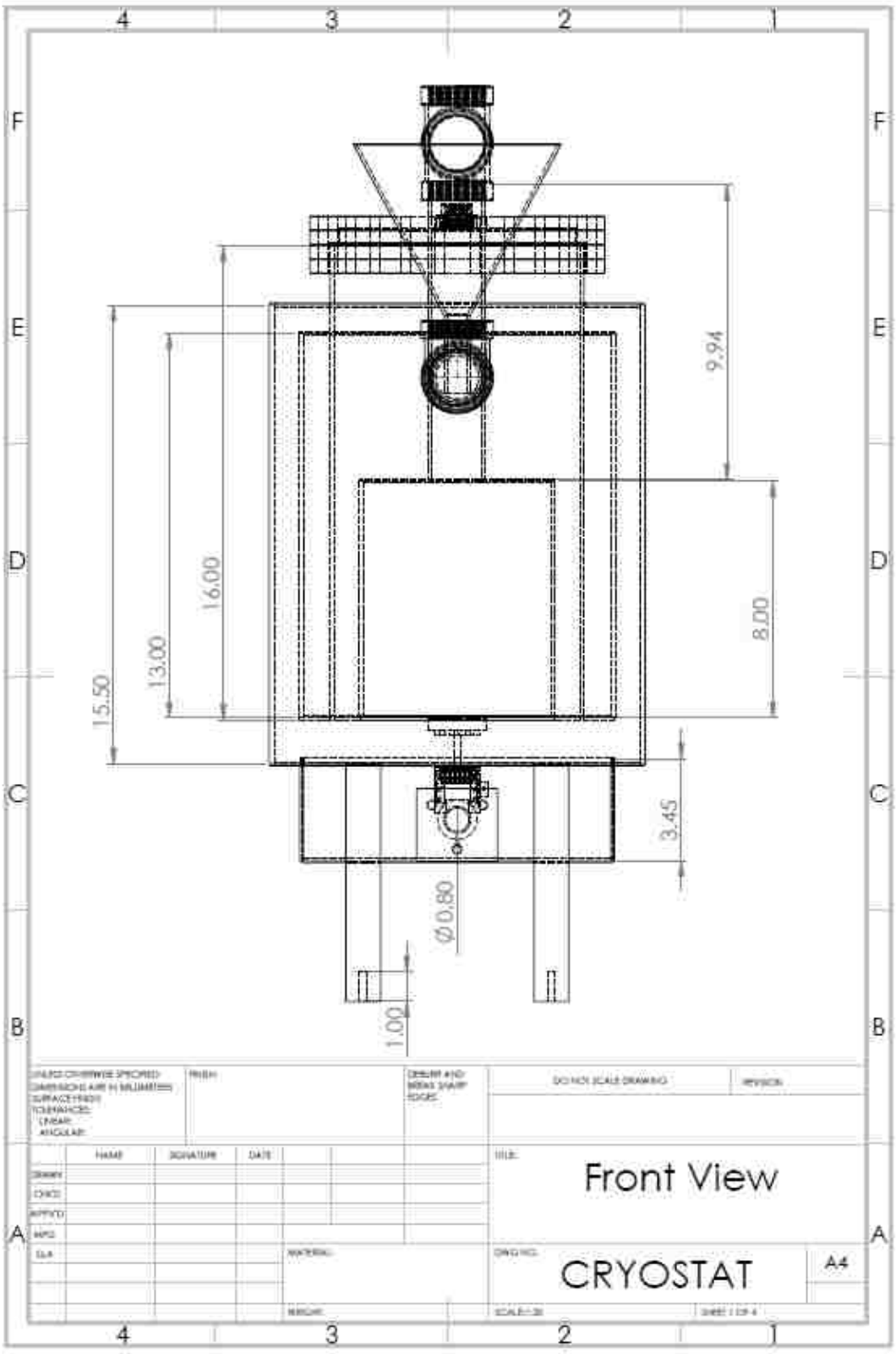
4
3
2
1
F
E
D
C
B
A
9.94
16.00
13.00
15.50
8.00
3.45
Ø0.80
1.00
Front View
CRYOSTAT
A4

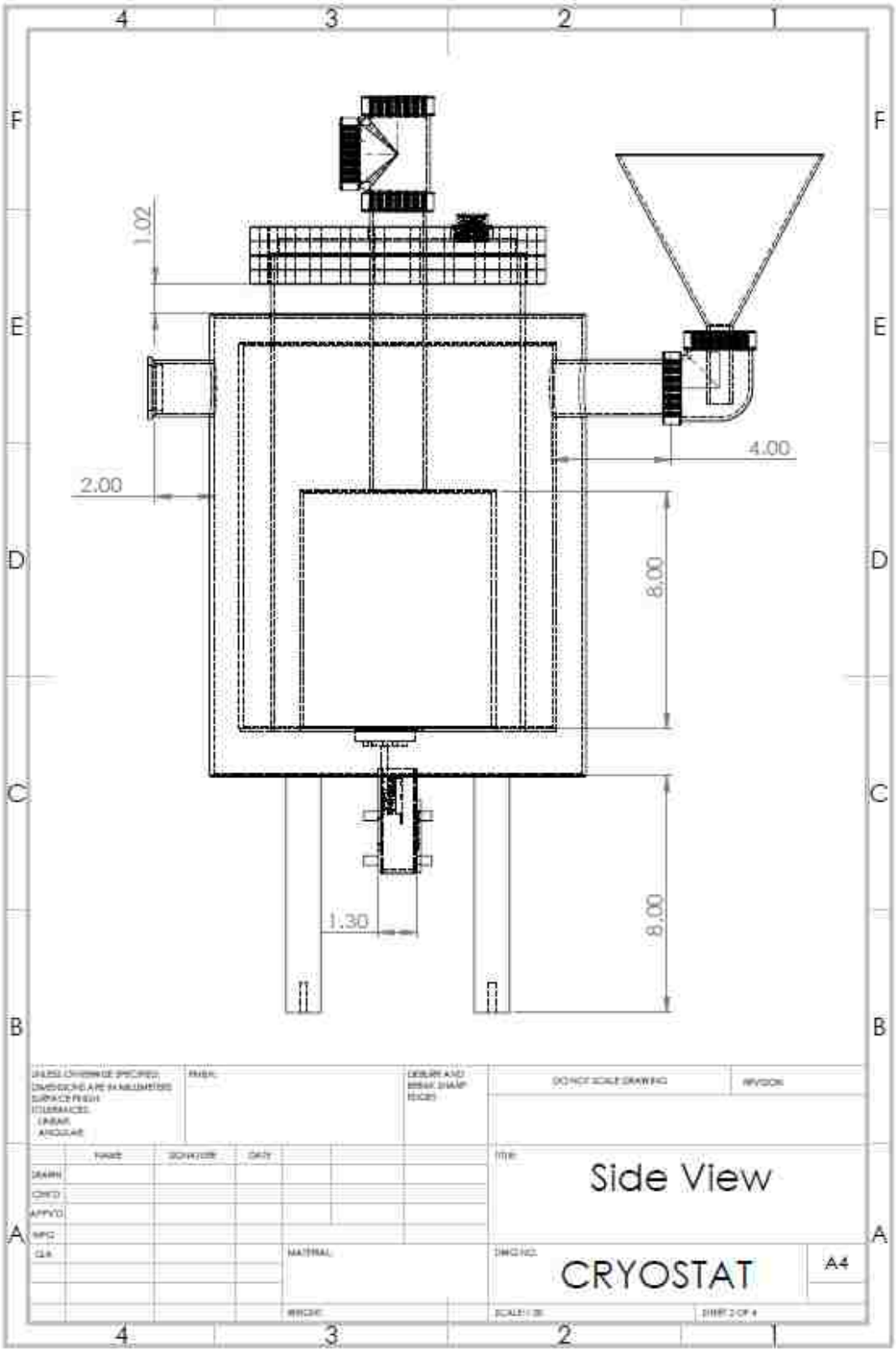
1.02
2.00
4.00
8.00
8.00
1.30
Side View
CRYOSTAT
A4

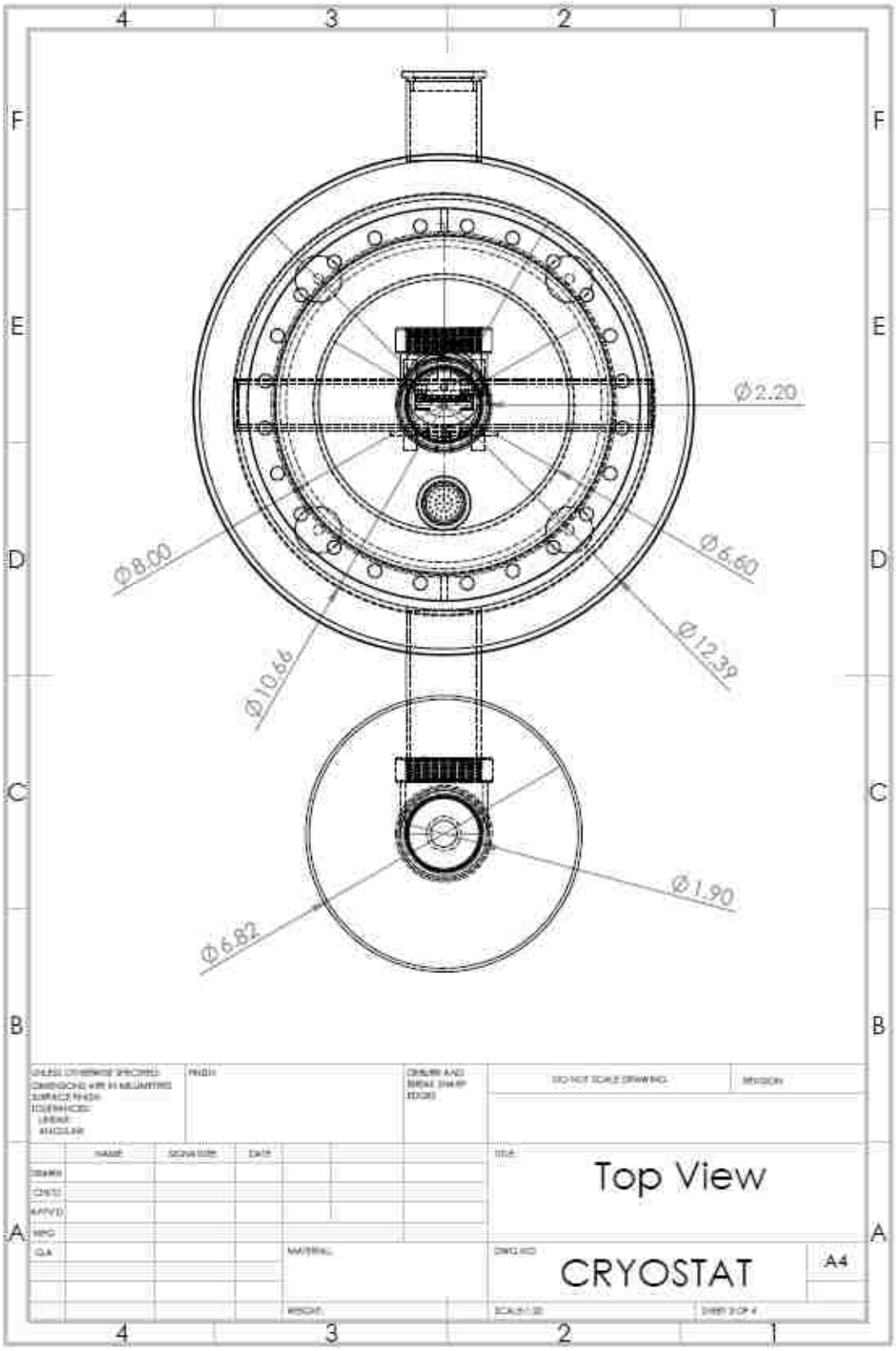
Ø2.20
Ø8.00
Ø6.60
Ø10.66
Ø12.39
Ø1.90
Ø6.82
Top View
CRYOSTAT
A4

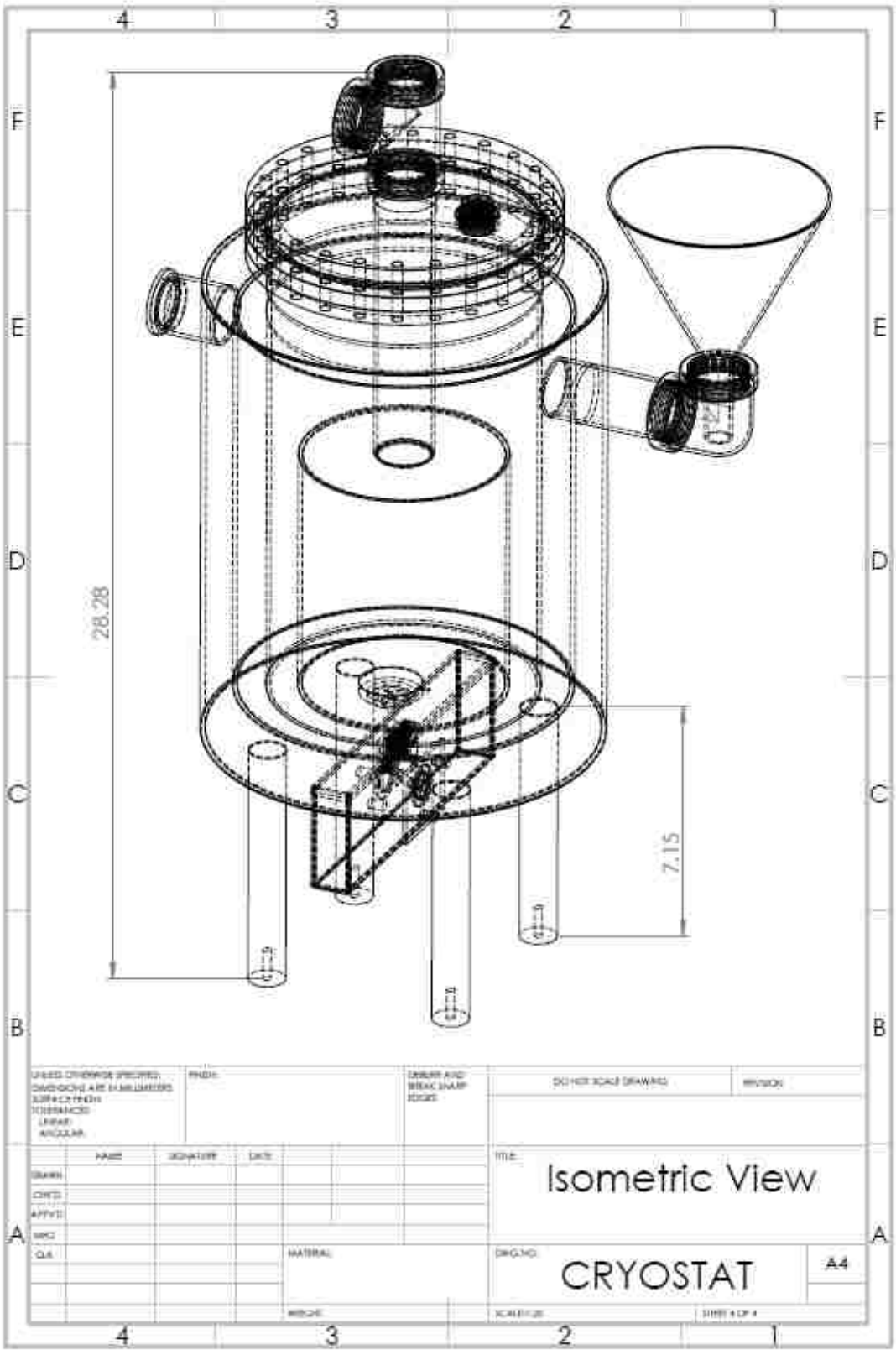
28.28
7.15
Isometric View
CRYOSTAT
A4

APPENDIX B

ENGINEERING DIAGRAMS FOR HOLDER

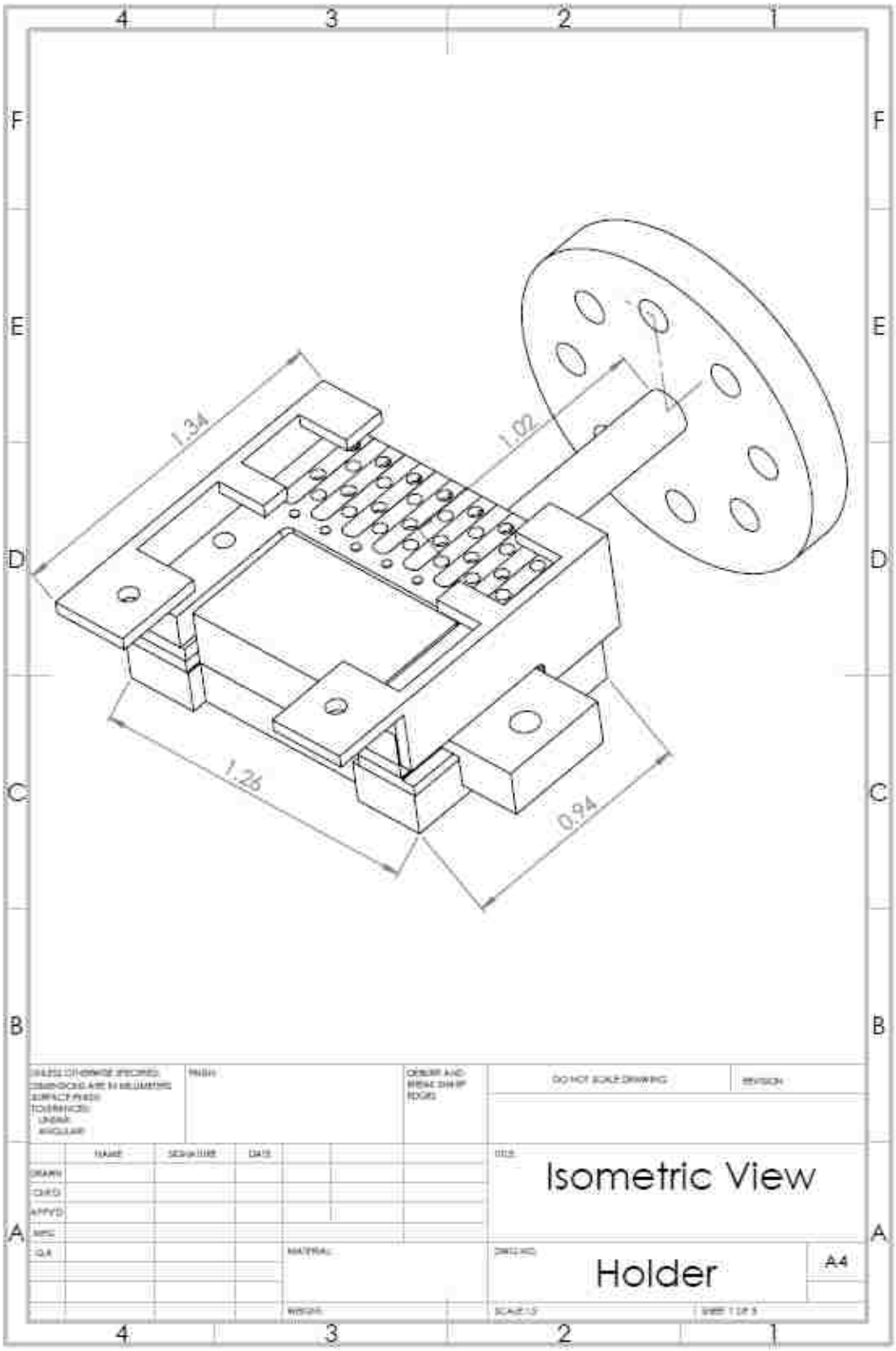
4
3
2
1
F
E
D
C
B
A
1.34
1.02
1.26
0.94
Isometric View
Holder
A4

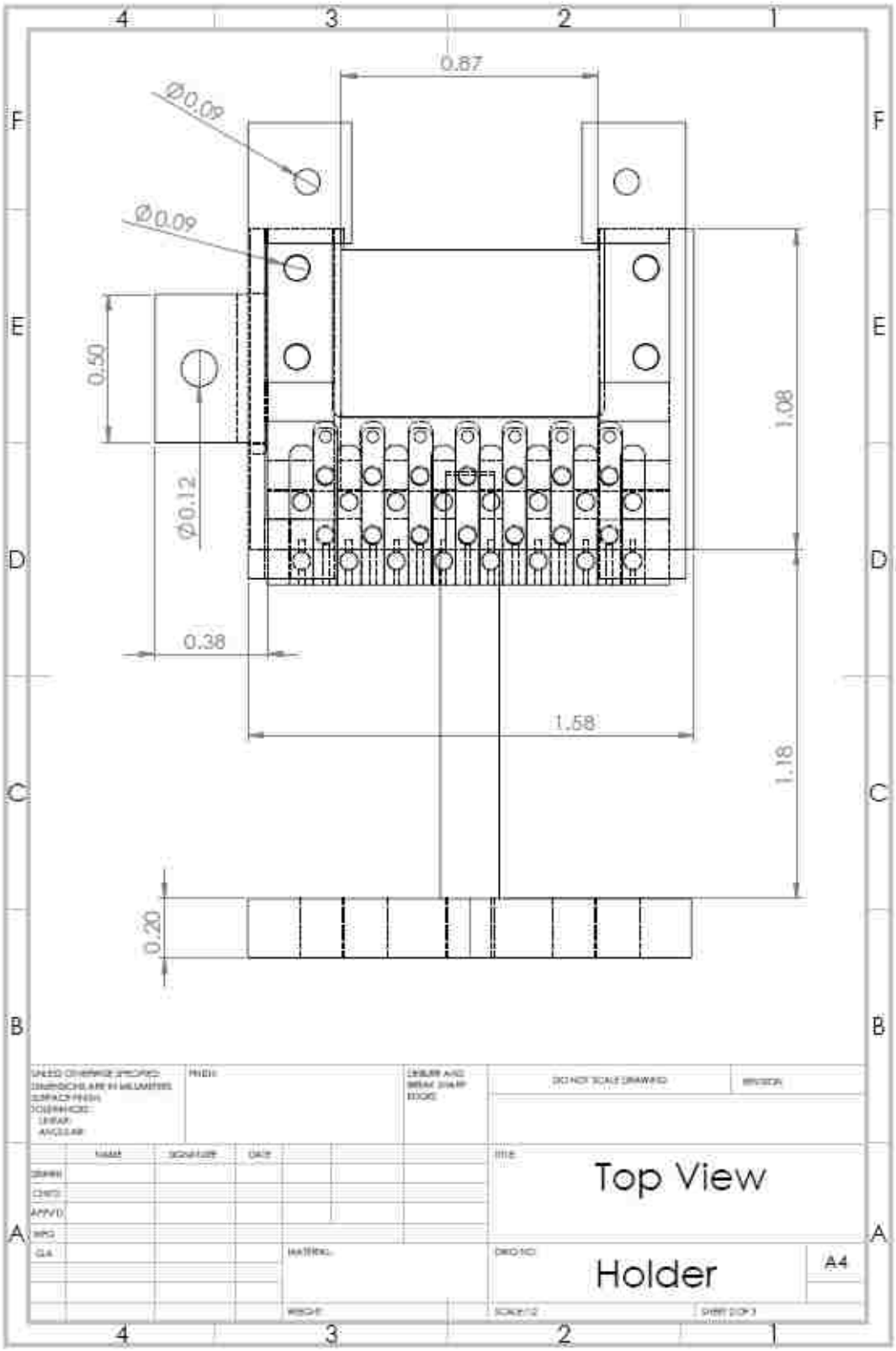
0.87
Ø0.09
Ø0.09
0.50
Ø0.12
0.38
1.08
1.58
1.18
0.20
Top View
Holder
A4

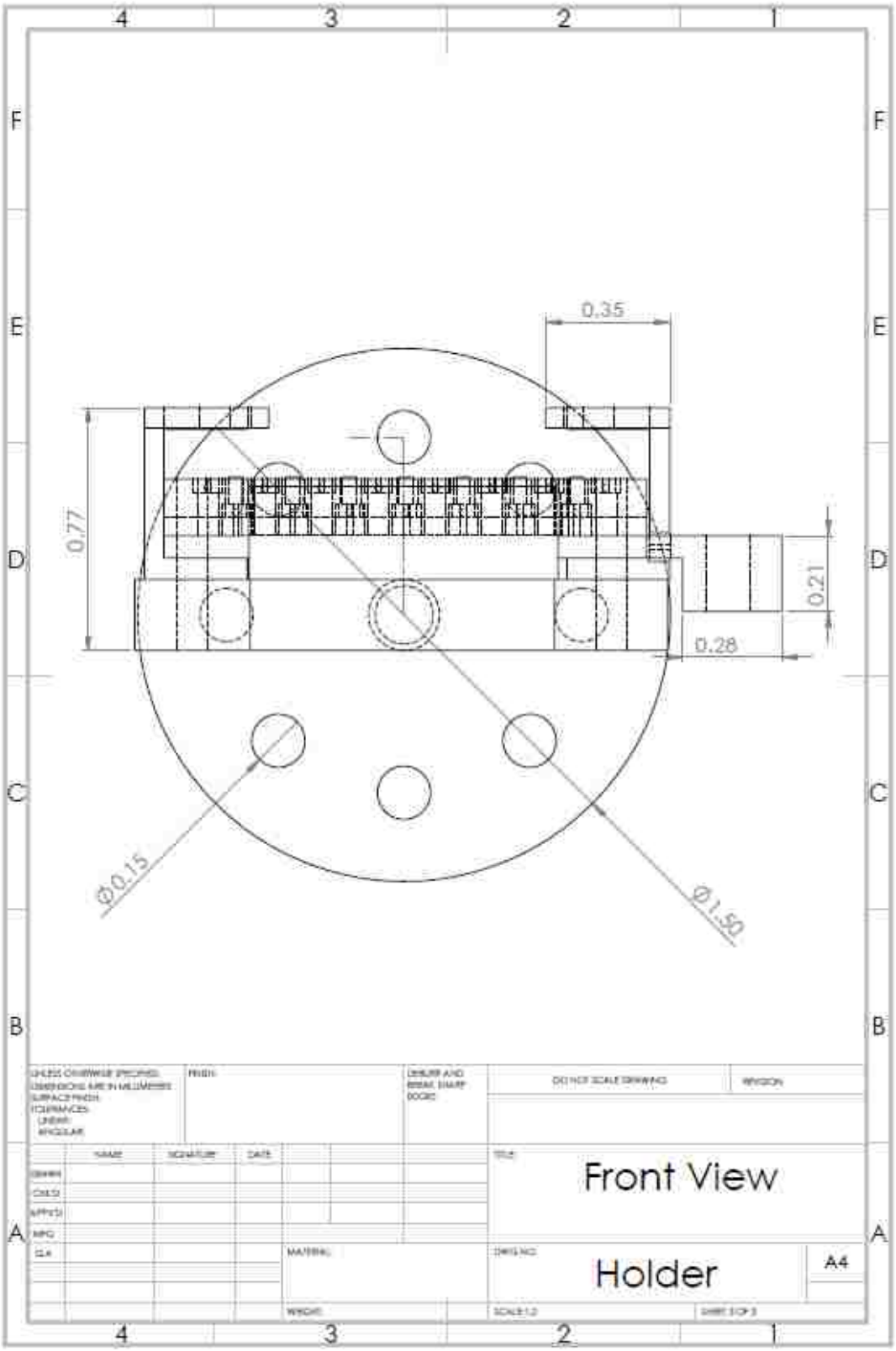
0.35
0.77
0.21
0.28
Ø0.15
Ø1.50
Front View
Holder
A4

APPENDIX C

FABRICATION FLOW FOR ACTUATORS AND SAMPLES

Wafer:	Prime SOI	
Device Layer	25 +/- 5 um	Polished
Box Layer	2 +/- 1% um	
Handling Layer	525 +/-10um	Polished

The author recommends using a thinner device layer of 20µm or less for easier lift off and release process.

ACTUATOR & SPECIMEN PATTERN:

Ensure device layer face up

Process Step	**Tool**	**Parameters**	**Comments**
HMDS Coat	HMDS Dispenser	Program 1, 100^0 C, 1 min	
Cool Down	Metal table surface	30 sec	Ensure surface is clean
Spin Coat	CEE Coater	AZ 1518,500rpm, 3 sec, 5000 rpm, 20 sec, 20 ml	Uniformly spread PR over whole wafer in circles
Soft Bake	Hot Plate	105^0 C, 90 sec	
Cool Down	Metal table surface	30 sec	Ensure surface is clean
Exposure	Karl Suss Mask Aligner	3.2 mW/cm^2, 16 sec, Vacuum contact at 40µm	Ensure good vacuum suction on Masks!
Develop	Caustic Bench	AZ400K 4:1, 3-4 min	Ensure the unwanted PR clears away
QDR	Caustic Bench	5 cycles	
Spin Rinse Dry	Verteq Spin Dryer	Resistivity DI water 15-18 MΩ	
Inspection	Nikon Microscope	5x,20x,40x, 100x	

The process results in 2µm uniform coat of PR.

DRIE ETCH

The following recipe is provided as an approximation and the actual etching process could not be completed at the University of New Mexico NanoFab due to technical malfunction of the etcher. The work then had to be contracted out to the NanoFab at the University of Washington, Seattle, WA. Nevertheless, all other processing was done exclusively at the University of New Mexico NanoFab at the Manufacturing Technology & Training Center.

Tool	**Parameters**	
Adixen AMS 100	Process time	25 min
(ICP Bosch Process)	He Pressure	10 mbar
	Substrate Position	200 mm
Program Name	Temperature	10 ^{o}C
(Std SOI 25 min)	Load	660
Temperature 10	Tune	907
Delay 30	Source Gen	Checked
Standard SOI 25 min	SH gen 2	Checked
	Passivation	**C_4F_8**
	Inactive State	0 sec
	Active State	120 sccm
	Priority	1
	Duration	2 sec
	Pressure	-
	Position	-
	Source G	1800 W
	SH gen	-
	H Power	50 W
	H time	20 msec
	L Power	0 W
	L Time	80 msec
	Etchant	**SF_6**

	Inactive State	0 sec
	Active State	300 sccm
	Priority	2
	Duration	7 sec
	Pressure	$4.5x10^{-2}$ mbar
	Position	20%
	Source G	1800 W

PIRANAH CLEANING

Process Step	Tool	Parameters
Piranha, Step 1	Acid Bench, Hot Plate	200 ml 95% Sulfuric Acid, 50 ml Hydrogen Peroxide, 175 ^{0}C, 5 min
Piranha, Step 1	Acid Bench, Hot Plate	200 ml 95% Sulfuric Acid, 50 ml Hydrogen Peroxide, 105 ^{0}C, 5 min
Water Cooling	Acid Bench	Dip in DI water, 2 min
QDR	Caustic Bench	5 cycles
Spin Rinse Dry	Verteq Spin Dryer	Resistivity DI water 15-18 MΩ

BOND PAD & SAMPLE PATTERN

Process Step	Tool	Parameters	Comments
HMDS Coat	HMDS Dispenser	Program 1, 100^0 C, 1 min	
Cool Down	Metal table surface	30 sec	Ensure surface is clean
Spin Coat	CEE Coater	AZ 9260,500rpm, 15 sec, 1600 rpm, 60 sec, 20 ml	Uniformly spread PR over whole wafer in circles
Soft Bake	Hot Plate	105^0 C, 90 sec	
Cool Down	Metal table surface	30 sec	Ensure surface is clean
Exposure	Karl Suss Mask Aligner	3.2 mW/cm^2 , 520 sec, Vacuum contact at 40µm	Ensure good vacuum suction on Masks!
Develop	Caustic Bench	AZ400K 4:1, 9 min	Ensure the unwanted PR clears away

QDR	Caustic Bench	5 cycles	
Spin Rinse Dry	Verteq Spin Dryer	Resistivity DI water 15-18 MΩ	
Inspection	Nikon Microscope	5x,20x,40x, 100x	

The process results in 10.9 µm uniform coat of PR. A thick PR coat is necessary to facilitate lift off and release steps. Also it is highly recommended that this step be separately performed on a bare Si wafer and sliced out to inspect the PR profile. If the PR profile is not good for lift off, then the exposure time should be decreased.

SPUTTERING

Metal Deposited	Tool	Parameters
Gold	AJA, RF Gun#2	Argon supply13 mtorr, Pressure set 4 mtorr, 99.99% Pure Gold Target, Plasma power 300W, 34nm/min
Titanium	AJA, DC Gun#3	Argon supply13 mtorr, Pressure set 4 mtorr, 99.99% Pure Ti Target, Plasma power 300W, 1.5nm/min
Iron	AJA, DC Gun#2	Argon supply13 mtorr, Pressure set 4 mtorr, 99.99% Pure Fe Target, Plasma power 300W, 6nm/min

BOND PAD LIFT OFF

Process Step	Tool	Parameters
Acetone Soak	Solvent Bench	2 hours with agitation. Do not use Sonic Bath!
Methanol Rinse	Solvent Bench	5 mins
IPA Soak	Solvent Bench	5 mins
QDR	Caustic Bench	5 cycles
Spin Rinse Dry	Verteq Spin Dryer	Resistivity DI water 15-18 MΩ
Inspection	Nikon Microscope	

SPECIMEN OPENING PATTERN

Process Step	Tool	Parameters	Comments
HMDS Coat	HMDS Dispenser	Program 1, 100^0 C, 1 min	
Cool Down	Metal table surface	30 sec	Ensure surface is clean
Spin Coat	CEE Coater	AZ 1518,500rpm, 3 sec, 5000 rpm, 20 sec, 20 ml	Uniformly spread PR over whole wafer in circles
Soft Bake	Hot Plate	105^0 C, 90 sec	
Cool Down	Metal table surface	30 sec	Ensure surface is clean
Exposure	Karl Suss Mask Aligner	3.2 mW/cm^2 , 16 sec, Vacuum contact at 40µm	Ensure good vacuum suction on Masks!
Develop	Caustic Bench	AZ400K 4:1, 3-4 min	Ensure the unwanted PR clears away
QDR	Caustic Bench	5 cycles	
Spin Rinse Dry	Verteq Spin Dryer	Resistivity DI water 15-18 MΩ	
Inspection	Nikon Microscope	5x,20x,40x, 100x	

Dice wafer to obtain individual dies

FREE STANDING BEAM RELEASE

XeF_2	Room Temperature
Etch chamber Vacuum	0.04 Torr
Expansion Chamber Pressure	0.25 Torr
No. of Pulses	15-Jan
Pulse Duration	60 sec

PHOTORESIST REMOVAL

Process Step	Tool	Parameters	
Ashing	March Plasma	Gas 2 (CF_4)	0 %
		Gas 4 (O_2)	95 %
		Pressure	600-630 mtorr
		Power	300 W
		End Pt	100
		Temp	0
		BP/RP	80
Rotate Wafer 180^0			
Repeat Ashing	March Plasma	Same as above	
Rotate Wafer 180^0			
Repeat Ashing	March Plasma	Same as above	

LIQUID & VAPOUR HF RELEASE

Process	Step	Parameters	
Liquid HF Release	Dip in HF	Concentration	49 %
		Time	4 hours
Vapor HF Release	Pre-Heat	Rheostat setting	60%
		Time	1 hour
		Temperature	35 ° C
	Load Wafer		
	HF Vapor Etch	Time	12 Hours
	Remove Wafer		
	Inspection		

End of Process